

Rapid fluctuations in mid-latitude siliceous plankton production during the Middle Eocene Climatic Optimum (ODP Site 1051, western North Atlantic)

Witkowski, Jakub; Edgar, Kirsty M; Bohaty, Steven; Harwood, David

DOI:

[10.1016/j.marmicro.2014.01.001](https://doi.org/10.1016/j.marmicro.2014.01.001)

License:

Creative Commons: Attribution-NonCommercial-NoDerivs (CC BY-NC-ND)

Document Version

Peer reviewed version

Citation for published version (Harvard):

Witkowski, J, Edgar, KM, Bohaty, S & Harwood, D 2014, 'Rapid fluctuations in mid-latitude siliceous plankton production during the Middle Eocene Climatic Optimum (ODP Site 1051, western North Atlantic)', *Marine Micropalaeontology*, vol. 106, pp. 110-129. <https://doi.org/10.1016/j.marmicro.2014.01.001>

[Link to publication on Research at Birmingham portal](#)

Publisher Rights Statement:

Published as above, final version of record available at <https://doi.org/10.1016/j.marmicro.2014.01.001>.

Checked 15/5/18

General rights

Unless a licence is specified above, all rights (including copyright and moral rights) in this document are retained by the authors and/or the copyright holders. The express permission of the copyright holder must be obtained for any use of this material other than for purposes permitted by law.

- Users may freely distribute the URL that is used to identify this publication.
- Users may download and/or print one copy of the publication from the University of Birmingham research portal for the purpose of private study or non-commercial research.
- User may use extracts from the document in line with the concept of 'fair dealing' under the Copyright, Designs and Patents Act 1988 (?)
- Users may not further distribute the material nor use it for the purposes of commercial gain.

Where a licence is displayed above, please note the terms and conditions of the licence govern your use of this document.

When citing, please reference the published version.

Take down policy

While the University of Birmingham exercises care and attention in making items available there are rare occasions when an item has been uploaded in error or has been deemed to be commercially or otherwise sensitive.

If you believe that this is the case for this document, please contact UBIRA@lists.bham.ac.uk providing details and we will remove access to the work immediately and investigate.

Rapid fluctuations in mid-latitude siliceous plankton production during the Middle Eocene Climatic Optimum (ODP Site 1051, western North Atlantic)

Jakub Witkowski^a, Steven M. Bohaty^b, Kirsty M. Edgar^c, David M. Harwood^d

^a Geology and Palaeogeography Unit, Faculty of Earth Sciences, University of Szczecin, ul. Mickiewicza 18, 70-383 Szczecin, Poland; Corresponding author: jakub.witkowski@univ.szczecin.pl

^b Ocean and Earth Science, University of Southampton, National Oceanography Centre, Southampton, SO14 3ZH, UK; e-mail address: S.Bohaty@noc.soton.ac.uk

^c School of Earth and Ocean Sciences, Cardiff University, Cardiff, CF10 3AT, UK; e-mail address: edgark1@cf.ac.uk

^d Department of Earth and Atmospheric Sciences, University of Nebraska-Lincoln, Lincoln, NE 68588-0340, USA; e-mail address: ddharwood1@unl.edu

Abstract

The Middle Eocene Climatic Optimum (MECO; ~40 million years ago [Ma]) is one of the most prominent transient global warming events in the Paleogene. Although the event is well documented in geochemical and isotopic proxy records at many locations, the marine biotic response to the MECO remains poorly constrained. We present new high-resolution, quantitative records of siliceous microplankton assemblages from the MECO interval of Ocean Drilling Program (ODP) Site 1051 in the subtropical western North Atlantic Ocean, which are interpreted in the context of published foraminiferal and bulk carbonate stable isotope ($\delta^{18}\text{O}$ and $\delta^{13}\text{C}$) records. High diatom, radiolarian and silicoflagellate accumulation rates between 40.5 and 40.0 Ma are interpreted to reflect a ~500 thousand year (kyr) interval of increased nutrient supply and resultant surface-water eutrophication that was associated with elevated sea-surface temperatures during the prolonged onset of the MECO. Relatively low pelagic siliceous phytoplankton sedimentation accompanied the peak MECO warming interval and the termination of the MECO during a ~70 kyr interval centered at ~40.0 Ma. Following the termination of the MECO, a ~200-kyr episode of increased siliceous plankton abundance indicates enhanced nutrient levels between ~39.9 and 39.7 Ma. Throughout the Site 1051 record, abundance and accumulation rate fluctuations in neritic diatom taxa are

similar to the trends observed in pelagic taxa, implying either similar controls on diatom production in the neritic and pelagic zones of the western North Atlantic or fluctuations in sea level and/or shelf accommodation on the North American continental margin to the west of Site 1051. These results, combined with published records based on multiple proxies, indicate a geographically diverse pattern of surface ocean primary production changes across the MECO. Notably, however, increased biosiliceous accumulation is recorded at both ODP Sites 1051 and 748 (Southern Ocean) in response to MECO warming. This may suggest that increased biosiliceous sediment accumulation, if indeed a widespread phenomenon, resulted from higher continental silicate weathering rates and an increase in silicic acid supply to the oceans over several 100 kyrs during the MECO.

Key words: Eocene; North Atlantic; Blake Nose; Middle Eocene Climatic Optimum; diatoms; siliceous microfossils, Ocean Drilling Program

1. Introduction

The Middle Eocene Climatic Optimum (MECO) is a global transient warming phase that occurred ~40 million years ago (Ma) (Bohaty and Zachos, 2003; Bohaty et al., 2009) and temporarily reversed the long-term early–middle Eocene cooling trend (Zachos et al., 2001, 2008; Cramer et al., 2009) for ~500–750 thousand years (kyr) (Bohaty et al., 2009; Edgar et al., 2010). MECO warming is interpreted to have begun gradually in response to rising levels of atmospheric CO₂ (Bijl et al., 2010). This phase of greenhouse warming terminated abruptly at ~40 Ma, perhaps facilitated by enhanced organic carbon burial (Spofforth et al., 2010). High-latitude surface- and deep-water warming of ~4–6° has been interpreted from foraminiferal stable isotope and organic geochemical proxies (Bohaty et al., 2009; Bijl et al., 2010), and profound biotic changes have been documented in conjunction with MECO warming (e.g., Luciani et al., 2010; Edgar et al., 2010, 2013; Toffanin et al., 2011; Witkowski et al., 2012; Boscolo Galazzo et al., 2013). Recent modeling efforts (Sluijs et al., 2013) indicate that the MECO poses a major challenge to the established understanding of the carbon cycle variations operating on intermediate (100–500 kyr) timescales. Further insight into the nature of this prominent warming event will therefore improve our understanding of Paleogene ocean–atmosphere–biosphere interactions, as well as associated feedbacks that influenced climate change in the geological past. Of particular interest for the MECO event are links between surface-ocean primary production and carbon sequestration, which may

provide clues, for example, to the mechanisms driving global temperature change during the event.

Siliceous microplankton are ubiquitous in marine environments and play a key role in marine primary production and carbon export. Several of the major siliceous groups, including diatoms and radiolarians, are characterized by an extensive fossil record and are widely used in paleoceanographic and paleoenvironmental reconstructions (e.g., Hollis et al., 1995; Stickley et al., 2008; Davies et al., 2009; Jordan and Stickley, 2010). However, there are relatively few paleoceanographic studies of diatoms in Paleogene successions compared to other microfossil groups (e.g., foraminifera, dinoflagellates, calcareous nannofossils), mainly due to the sensitivity of the opaline frustules of diatoms to post-depositional diagenetic alteration. Yet, quantitative studies of diatoms from well-dated deep-sea successions are crucial for developing new productivity, temperature and salinity proxies for the Paleogene, and further development of high-resolution diatom assemblage records will aid in refinement of biostratigraphic zonations. Given the importance of diatoms in primary production, elemental cycling, and carbon export and burial in the modern oceans (Ragueneau et al., 2000; Tréguer and De La Rocha, 2013), an understanding of diatom response to past climate perturbations may also help to predict and model future changes in the climate–ocean system.

Drillcores recovered during Ocean Drilling Program (ODP) Leg 171B contain an expanded record of Paleogene climate variability (e.g., Bains et al., 1999; Wade and Kroon, 2002), and a thick, middle Eocene section of siliceous nannofossil ooze spanning Chron C18, during which the MECO event occurred, was obtained at ODP Site 1051 (Shipboard Scientific Party, 1998a). The Site 1051 cores therefore provide an opportunity to apply existing diatom paleoecological tools to further elucidate paleoceanographic variability during the MECO (Bohaty et al., 2009; Edgar et al., 2010), as well as refine siliceous microfossil paleoenvironmental proxies through comparison with foraminiferal datasets.

The specific goals of this study were to: (1) generate detailed siliceous microfossil assemblage records across a ~2.6 million year (myr) interval spanning the MECO event; (2) interpret assemblage changes in the context of published foraminiferal and bulk carbonate stable isotope ($\delta^{13}\text{C}$, $\delta^{18}\text{O}$) records and planktic foraminiferal assemblage records; (3) reconstruct the paleoenvironmental setting in which siliceous nannofossil ooze and chalk were deposited at Site 1051; and (4) use the siliceous microfossil data from Site 1051 to assess changes in subtropical siliceous plankton production in a regional and global context.

2. Materials and methods

2.1. Geological setting and site location

ODP Site 1051 (30°03'N, 76°21'W) was drilled on Blake Nose, an eastward projection of the Blake Plateau, in the western subtropical North Atlantic Ocean (Fig. 1). Two holes (1051A and 1051B) were drilled at a water depth of ~1980 m (Shipboard Scientific Party, 1998a). A 630-m thick Paleogene succession was recovered at Site 1051, including a ~370-m thick middle Eocene interval characterized by high sedimentation rates (~4 cm/kyr) relative to many other pelagic deep-sea sections spanning this time interval (Edgar et al., 2010). A well-constrained magnetobiostratigraphic age model is available for the middle Eocene section of Site 1051 (Ogg and Bardot, 2001; Edgar et al., 2010). The paleodepth for Site 1051 during the late Paleocene through middle Eocene interval is estimated at ~1000–2000 m (Shipboard Scientific Party, 1998a).

The middle Eocene interval recovered at Site 1051 between 161.9 and 61.7 meters composite depth (mcd) was selected for this study. Within this interval, the dominant lithology is siliceous nannofossil ooze, which grades downhole into siliceous nannofossil chalk at ~148.5 mcd. With the exception of one poorly recovered core (Core 1051B-10H), drilling disturbance is generally minor within the advanced piston-cored (APC) ooze-dominated interval. However, the chalk-dominated interval below ~148.5 mcd was cored using the rotary extended core barrel (XCB) system and is moderately disturbed from the drilling process (Shipboard Scientific Party, 1998a; Fig. 2).

2.2. Biostratigraphy and age model

Although diatoms generally occur in high abundance in the upper middle Eocene section of Site 1051, the number of diatom bioevents is insufficient to provide reliable high-resolution age control. Instead, magnetostratigraphy combined with calcareous nannofossil and planktic foraminiferal biostratigraphy (Fig. 2g) provides the primary means of age control for the Eocene section of Site 1051 (Shipboard Scientific Party, 1998a; Mita, 2001; Ogg and Bardot, 2001; Edgar et al., 2010). We utilize the magnetobiostratigraphic age model recently developed by Edgar et al. (2010), and, using this age model, our study interval spans a ~2.6 myr interval between 42.1 and 39.5 Ma. However, because of significant biscuiting of the sediment below ~148.5 mcd (~41.7 Ma), we focus our high-resolution analyses on the interval above this level (Fig. 2). In order to enable direct correlation of our results to other published

records, all ages in this paper are reported relative to the timescale of Cande and Kent (1995), but additional age axes calibrated to the GTS2012 timescale (Gradstein et al., 2012) are also provided for reference in the relevant figures.

2.3. Sample collection and processing

In total, 175 samples from the shipboard splice of Holes 1051A and 1051B were examined for siliceous microfossils in this study (Shipboard Scientific Party, 1998a; Fig. S1c). An initial pilot study was performed at a stratigraphic resolution of 60–150 cm, but the sampling interval was subsequently decreased to 10–30 cm spacing between 106.2 and 73.1 mcd where the largest variations in siliceous microfossil assemblages were observed in the pilot results (Fig. 2b). Sample treatment methods and preparation of permanent slides followed Witkowski et al. (2012). The only modification to this methodology was that samples were not heated during H₂O₂ treatment because their low organic matter content enabled total digestion at room temperature.

2.4. Quantitative siliceous microfossil counts

Siliceous microfossil counts were performed on two slides from each sample. At least three random traverses across the coverslip were made at ×1000 magnification. For samples with low siliceous microfossil abundance, at least 100 siliceous microfossils were counted in multiple traverses. On average, ~200 siliceous microfossils were counted on each slide. Diatoms, silicoflagellates, ebridians, siliceous dinoflagellates and synurophyte scales were identified to species level and counted following the method outlined by Schrader and Gersonde (1978). Radiolarians and chrysophyte cysts were also counted, but not identified. The technique for absolute siliceous microfossil abundance estimation follows the random settling method modification used by Witkowski et al. (2012). Range charts for all of the siliceous microfossil groups identified in this study are available in the online Supplementary Materials section (Tables S1–S2). Taxonomic references are provided in Tables S3–S5.

2.5. Paleoecological assignments

This study is based on both autotrophic and heterotrophic siliceous microplankton groups. Diatoms, silicoflagellates, synurophytes and chrysophytes are photosynthetic algal groups (Tappan, 1980; Andersen, 1987; Round et al., 1990). The nutrition of the siliceous motile, thecate dinoflagellate *Peridinites* (Harding and Lewis, 1994) is unknown, but fossil actiniscidians (e.g., *Carduifolia*) were likely naked, heterotrophic forms with internal spicular

skeletons (Preisig, 1994). Although radiolarians display several feeding strategies, they are generally considered heterotrophic (Matsuoka, 2007); both heterotrophic and mixotrophic behavior is reported for ebridians (Witkowski et al., 2012).

Most of the diatom taxa recorded in this study are extinct, thus detailed paleoecological classification is challenging. To distinguish pelagic and neritic groups, we considered the global paleobiogeographic distribution of taxa, morphological features, and comparison to extant relatives, where applicable. Lists of diatom taxa and their inferred paleoecology are provided in Tables S3–S5 in the online Supplementary Materials, and paleobiogeographic data from the published literature are compiled in Tables S6–S15.

2.6. Sediment density and accumulation rate calculations

Accumulation rate estimates account both for changes in bulk sedimentation rate and dilution by other sedimentary components (biogenic and non-biogenic), and thus provide a more accurate measure of changes in sedimentation through time than variations in the absolute abundance of microfossils. Sediment density and linear sedimentation rates (LSRs) are required to calculate sediment accumulation rates. In pelagic settings such as Site 1051 where silt and clay input is limited, variation in sediment density primarily reflects variations in the relative concentration of CaCO_3 and SiO_2 , and thus can be used as an indirect proxy for biogenic opal concentration (Weber, 1998). In the Site 1051 study interval, high-resolution wet bulk density data, determined using the gamma ray attenuation porosity evaluator (GRAPE) method, correlate well with discrete dry bulk density (DBD) measurements made during routine shipboard analysis (Shipboard Scientific Party, 1998a). Therefore, it is possible to estimate DBD at high resolution by calibrating the GRAPE record with the discrete DBD data (Fig. S2). Total siliceous microfossil, diatom, silicoflagellate and radiolarian accumulation rates were calculated using these high-resolution DBD estimates and the LSRs derived from the Edgar et al. (2010) age model.

2.7. Stable isotope records

In order to explore the possible links between surface-ocean primary production and late middle Eocene greenhouse warming at Site 1051, siliceous microfossil assemblage changes are interpreted in the context of published stable isotope records ($\delta^{18}\text{O}$, $\delta^{13}\text{C}$) (Bohaty et al., 2009; Edgar et al., 2010). The abundance of benthic foraminifera is low within the MECO interval of Site 1051, hindering development of a high-resolution stable isotope stratigraphy

(Edgar et al., 2010). However, a high-resolution bulk-sediment stable isotope record is available across our study interval (Bohaty et al., 2009; Fig. 2e-f), which provides a surface-water signal from calcareous nannofossils—the dominant sedimentary component of Eocene sediments at Site 1051 (Shipboard Scientific Party, 1998a). In comparison of planktic foraminiferal and fine-fraction stable isotope records in Miocene pelagic sediments, Ennyu et al. (2002) inferred that the fine-fraction (calcareous nannofossil) stable isotope records are strongly influenced by the season of calcification, and likely reflect blooms during periods of deep mixing in the late winter or early spring characterized by cool, high-nutrient conditions. Therefore, the bulk stable isotope signals at Site 1051 may be similarly biased towards cool conditions that are not representative of summer sea-surface temperatures. This may explain why, for instance, the bulk and benthic $\delta^{18}\text{O}$ values overlap in some intervals of the Site 1051 study section (Fig. S1a), although vital-effect offsets or diagenetic alteration also cannot be ruled out. The trends and relative changes, however, are similar between the bulk $\delta^{18}\text{O}$ record and the lower-resolution benthic foraminiferal $\delta^{18}\text{O}$ record (Fig. 2e-f), providing parallel indications of relative temperature change.

3. Results

3.1. Siliceous microfossil abundance

Siliceous microfossils are present throughout the Site 1051 study interval, and a diverse range of siliceous microfossil groups was identified, including diatoms (average ~73% of the total siliceous microfossil assemblage), radiolarians (~24%), ebridians (~0.8%), silicoflagellates (~0.1%), and chrysophyte cysts, siliceous dinoflagellates, and synurophyte scales (~2.1% of the assemblage combined) (Fig. 2a). Taxonomic lists of all siliceous microfossil taxa identified in this study are presented in Tables 1-3. The absolute total siliceous microfossil (TSM) abundance is relatively low ($\sim 2.6 \times 10^6$ siliceous microfossils per gram of sediment [g^{-1}] on average) and shows little variability below the MECO between ~148.5 and 106.2 mcd, and above the MECO interval between 73.2 and 61.7 mcd (Fig. 2b). A broad interval of elevated TSM abundance, with two maxima, is recorded between 106.2 and 73.2 mcd—here defined as 'TSM Maximum 1' and 'TSM Maximum 2.' Within TSM Maximum 1, between 106.2 and 86.3 mcd, and TSM Maximum 2 between ~83.0 and 73.2 mcd, TSM abundance exceeds $\sim 9 \times 10^6 \text{ g}^{-1}$ (Fig. 2b). TSM Maximum 1 is associated with decreases in bulk and benthic $\delta^{18}\text{O}$ values and bulk $\delta^{13}\text{C}$ values (Fig. 2e-f), whereas TSM maximum 2 is associated with an increase in bulk $\delta^{13}\text{C}$ and a short-lived decrease in bulk $\delta^{18}\text{O}$ values at 79.5 mcd (Figs.

2b, e-f). TSM abundance decreases to minimum values between the two TSM maxima (Fig. 2b), coincident with the interval of the lowest bulk and benthic $\delta^{18}\text{O}$ and $\delta^{13}\text{C}$ values and a sharp $\sim 1\text{‰}$ positive shift in both bulk and benthic $\delta^{18}\text{O}$ and $\delta^{13}\text{C}$ values at 83.9 mcd (Fig. 2e-f).

3.2. Diatoms

A total of ~ 150 diatom taxa were identified in Site 1051 samples (Table 1). Neritic taxa comprise $\sim 78\%$ of the diatom assemblage while pelagic forms and resting spores account for $\sim 13\%$ and $\sim 5\%$, respectively (Fig. 2c-d). The paleoecological associations of $\sim 4\%$ of the diatom assemblage are uncertain due to provisional identifications (tabulated as ‘Unidentified diatoms, vegetative valves’ in Table S1) and thus are not discussed further (Fig. 2c). Trends in diatom absolute abundance parallel variations in TSM abundance, as expected given the dominance of diatoms in the siliceous microfossil assemblages (Fig. 2a-b, d).

The most abundant neritic diatom taxa present at Site 1051 are *Paralia* spp. (Pl. I, Figs. 9-10), *Pseudopodosira* spp. (Pl. I, Fig. 8), *Rutilaria* spp., and *Rhaphoneis* spp. (Pl. I, Fig. 1). *Pseudopodosira* spp. are more abundant than *Paralia* spp. between 148.5 and 102.1 mcd and between 83.92 mcd and the top of the study interval at 61.7 mcd (Fig. 3a). However, there is a transient interval of increased relative abundance of *Paralia* between 102.1 and 83.9 mcd (Fig. 3a).

Among the pelagic diatoms (Fig. 3b), the most abundant taxa are *Distephanosira* spp. (Pl. I, Figs. 17-18), *Hemiaulus* spp. (Pl. I, Figs. 12-13), *Rocella praeinitida* (Pl. I, Fig. 20), *Triceratium inconspicuum* (Pl. I, Figs. 14-15) and *Coscinodiscus decrescens* (Pl. I, Fig. 16). A distinct increase in the relative abundance of *T. inconspicuum* occurs between 106.2 and 86.3 mcd ($\sim 15.5\%$ on average, Fig. 3b). *Rocella praeinitida* is moderately abundant between 148.5 and 106.2 mcd ($\sim 7.6\%$), but its abundance gradually diminishes and shows an abrupt decline at 86.3 mcd (Fig. 3b). The abundance of *Hemiaulus* spp. (predominantly *H. polycystinorum* var. *mesolepta*, Fig. 3c) varies considerably throughout the study section, averaging $\sim 15.0\%$ of the pelagic diatom assemblage between 148.5 and 106.2 mcd, $\sim 32.0\%$ between 86.3 and 83.0 mcd, and $\sim 23.5\%$ between 83.0 and 61.7 mcd (Fig. 3b). The relative abundance of *Distephanosira* is high throughout the study interval ($>55\%$; Fig. 3b), with only a transient decrease to $\sim 14.3\%$ between 86.3 and 83.0 mcd (Fig. 3b). This interval of low *Distephanosira* abundance is characterized by high relative abundance of *C. decrescens* (up to $\sim 29.7\%$; Fig. 3b).

The diatom resting spore assemblages are represented by only a few taxa, with *Pterotheca* (Pl. I, Fig. 23), *Quadrocistella* (Pl. I, Fig. 22), and *Xanthiopyxis* (Pl. I, Fig. 21) as the dominant genera. Although there are large variations in the relative abundance of resting spore taxa in the lower part of the section, the assemblage is dominated by *Xanthiopyxis* below 106.2 mcd, *Quadrocistella* between 106.2 and 86.3 mcd, and *Pterotheca* above 83.0 mcd (Fig. 3d). Between 86.3 and 83.0 mcd, there are rapid variations in resting spore abundance, and, within a narrow interval at 84.2 mcd, *Xanthiopyxis* accounts for 100% of the resting spore assemblage (Fig. 3d).

3.3. Other siliceous microfossil groups

Previous studies reported diverse and well-preserved middle Eocene radiolarian assemblages from Site 1051 (Shipboard Scientific Party, 1998a; Sanfilippo and Blome, 2001). Radiolarians comprise ~23% of the siliceous microfossil assemblage on average throughout the study interval, with the exception of a large increase in their relative abundance between 87.2 and 83.0 mcd (up to ~60%). This interval is coincident with a minimum in diatom abundance (Fig. 2a-b, Fig. S3a).

Throughout the study section, the abundances of silicoflagellates (Pl. II, Figs. 1-2), ebridians (Pl. II, Figs 3, 6-7), chrysophyte cysts (Pl. II, Figs 4-5), siliceous dinoflagellates (Pl. II, Figs. 8-9) and synurophyte scales (Pl. II, Figs 10-12) are generally low (Figs. S3b-S4). All of these groups, however, display similar trends to those observed in the diatom record, with elevated abundances between 106.2 and 86.3 mcd and between 83.0 and 73.2 mcd (Figs. S3b-S4).

3.4. Sediment density and accumulation rates

There is an up-section decrease in sediment density beginning at ~110 mcd with a transient minimum at ~85.8 mcd, where sediment density values reach as low as ~1.6 g/cm³ (Fig. S5a). A decrease in sediment density is indicative of increasing biogenic opal content (Weber, 1998), which is consistent with our newly developed TSM record prior to the peak of TSM Maximum 1 at 93.4 mcd. Within the uppermost interval of the MECO, however, the sediment density record is likely biased by high radiolarian concentrations, perhaps due to the large size and high porosity of radiolarian tests (Fig. S5a-b). These observations support the use of sediment density as an indicator of sediment composition, but also demonstrate that detailed microfossil assemblage records are necessary to aid the interpretation of GRAPE and DBD data.

Assessment of accumulation rates requires switching from the depth to age domain, which will be discussed from this point onwards. It should be noted that because of the low number of age control tie points in the available age model, the accumulation rate calculations presented here are approximate and likely average out short-term changes. Despite this caveat, elevated TSM accumulation rates are correlative with TSM maxima (Fig. S5d), suggesting that TSM abundance variations reflect pronounced changes in siliceous plankton production and sedimentation in the pelagic zone of the western North Atlantic Ocean (see further discussion in Section 5.1). Separate accumulation rate calculations were also made for total diatoms, neritic diatoms, pelagic diatoms, and resting spores (Fig. S5e), as well as for radiolarians and silicoflagellates (Fig. S5f-g). With the exception of radiolarians, accumulation rate changes for each of these groups parallel the overall trends in TSM fluxes.

4. Interpretation

4.1. Diatom preservation

The high alkalinity of pore-waters in carbonate-rich sediments tends to facilitate biogenic opal dissolution (Flower, 1993). For instance, diatom valves in middle Eocene sediments from Site 1051 commonly lack the most delicate parts of the valves, e.g., pore fields or areolae occlusions (Fig. S6c-e). However, *Liostephanina* (Pl. I, Fig. 19), internal casts of diatoms regarded as indicators of enhanced dissolution (e.g., Hanna and Brigger, 1970) are sparse at Site 1051. Therefore, we interpret an overall moderate level of diatom dissolution across the entire study interval. Breakage is more common than dissolution at Site 1051, which most likely resulted from the offshore transport of neritic diatoms and a high degree of sediment bioturbation (Shipboard Scientific Party, 1998a).

Neritic diatoms are typically more heavily silicified than pelagic taxa, and their dominance throughout the study section is at least in part affected by preferential dissolution of pelagic taxa in the water column and on the seafloor. However, neritic diatoms consistently show poor-to-moderate preservation, while pelagic diatoms and resting spores identified tend to be moderately to well-preserved throughout the study interval. This suggests that there are no major temporal changes in siliceous microfossil preservation, and that diagenetic alteration is approximately uniform throughout the section. Thus, we interpret the intervals of elevated siliceous microfossil abundance and flux at Site 1051 to reflect primary changes in siliceous microfossil production and sedimentation in the western North Atlantic Ocean across the MECO, rather than secondary processes such as post-burial diagenesis.

4.2. Diatom paleoecology

Diatom-based paleoreconstructions commonly assume that all of the diatom assemblage is composed of *in situ* valves. Whereas such assumption is justified in studies on distal successions (e.g., Davies et al., 2009), diatom assemblages from more proximal localities, like ODP Sites 1051 or 1260 (Renaudie et al., 2010) (Fig. 1) need to be interpreted cautiously, as not all diatoms are well-suited for being indicators of open-ocean surface water conditions. Furthermore, our understanding of diatom paleoecology is often insufficient, which considerably reduces the paleoceanographic utility of early Paleogene diatoms. Based on the available paleobiogeographic, morphological, and ecological data, we provide a discussion below regarding the paleoecological preferences of the key diatom taxa observed in the Site 1051 study interval. These paleoecological inferences provide a basis for further paleoceanographic interpretation of the records.

Distephanosira architecturalis is one of the most common diatoms worldwide in middle-to-late Eocene sections. A compilation of published records (Tables S6-S7) indicates that this taxon had a cosmopolitan distribution in coastal, neritic and pelagic sites throughout its stratigraphic range (Fig. 4a). Careful examination of morphological features (Fig. S6a-b) reveals a special adaptation for a planktic mode of life in the form of an empty chamber within the valve, presumably to increase buoyancy. Similarly, *T. inconspicuum* is common in both neritic and pelagic middle Eocene sediments (Tables S8-S9), which indicates a planktic mode of life (Fig. 4b). Despite the scarcity of reports of *H. polycystinorum* var. *mesolepta* and *C. decrescens* in the literature (Tables S10-S13), the cosmopolitan distribution of these species (Fig. 5a-b), including numerous pelagic sites, strongly suggests a preference for an open-marine habitat. *Rocella praenitida* is absent from the Eocene-Oligocene intervals of tropical sites (Tables S14-S15), but it has a broad distribution in mid- and high-latitude Atlantic Ocean and at several Southern Ocean sites, which corroborates its pelagic affinity (Fig. 5c). Based on these lines of reasoning, we regard the taxa assigned here as pelagic diatoms as representative of the paleoenvironmental conditions in the photic zone above Site 1051 in the pelagic western mid-latitude Atlantic Ocean. Thus, variations in abundance and assemblage structure of these pelagic diatoms (Fig. 3b) are used to infer changes in local siliceous microfossil production and surface-ocean hydrography.

The diatom assemblage at Site 1051 includes a number of heavily silicified, chain-forming taxa, including, *Paralia*, *Pseudopodosira*, and *Rutilaria*. A neritic paleoecology for these

genera is inferred primarily by comparison to the environmental preferences of extant taxa (e.g., Ross, 1995; McQuoid and Nordberg, 2003). Given the distribution of *Paralia* in the modern oceans, where it is restricted to littoral waters (e.g., Sawai et al., 2005; Gebühr et al., 2009), we infer that it is unlikely that Paleogene species of *Paralia* had a pelagic affinity. Even early in its evolutionary history in the Cretaceous, *Paralia* was common in neritic environments (e.g., Canadian Margin, see Witkowski et al., 2011), and absent from pelagic settings (e.g., CESAR-6 drillcore; Davies et al., 2009). As a tychoplanktic diatom, *Paralia* can be transported over large distances, but its heavy silicification makes it primarily a neritic form (Round et al., 1990).

The high abundance of neritic diatoms at Site 1051 (Figs. 2c-d) conflicts with the interpreted pelagic setting of this site during the middle Eocene, inferred mainly from sediment lithology (carbonate-rich oozes with low siliciclastic content), deep outer slope position on Blake Nose, and high abundance of planktic relative to benthic foraminifera (Shipboard Scientific Party, 1998a). Thus, the neritic diatoms deposited at Site 1051 are allochthonous and were transported from the adjacent shelf environments located to the west of Blake Plateau during the middle Eocene (see paleogeographic reconstruction in Galloway et al., 2011). The high abundance of tychoplanktic and neritic planktic taxa implies intense lateral transport by surface currents (e.g., Martin, 2003), and the presence of benthic diatoms such as *Actinoptychus*, *Diplomenora*, *Mastogloia* and *Rhaphoneis* (Table S3; see Pl. I, Figs. 1-5) also indicates the role of bottom currents in transporting diatoms downslope from the shelf to Site 1051 (e.g., Kennett, 1982; see also Fenner and Hoff, 2011). Based on the absence of diatom zonal marker species that were extinct by the late middle Eocene (e.g., *Triceratium kanayae*, *Pyrgopyxis caput-avis*; see Fenner, 1985), we think it unlikely that erosion and reworking of older strata provided the source of neritic diatoms recorded at Site 1051, and assume that the allochthonous diatoms are contemporaneous with the pelagic deposition at this site. Dinocyst assemblages at ODP Site 1053 (paleodepth: 500-700 m; Shipboard Scientific Party, 1998b) (Fig. 1) also show a high percentage of transported neritic forms (van Mourik et al., 2001). Site 1053, spanning magnetochrons C17r through C13r (mid- to late Eocene; Shipboard Scientific Party, 1998b) is more proximal, and is located at a shallower water depth than Site 1051. However, the high abundance of neritic dinocysts at Site 1053 corroborates persistent transport of shelf-dwelling microplankton from the North American continental margin in the Blake Nose area. Finally, the presence of allochthonous neritic diatoms and dinocysts in pelagic sediments at the Blake Nose indicates that other sedimentary components and

microfossil groups may also be displaced from the adjacent shelf environments, although to date no direct evidence of transport from the shelf has been reported, e.g., in the foraminiferal or calcareous nannofossil assemblage records.

Some of the most abundant resting spore taxa at Site 1051, such as *Quadrocistella* and *Xanthiopyxis* (Fig. 3d), were likely produced by the planktic genus *Chaetoceros* (Suto, 2004, 2006). In the modern oceans, *Chaetoceros* is common in the neritic plankton (e.g., Hernández-Becerril, 1996; Hasle and Syvertsen, 1997), but pelagic species are also known (e.g., Aizawa et al., 2005). *Pterotheca* is also present in high abundance at Site 1051 (Fig. 3d); this taxon is common in neritic settings from the Cretaceous onward, but its corresponding vegetative valves have not been determined (Suto et al., 2009). Therefore, based on both possible neritic and pelagic paleoecological associations of the resting spore taxa recorded in this study, the resting spores were either part of neritic plankton communities that were transported to the open ocean, or they were produced and deposited in the pelagic zone in close proximity to Site 1051. Changes in the abundance of resting spore taxa may provide only indirect evidence for nutrient or stratification changes in surface waters either locally or in nearby shelf environments across the MECO, because their provenance is uncertain.

4.3. Succession of diatom assemblages

Based on the changes in relative abundance of neritic, pelagic and resting spore taxa, four diatom assemblage zones are distinguished at Site 1051 (Figs. 3, 6, Table 4):

(1) **Assemblage Zone I** (41.68–40.52 Ma) is characterized by higher abundances of *Pseudopodosira* than *Paralia* (Fig. 3a), generally higher abundances of *R. praenitida* than *T. inconspicuum* (Fig. 3b), and the dominance of *Xanthiopyxis* among the resting spores (Fig. 3d).

(2) In **Assemblage Zone II** (40.52–40.06 Ma), *Paralia* is more abundant than *Pseudopodosira* (Fig. 3a), *T. inconspicuum* occurs in higher abundance than *R. praenitida* (Fig. 3b), *H. polycystinorum* var. *mesolepta* is the dominant species of *Hemiaulus* (Fig. 3c), and *Quadrocistella* is the dominant resting spore genus (Fig. 3d).

(3) In **Assemblage Zone III** (40.06–39.98 Ma), *Paralia* and *Pseudopodosira* are present in approximately equal abundance (Fig. 3a), *Hemiaulus* replaces *Distephanosira* as the most abundant pelagic form (Fig. 3b), and there is a high percentage of *C. decrescens* present (Figs.

3b). Among resting spores, the abundance of *Pterotheca* and *Xanthiopyxis* is highly variable (Fig. 3d).

(4) **Assemblage Zone IV** (39.98–39.50 Ma) is characterized by abundant *Pseudopodosira* (Fig. 3a). Secondly, among the pelagic diatoms, there is also a high abundance of *Distephanosira* in this zone (Fig. 3b), and *H. polycystinorum* var. *mesolepta* is less abundant than other *Hemiaulus* spp. (Fig. 3c). The dominant resting spore is *Pterotheca* spp. (Fig. 3d).

The diatom assemblage zones defined here correspond to four distinct stages of sea-surface temperature (SST) evolution evidenced by benthic foraminiferal and bulk $\delta^{18}\text{O}$ records (Fig. 6): Stage I includes the terminal phase of pre-MECO cooling (41.68–40.52 Ma); Stage II encompasses the prolonged onset of MECO warming (40.52–40.06 Ma); Stage III is a short interval spanning peak MECO warming and termination (40.06–39.98 Ma); and Stage IV spans the post-MECO cooling interval (39.98–39.50 Ma).

4.4. Temperature and nutrient level changes

Surface-to-deep $\delta^{13}\text{C}$ gradients ($\Delta\delta^{13}\text{C}_{\text{bulk carbonate-benthic}}$) are generally stable throughout Stage I and diatom flux is consistently low (Fig. 6a, g), implying no significant changes in phytoplankton production during this interval. There is also minimal bulk and benthic $\delta^{18}\text{O}$ variation between 41.68 and 40.80 Ma, further indicating no significant temperature change in surface or deep waters. The gradual onset of MECO warming is suggested by the progressive decrease in bulk $\delta^{18}\text{O}$ values starting at ~40.80 Ma (Fig. 6e). However, there is no apparent response to the interpreted onset of warming in the siliceous microfossil record (Fig. 6a-b), which may suggest that SST warming was not associated with concomitant changes in nutrient levels and/or pelagic siliceous plankton production—reflecting either a low sensitivity or a small degree of environmental change at this time. In contrast, the thermophilic planktic foraminiferal genus *Morozovelloides* does increase in abundance synchronously with the onset of warming indicated by the $\delta^{18}\text{O}$ records (Fig. 6d), perhaps implying a greater temperature sensitivity of foraminifera than siliceous microfossils. Surface waters over Site 1051 were more oligotrophic prior to than during the MECO based on the low flux of pelagic diatoms and silicoflagellates in Stage I (Fig. 6a-b). This interpretation is consistent with the high relative abundances of warm-water favoring, photosymbiotic taxa (e.g., *Acarinina* and *Morozovelloides*; Edgar et al., 2013) in planktic foraminiferal assemblages (Fig. 6c). The relatively high flux of neritic diatoms during Stage I also implies continuous transport of diatoms to Site 1051 by surface and bottom currents (Figs. 6a, 7a).

A pronounced increase in pelagic diatom flux at the beginning of Stage II (Figs. 6a, 7b) points to an increase in primary production in surface waters over Site 1051. The onset of this trend (~40.52 Ma) is coeval with the initiation of the MECO at other sites as identified by Bohaty et al. (2009), but postdates the gradual onset of warming at Site 1051. This increase in primary production is associated with continued surface and deep-water warming interpreted from decreasing bulk and benthic $\delta^{18}\text{O}$ values (Fig. 6e). Eutrophication of surface waters is supported by relative decreases in the inferred warm, oligotrophic surface-dweller *Acarinina* (Fig. 6c; Edgar et al., 2013). There is also an associated decrease in the $\Delta\delta^{13}\text{C}_{\text{bulk carbonate-benthic}}$ gradient in this interval, with values approaching 0 (Fig. 6g), which could be interpreted to indicate a decline in export production or a decrease in nutrient utilization in the photic zone. However, compelling evidence for increased surface-water nutrient levels from multiple marine plankton groups argues against either of these alternative scenarios. Despite the evidence for continued increase in nutrient levels, both pelagic and total diatom fluxes peak at ~40.2 Ma, and subsequently diminish (Fig. 8b). This may indicate that at this time diatoms were outcompeted by other phytoplankton, who presumably utilized the available nutrients more efficiently.

Stage III is defined by a short-lived minimum in the flux of pelagic diatoms suggesting low diatom production during peak MECO warming and subsequent cooling (Fig. 6a, 7c). However, maximum radiolarian accumulation rates also occur in this interval at 40.05 Ma (Fig. 8c). One plausible explanation for this peak in radiolarian abundance, offset ~150 kyr from the peak in total diatom flux, is that radiolarians grazed on the groups of non-siliceous phytoplankters that outcompeted diatoms during the interval of peak warming. Alternatively, the observed offset could result from increased radiolarian concentration due to winnowing. A rapid decline in radiolarian flux immediately follows this interval between 40.05 and 40.02 Ma (Fig. 6b, 8c). Together, low diatom, silicoflagellate and radiolarian flux (Fig. 6b) suggest a decrease in pelagic plankton production associated with rapid cooling (Fig. 7c). Changes in planktic foraminiferal assemblages, most notably a rapid drop in the relative abundance of the thermophilic genus *Morozovelloides* (Fig. 6d) support rapid sea-surface cooling interpreted from increasing $\delta^{18}\text{O}$ values. The $\Delta\delta^{13}\text{C}_{\text{bulk carbonate-benthic}}$ values initially increase at 40.06 Ma within Stage III (Fig. 6g), possibly indicating a transient rise in phytoplankton export production concomitant with the short-lived increase in radiolarian abundance.

At the beginning of Stage IV, pelagic diatom and silicoflagellate fluxes increase between 39.98 and 39.76 Ma, pointing to elevated nutrient levels in the surface ocean over Site 1051

(Figs. 6a-b, 7d). High flux of resting spores between 39.98 and 39.94 Ma (Fig. 6a) may suggest not only increased diatom production but also periodic stratification with nutrient depletion in the photic zone. $\Delta\delta^{13}\text{C}_{\text{bulk carbonate-benthic}}$ values increase at ~39.9 Ma (Fig. 6g), possibly indicating more efficient nutrient utilization or elevated export production in the photic zone. The onset of this trend is associated with a relatively short-lived (<100 kyr) negative excursion in bulk $\delta^{18}\text{O}$ and $\delta^{13}\text{C}$ values (Fig. 6e-f), which can be interpreted as a minor warming event within the post-MECO cooling phase, as also suggested by a transient increase in the relative abundance of *Morozovelloides* (Fig. 6d). After 39.76 Ma the diatom flux decreases, suggesting reduced nutrient availability in the surface waters at Site 1051 (Fig. 6a) and a return to baseline conditions similar to, or warmer than, those immediately prior to the MECO event (Fig. 7a, d). Similarly, planktic foraminiferal assemblages indicate a return to pre-MECO like conditions with relative increases and decreases in the percentage of *Acarinina* and *Globigerinatheka*, respectively (Fig. 6c). However, the relative abundance of the warm-water indicator species *Orbulinoides beckmanni* also diminishes through Stage IV (Fig. 6d) and may indicate SST cooling throughout this time interval (Edgar et al., 2010).

To summarize, we interpret changes in siliceous microfossil assemblages at Site 1051 as a record of rapid fluctuations in pelagic siliceous phytoplankton production (Fig. 7). Two episodes of nutrient enrichment in the surface ocean are interpreted from siliceous microfossil assemblage changes between 41.7 and 39.5 Ma: a ~460 kyr interval during the initial warming phase of the MECO (TSM Maximum 1 within Stage II), and a ~220 kyr period of nutrient enrichment within the initial post-MECO cooling phase (TSM Maximum 2 within Stage IV). The interpreted minimum in siliceous phytoplankton production between 40.06 and 39.98 Ma spans the interval of peak warming and abrupt cooling which terminated the MECO event (Fig. 8b).

5. Discussion

5.1. Planktic vs. neritic diatom paleoenvironmental signals

During initial shipboard work, the high abundance of diatoms in Eocene sediments at Site 1051 was interpreted to represent persistent high siliceous phytoplankton primary production (Shipboard Scientific Party, 1998a). In contrast, our high-resolution study shows that siliceous phytoplankton production was variable across the MECO interval. Due to a number of syn- and post-depositional processes, it is not possible to quantify past surface-water nutrient levels based on siliceous microfossil assemblage and accumulation rate variations alone. However,

biosiliceous sediments deposited under upwelling regimes typically show diatom abundance in the range of 10^9 g^{-1} (Davies et al., 2009). Maximum TSM concentration recorded here is in the range of 10^6 g^{-1} . Therefore, given the preservational issues outlined in section 4.1, we conservatively interpret our diatom records to indicate that the trophic regime at Site 1051 ranged from moderately oligotrophic to mesotrophic—an interpretation consistent with planktic foraminiferal assemblages (Shipboard Scientific Party, 1998a; Edgar et al. 2010, 2013). Thus, continuous highly eutrophic conditions with sustained high siliceous phytoplankton production in surface waters are unlikely at Site 1051 during the late middle Eocene. Furthermore, it is also apparent that multiple paleoenvironmental signals are embedded in the middle Eocene diatom record at Site 1051. Our interpretation of the siliceous plankton production changes during the MECO at Site 1051 relies mainly on the pelagic diatoms and silicoflagellates. However, the dominant component of the siliceous microfossil assemblages are neritic diatoms (Fig. 6a). Thus, an important question arises: whether the variations in neritic diatom abundance and accumulation rates can be used to interpret changes in neritic diatom production on the adjacent continental shelf located to the west of Site 1051 (see paleogeographic reconstruction in Galloway et al., 2011).

While pelagic and neritic diatom assemblages show a similar pattern of variation between 41.7 and 39.5 Ma, the abundance and flux of neritic diatoms are considerably higher than those of pelagic diatoms and resting spores (Fig. 6a). This may suggest that nutrient levels were higher in the coastal zone of the western North Atlantic than in the open ocean at Site 1051. However, the high relative abundance of neritic diatoms, and, in particular, heavily silicified tychoplanktic diatoms (*Pseudopodosira* spp. and *Paralia* spp.) may be the result of preferential dissolution of the lightly silicified pelagic diatoms. Therefore, the changes in trophic status in the neritic zone of the western North Atlantic during the MECO may have followed the same pattern as in the pelagic zone, but their magnitude cannot be quantitatively constrained based on the displaced neritic diatom assemblages.

Another plausible interpretation of the high percentage of neritic diatoms at Site 1051 is that intervals of high neritic diatom flux may reflect changes in sea level or shelf accommodation space on the adjacent North American continental margin. Recent modelling efforts (Sømme et al., 2009) indicate that continental shelves during the Paleogene were broad and relatively shallow, which enabled high sediment supply to the continental slope and basin floor. Increased sediment supply to the shelf, which should be expected during a period of a greenhouse warming because of the intensified hydrological cycle and elevated continental

weathering rates (e.g., Sluijs et al., 2013), would have further reduced shelf accommodation space, possibly leading to increased neritic diatom flux offshore. This might explain the high abundance of neritic diatoms at Site 1051 within TSM Maximum 1 during Stage II. Furthermore, a relative rise in sea level during the peak warming phase would have increased the accommodation space, and thus caused a drop in neritic diatom accumulation during Stage III. Alternatively, high flux of neritic diatoms could have been caused by relative sea level rise or an increase in shelf accommodation space which created a broader neritic zone and thus more area for shelf diatom production. Such speculations require verification by other microfossil groups and independent sea-level proxies.

Overall, we infer that the high abundance of neritic diatoms at Site 1051 resulted from sustained transport of contemporaneous shelf-derived biogenic material by both surface and bottom currents throughout the middle Eocene study interval. In addition, the diatom assemblages have been subject to a minor-to-moderate degree of preferential dissolution which likely elevated the percentages of the heavily-silicified neritic diatoms. As such, the intervals of high neritic diatom abundance may reflect elevated diatom flux resulting from higher siliceous phytoplankton production in the neritic zone of the western North Atlantic Ocean during the onset of the MECO (TSM Maximum 1), and within the early phase of post-MECO cooling (TSM Maximum 2). Alternatively, the intervals of elevated neritic diatom accumulation rates could indicate changes in shelf accommodation space and/or sea level fluctuations. Given the evidence for downslope transport provided by diatoms from Site 1051 and dinocyst assemblages from Site 1053 (van Mourik et al., 2001), future studies on the Leg 171B sites should consider possible evidence for downslope transport in paleoenvironmental interpretations derived from micropaleontological and geochemical proxies.

5.2. Integration of Site 1051 paleoproductivity signals with other MECO records

Variations in surface-ocean primary production across the MECO have been interpreted at several sites around the globe based on a variety of proxies (Fig. 9a). At ODP Site 1218 in the equatorial Pacific, biogenic opal accumulation rates are highly variable throughout the Eocene (Lyle et al., 2005) and the MECO occurs within an interval of reduced biogenic opal accumulation (Lyle et al., 2005; Fig. 9a-b)—although opal accumulation remained relatively high at this site for the entire late middle Eocene interval between ~42 and 38 Ma. Despite uncertainties in accumulation rate estimates at Site 1051 (e.g., due to the low-resolution age model and the LSRs), the record of pelagic diatom production at this site shows a different

pattern than at Site 1218, with generally low flux inferred for the period prior to 40.5 Ma, and high accumulation rates interpreted during the MECO event (Fig. 9b). These differences are likely influenced by the contrasting paleoceanographic regimes of the sites in the middle Eocene: Site 1051 was located on a mid-latitude continental slope, and thus sensitive to changes in upwelling along the North American shelf margin and the local continental hydrological cycle which influenced nutrient supply to surface waters. In contrast, Site 1218 is an equatorial, open-ocean site at a paleodepth of ~3000 m (Shipboard Scientific Party, 2002). In part because of the scarcity of deep-sea successions with well-preserved diatoms and reliable age control, the currently available datasets are insufficient to confidently speculate on global changes in biogenic silica accumulation across the MECO. These preliminary observations call for an increased effort to generate high-resolution biogenic opal records and quantitative siliceous microfossil accumulation records from other deep-sea successions, in order to provide an improved perspective on ocean fertility changes and silica cycling during the major climatic perturbations of the Paleogene.

A direct comparison of the timing of eutrophication between ODP Site 1051 and ODP Site 748 (~58°S, Kerguelen Plateau, Southern Ocean) may be complicated by a ~50 kyr misalignment of the peak of the MECO based on the current age models available for each site (Fig. S7c). The Eocene interval of Site 748 has an uninterpretable paleomagnetic signal (Roberts et al., 2003), and the age model developed by Bohaty et al. (2009) is based on correlation of stable isotope records between Site 748 and Southern Ocean ODP sites 702 (50°S, Islas Orcadas Rise, South Atlantic) and 738 (62°S, Kerguelen Plateau, Southern Ocean) that have interpretable, but not high quality, magnetostratigraphic age control. At Site 1051, the magnetostratigraphy is generally good, but a weak magnetic signal hinders confident placement of the base of Subchron C18n.2n (± 0.55 m), which is crucial for dating of the peak of the MECO (Edgar et al., 2010). Future studies of the MECO in deep-sea successions with better age control, most notably sediments recovered during Integrated Ocean Drilling Program (IODP) Expeditions 320 (equatorial Pacific) and 342 (Newfoundland margin, North Atlantic), should help to resolve this discrepancy (Fig. S7c).

Despite problems aligning the peak of the MECO, the overall trends in siliceous plankton accumulation through the MECO at Site 748 in the Southern Ocean (Witkowski et al., 2012; Fig. 9a) are similar to those observed at Site 1051. Oligotrophic surface waters are interpreted at both sites prior to the MECO, and an increase in pelagic siliceous phytoplankton production indicative of a shift to more eutrophic conditions is associated with increasing surface ocean

SSTs during the initial warming phase of the MECO at both sites (Fig. 9c). Rapid cooling following the MECO coincides with a minimum in siliceous plankton production at Site 1051 and with a decline at Site 748 (Fig. 9c). However, biotic records from the MECO intervals of Sites 748 and 1051 display considerable differences in the taxonomic composition of the assemblages (Fig. S7a-b). At Site 1051, diatoms are the dominant siliceous microfossil group, and silicoflagellates and ebridians are nearly absent (Fig. S7a-b), whereas at the Southern Ocean Site 748, silicoflagellates are the most abundant siliceous primary producer group, and ebridians and radiolarians make up the bulk of the siliceous microfossil assemblage (Fig. S7a-b). Furthermore, a post-MECO (~39.9-39.7 Ma) increase in biosiliceous productivity (roughly equivalent to the peak flux during the MECO) is recorded at Site 1051 in the Atlantic Ocean but not in the Southern Ocean (Fig. 9c).

In outcrop sections at Alano di Piave (Southern Alps, northern Italy; Fig. 9a), and Contessa Highway (northeastern Apennines, central Italy) (Jovane et al., 2007; Luciani et al., 2010), geochemical proxies and foraminiferal and nannofossil assemblages also indicate significant eutrophication on the Tethyan margin in conjunction with the MECO event (Spofforth et al., 2010; Luciani et al., 2010; Toffanin et al., 2011; Boscolo Galazzo et al., 2013). A more direct comparison between the deep-sea successions from sites 748 and 1051, and the Tethyan localities is hindered by the lack of biogenic opal/siliceous microfossil assemblage data from the Italian sections. Similarly, no siliceous microplankton assemblage data are currently available for the hemipelagic ODP Site 1172 (44°S, East Tasman Plateau, southwest Pacific). However, changes in the peridinioid-gonyaulacoid ratio in dinocyst assemblages indicate a decrease in nutrient levels across the MECO at this site (Bijl et al., 2010; Fig. 9a).

Based on the current range of available datasets, it is clear that the MECO had a geographically varied, but profound impact on plankton assemblages worldwide. A similar pattern of geographically disparate trends in surface ocean primary production is also identified at the Paleocene-Eocene Thermal Maximum (PETM) (e.g., Gibbs et al., 2006; Stoll et al., 2007), reflecting the different relative influences of latitude, proximity to continents, upwelling zones, etc. Further study of the changes in surface ocean primary production during the major Paleogene global warming events may help to determine whether the geographically variable productivity patterns result from similar mechanisms—and whether productivity patterns can provide insight on the operation of the carbon cycle (e.g., variations and mechanisms of marine carbon burial) during short-lived perturbations to the climate system.

5.4. Global implications of the Site 1051 siliceous microfossil record across the MECO

Diatoms are one of the key groups of primary producers in the modern oceans (Ragueneau et al., 2000). Owing to their rapid sinking as particulate debris in marine snow and within fecal pellets, diatoms also play an important role in organic carbon export to the deep ocean, which leads to carbon recycling or burial, and thus represents one mechanism regulating the quantity and cycling carbon in the ocean–atmosphere system (e.g., Yool and Tyrrell, 2003). The silicon residence time in the ocean is estimated at ~10 kyr (Tréguer and De La Rocha, 2013). Therefore, the siliceous microfossil record across the MECO interval of Site 1051 raises an important question: what conditions are necessary to sustain periods of elevated siliceous plankton production on the timescales of several 100 kyrs?

Diatom growth is controlled by the availability of a range of nutrients, including nitrogen and phosphorus (Tappan, 1980), and silicic acid, which is supplied to the oceans mainly from riverine discharge, aeolian input, and hydrothermal and seafloor weathering sources (Yool and Tyrrell, 2003; Tréguer and De La Rocha, 2013). Of these, the riverine input of continental weathering-derived silica provides the highest contribution to the total silica input flux to the ocean, and biogenic silica burial represents the primary output flux (Tréguer and De La Rocha, 2013). Thus, given the short residence time of silicon in the oceans, if diatom accumulation was elevated in some regions for ~500 kyrs, it implies that continental silicate weathering rates were enhanced during the MECO. This interpretation is consistent with an intensified hydrological cycle resulting from elevated atmospheric humidity, as previously invoked to explain the negative feedback mechanisms associated with climate warming during the PETM (e.g., Bowen et al., 2004).

Silicate weathering, in conjunction with carbonate deposition in the oceans, is the major sink for CO₂ in the long-term carbon cycle (Walker et al., 1981; Brady, 1991). The feedback between silicate weathering and atmospheric CO₂ concentrations operates on timescales of 100 kyrs and longer (Zachos et al., 2008; Sluijs et al., 2013), and thus is an important consideration for the relatively long duration of the MECO (~500 kyrs). Increased rates of silicate weathering likely modulated the rise in atmospheric CO₂ levels during the MECO (Sluijs et al., 2013). Our records indicating increased rates of marine biogenic silica accumulation at Sites 748 and 1051 provide some support for the hypothesized increase in continental weathering during the MECO. However, the global picture of opal accumulation over the Cenozoic is not yet resolved, requiring data from many sites worldwide.

Additionally, the causal mechanisms that drove the greenhouse warming during the MECO are still largely uncertain, and the relationship between elevated silicate weathering on land and long-lived periods of carbonate dissolution in the deep sea poses a ‘MECO conundrum’ (see Sluijs et al., 2013). Further research on the distribution of biogenic silica sedimentation and marine primary production, as well as new data from shallow marine and terrestrial sedimentary systems, may shed more light on perturbations in continental weathering regimes during the MECO.

Conclusions

We document abundant siliceous microfossils within pelagic sediments at ODP Site 1051 across the late middle Eocene interval between 41.7 and 39.5 Ma. Diatoms and radiolarians are the most abundant siliceous microfossil groups in these sediments, while ebridians, silicoflagellates, chrysophyte cysts, siliceous dinoflagellates, and synurophyte scales constitute a minor component of the assemblages. Pronounced fluctuations in siliceous microfossil accumulation rates are recorded across the study interval. Two siliceous microfossil abundance maxima are identified: between 40.52 and 40.06 Ma during the initial warming stage of the MECO (TSM Maximum 1), and between 39.98 and 39.76 Ma during the post-MECO cooling phase (TSM Maximum 2). These events are characterized by moderately high pelagic diatom and silicoflagellate accumulation rates, and are interpreted to represent enhanced pelagic siliceous plankton production. A prominent minimum in pelagic productivity is interpreted over a short interval between 40.06 and 39.98 Ma, which spans peak warming and the subsequent rapid cooling that terminated the MECO.

The diatom assemblage at Site 1051 is composed predominantly of allochthonous neritic diatoms, including mainly tychoplanktic, but also planktic and benthic forms. Therefore, sustained surface and bottom current transport of contemporaneous diatoms and sediment from the North American continental shelf is interpreted throughout the interval of study. We propose that the trends in neritic diatom accumulation rates may be interpreted as evidence for fluctuations in neritic primary production, or – alternatively – variations in sea level and/or shelf accommodation space on the North American margin located to the west of Site 1051. It is not clear, however, whether increases in accommodation space or a sea-level rise would result in an increase or decrease in transport of neritic diatom to offshore Site 1051.

Comparison of Site 1051 microfossil and stable isotope records with other sites across the MECO interval suggests a geographically varied response in surface ocean primary

production to late middle Eocene greenhouse warming. The increase in siliceous plankton production over timescales of several 100 kyrs recorded at ODP sites 748 and 1051 indicates that elevated opal accumulation during the MECO may have been a widespread phenomenon and linked to enhanced input of silicic acid to the oceans. Thus, the siliceous microfossil record from Site 1051 lends support to the role of silicate weathering on land responding to and modulating an increase in atmospheric CO₂ levels during the MECO.

Acknowledgements

This paper represents the second part of a PhD project completed by JW at the University of Warsaw under the advisorship of Ireneusz Walaszczyk. Funding for this research was provided by the Polish Ministry of Science and Higher Education with grant no. N N307 140838 to JW. Additional financial support for JW was provided by the Foundation for Polish Science ('Start' programme). KE acknowledges research fellowship funding from the Natural Environment Research Council (NERC). The samples utilized in this study were provided by the Integrated Ocean Drilling Program. We thank Walter Hale and staff at the IODP Bremen Core Repository for efficient handling of several sample requests. We also wish to thank A. Sanfilippo, K. McCartney, B. Wawrzyniak-Wydrowska, S. Skompski, and W. Majewski for insightful discussions, constructive criticism, and numerous helpful suggestions. Chris Hollis and Peter Bijl are thanked for their constructive reviews and comments that greatly improved this paper.

References

- Aizawa, C., Tanimoto, M., Jordan, R.W., 2005. Living diatom assemblages from North Pacific and Bering Sea surface waters during summer 1999. *Deep-Sea Research II* 52, 2186-2205. doi: 10.1016/j.dsr2.2005.08.008
- Andersen, R.A., 1987. Synurophyceae Classis Nov., a new class of algae. *American Journal of Botany* 74, 337-353.
- Bains, S., Corfield, R.M., Norris, R.D., 1999. Mechanisms of climate warming at the end of the Paleocene. *Science* 285, 724-727. doi: 10.1126/science.285.5428.724
- Bijl, P.K., Houben, A.J.P., Schouten, S., Bohaty, S.M., Sluijs, A., Reichert, G.J., Sinninghe Damsté, J.S., Brinkhuis, H., 2010. Transient Middle Eocene Atmospheric CO₂ and Temperature Variations. *Science* 330, 819-821. doi: 10.1126/science.1193654
- Boscolo Galazzo, F., Giusberti, L., Luciani, V., Thomas, E., 2013. Paleoenvironmental changes during the Middle Eocene Climatic Optimum (MECO) and its aftermath: the benthic foraminiferal record from the Alano section (NE Italy). *Palaeogeography, Palaeoclimatology, Palaeoecology* 378, 22-35. doi: 10.1016/j.palaeo.2013.03.018
- Bohaty, S.M., Zachos, J.C., 2003. Significant Southern Ocean warming event in the late middle Eocene. *Geology* 31, 1017-1020.
- Bohaty, S.M., Zachos, J.C., Florindo, F., Delaney, M.L., 2009. Coupled greenhouse warming and deep-sea acidification in the middle Eocene. *Paleoceanography* 24, PA2207. doi: 10.1029/2008PA001676
- Bowen, G.J., Beerling, D.J., Koch, P.L., Zachos, J.C., Quattlebaum, T., 2004. A humid climate state during the Palaeocene/Eocene thermal maximum. *Nature* 432, 495-499.
- Brady, P.V., 1991. The effect of silicate weathering on global temperature and atmospheric CO₂. *Journal of Geophysical Research* 96, 18101-18106. doi:10.1029/91JB01898
- Cande, S.C., Kent, D.V., 1995. Revised calibration of the geomagnetic polarity timescale for the Late Cretaceous and Cenozoic. *Journal of Geophysical Research* 100, 6093-6095.
- Cramer, B.S., Toggweiler, J.R., Wright, J.D., Katz, M.E., Miller, K.G., 2009. Ocean overturning since the Late Cretaceous: inferences from a new benthic foraminiferal isotope compilation. *Paleoceanography* 24, PA4216. doi: 10.1029/2008PA001683

751 Davies, A., Kemp, A.E.S., Pike, J., 2009. Late Cretaceous seasonal ocean variability from the
752 Arctic. *Nature* 460, 254-259. doi: 10.1038/nature08141

753 Edgar, K.M., Bohaty, S.M., Gibbs, S.J., Sexton, P.F., Norris, R.D., Wilson, P.A., 2013.
754 Symbiont 'bleaching' in planktic foraminifera during the Middle Eocene Climatic Optimum.
755 *Geology* 41, 15-18. doi: 10.1130/G33388.1

756 Edgar, K.M., Wilson, P.A., Sexton, P.F., Gibbs, S.J., Roberts, A.P., Norris, R.D., 2010. New
757 biostratigraphic, magnetostratigraphic and isotopic insights into the Middle Eocene Climatic
758 Optimum in low latitudes. *Palaeogeography, Palaeoclimatology, Palaeoecology* 297, 670-682.
759 doi: 10.1016/j.palaeo.2010.09.016

760 Ennyu, A., Arthur, M.A., Pagani, M., 2002. Fine-fraction carbonate stable isotopes as
761 indicators of seasonal shallow mixed-layer paleohydrography. *Marine Micropaleontology* 46,
762 317-342.

763 Fenner, J., 1985. Late Cretaceous to Oligocene planktic diatoms. In: Bolli, H.M., Saunders,
764 J.B., Perch-Nielsen, K. (Eds.), *Plankton stratigraphy*, Cambridge University Press,
765 Cambridge, 713-762.

766 Fenner, J., Hoff, U., 2011. Marine diatoms in the Paleocene of the SW-Pacific. In: Egger, H.
767 (Ed.), *Climate and Biota of the Early Paleogene, Conference Program and Abstracts. Berichte*
768 *der Geologischen Bundesanstalt* 85, 73.

769 Flower, R.J., 1993. Diatom preservation: experiments and observations on dissolution and
770 breakage in modern and fossil material. *Hydrobiologia* 269/270, 473-484.

771 Galloway, W.E., Whiteaker, T.L., Ganey-Curry, P., 2011. History of Cenozoic North
772 American drainage basin evolution, sediment yield, and accumulation in the Gulf of Mexico
773 basin. *Geosphere* 7, 938-973. doi: 10.1130/GES00647.1

774 Gebühr, C., Wiltshire, K.H., Aberle, N., van Beusekom, J.E.E., Gerdts, G., 2009. Influence of
775 nutrients, temperature, light and salinity on the occurrence of *Paralia sulcata* at Helgoland
776 Roads, North Sea. *Aquatic Biology* 7, 185-197. doi: 10.3354/ab00191.

777 Gibbs, S.J., Bralower, T.J., Bown, P.R., Zachos, J.C., Bybell, L.M., 2006. Shelf and open-
778 ocean calcareous phytoplankton assemblages across the Paleocene-Eocene Thermal

779 Maximum: implications for global productivity gradients. *Geology* 34, 233-236. doi:
 780 10.1130/G22381.1

781 Gradstein, F.M., Ogg, J.G., Schmitz, M.D., Ogg, G.M. (Eds.), *The Geologic Time Scale*
 782 2012. Elsevier, Oxford.

783 Hanna, G.D., Brigger, A.L., 1970. Observations on *Liostephania*. In: Gerloff, J., Chalnoky,
 784 B.J. (Eds.), *Diatomaceae II. Friedrich Hustedt Gedenkband. Nova Hedwigia, Beiheft 31*, 89-
 785 100.

786 Harding, I.C., Lewis, J., 1994. Siliceous dinoflagellate thecal fossils from the Eocene of
 787 Barbados. *Palaeontology* 37, 825-840.

788 Hasle, G.R., Syvertsen, E.E., 1997. Marine diatoms. In: Tomas, C.R. (Ed.), *Identifying*
 789 *Marine Phytoplankton*. Academic Press, San Diego, 5-386.

790 Hernández-Becerril, D.U., 1996. A morphological study of *Chaetoceros* species
 791 (Bacillariophyta) from the plankton of the Pacific Ocean of Mexico. *Bulletin of the Natural*
 792 *History Museum, Botany Series* 26, 1-73.

793 Hollis, C.J., Rodgers, K.A., Parker, R.J., 1995. Siliceous plankton bloom in the earliest
 794 Tertiary of Marlborough, New Zealand. *Geology* 23, 835-838.

795 Jordan, R.W., Stickley, C.E., 2010. Diatoms as indicators of paleoceanographic events. In:
 796 Smol, J.P., Stoermer, E.F. (Eds.), *The Diatoms: Applications for the Environmental and Earth*
 797 *Sciences*, 2nd edition, Cambridge University Press, Cambridge, 424-453.

798 Jovane, L., Florindo, F., Coccioni, R., Dinarès-Turell, J., Marsili, A., Monechi, S., Roberts,
 799 A.P., Sprovieri, M., 2007. The middle Eocene climatic optimum event in the Contessa
 800 Highway section, Umbrian Apennines, Italy. *GSA Bulletin* 119, 413-427. doi:
 801 10.1130/B25917.1

802 Kennett, J.P., 1982. *Marine Geology*. Prentice-Hall, New Jersey.

803 Luciani, V., Giusberti, L., Agnini, C., Fornaciari, E., Rio, D., Spofforth, D.J.A., Pälike, H.,
 804 2010. Ecological and evolutionary response of Tethyan planktonic foraminifera to the middle
 805 Eocene climatic optimum (MECO) from the Alano section (NE Italy). *Palaeogeography*,
 806 *Palaeoclimatology, Palaeoecology* 292, 82-95. doi: 10.1016/j.palaeo.2010.03.029

807 Lyle, M., Olivarez Lyle, A., Backman, J., Tripathi, A., 2005. Biogenic sedimentation in the
 808 Eocene equatorial Pacific – the stuttering greenhouse and Eocene carbonate compensation
 809 depth. In: Wilson, P.A., Lyle, M., Firth, J.V. (Eds.), Proceedings of the Ocean Drilling
 810 Program, Scientific Results 199, 1-35 (Online). doi: 10.2973/odp.proc.sr.199.219.2005

 811 Martin, A.P., 2003. Phytoplankton patchiness: the role of lateral stirring and mixing. Progress
 812 in Oceanography 57, 125-174. doi: 10.1016/S0079-6611(03)00085-5

 813 Matsuoka, A., 2007. Living radiolarian feeding mechanisms: new light on past marine
 814 ecosystems. Swiss Journal of Geosciences 100, 273-279. doi: 10.1007/s00015-007-1228-y

 815 McQuoid, M.R., Nordberg, K., 2003. The diatom *Paralia sulcata* as an environmental
 816 indicator species in coastal sediments. Estuarine, Coastal and Shelf Science 56, 339-354. doi:
 817 10.1016/S0272-7714(02)00187-7

 818 Mita, I., 2001. Data report: Early to Late Eocene calcareous nannofossil assemblages of Sites
 819 1051 and 1052, Blake Nose, Northwestern Atlantic Ocean. In: Kroon, D., Norris, R.D., Klaus,
 820 A. (Eds.), Proceedings of the Ocean Drilling Program, Scientific Results 171B, 1-28 (Online).
 821 doi: 10.2973/odp.proc.sr.171B.122.2001

 822 Ogg, J.G., Bardot, L., 2001. Aptian through Eocene magnetostratigraphic correlation of the
 823 Blake Nose Transect (Leg 171B), Florida Continental Margin. In: Kroon, D., Norris, R.D.,
 824 Klaus, A. (Eds.), Proceedings of the Ocean Drilling Program, Scientific Results 171B, 1-58
 825 (Online). doi: 10.2973/odp.proc.sr.171B.104.2001

 826 Preisig, H.R., 1994. Siliceous structures and silicification in flagellated protists. Protoplasma
 827 181, 29-42. doi: 10.1007/BF01666387

 828 Ragueneau, O., Tréguer, P., Leynaert, A., Anderson, R.F., Brzezinski, M.A., DeMaster, D.J.,
 829 Dugdale, R.C., Dymond, J., Fischer, G., François, R., Heinze, C., Maier-Reimer, E., Martin-
 830 Jézéquel, V., Nelson, D.M., Quéguiner, B., 2000. A review of the Si cycle in the modern
 831 ocean: recent progress and missing gaps in the application of biogenic opal as a
 832 paleoproductivity proxy. Global and Planetary Change 26, 317-365. doi: 10.1016/S0921-
 833 8181(00)00052-7

 834 Renaudie, J., Danelian, T., Saint Martin, S., Le Callonec, L., Tribovillard, N., 2010. Siliceous
 835 phytoplankton response to a Middle Eocene warming event recorded in the tropical Atlantic

836 (Demerara Rise, ODP Site 1260A). *Palaeogeography, Palaeoclimatology, Palaeoecology* 286,
837 121-134. doi: 10.1016/j.palaeo.2009.12.004

838 Roberts, A.P., Bicknell, S.J., Byatt, J., Bohaty, S.M., Florindo, F., Harwood, D.M., 2003.
839 Magnetostratigraphic calibration of Southern Ocean diatom datums from the Eocene-
840 Oligocene of Kerguelen Plateau (Ocean Drilling Program sites 744 and 748).
841 *Palaeogeography, Palaeoclimatology, Palaeoecology* 198, 145-168. doi: 10.1016/S0031-
842 0182(03)00397-3

843 Ross, R., 1995. A revision of *Rutilaria* Greville (Bacillariophyta). *Bulletin of the British*
844 *Museum (Natural History), Botany Series* 25, 1-93.

845 Round, F.E., Crawford, R.M., Mann, D.G., 1990. The diatoms. Biology & morphology of the
846 genera. Cambridge University Press, Cambridge.

847 Sanfilippo, A., Blome, C.D., 2001. Biostratigraphic implications of mid-latitude Palaeocene-
848 Eocene radiolarian faunas from Hole 1051A, ODP Leg 171, Blake Nose, western North
849 Atlantic. In: Kroon, D., Norris, R.D., Klaus, A. (Eds.), *Western North Atlantic Palaeogene*
850 *and Cretaceous Palaeoceanography*. Geological Society of London Special Publications 183,
851 185-224.

852 Sawai, Y., Nagumo, T., Toyoda, K., 2005. Three extant species of *Paralia*
853 (Bacillariophyceae) along the coast of Japan. *Phycologia* 44, 517-529.

854 Schrader, H.-J., Gersonde, R., 1978. Diatoms and silicoflagellates. In: Zachariasse, W.J. (Ed.),
855 *Micropaleontological Counting Methods and Techniques: An Exercise of an Eight Metres*
856 *Section of the Lower Pliocene of Cap Rossello, Sicily*. Utrecht Micropalaeontological
857 *Bulletin* 17, 129-176.

858 Shipboard Scientific Party, 1998a. Site 1051. In: Norris, R.D., Kroon, D., Klaus, A., et al.
859 (Eds.), *Proceedings of the Ocean Drilling Program, Initial Reports 171B*, 171-239. doi:
860 10.2973/odp.proc.ir.171B.105.1998

861 Shipboard Scientific Party, 1998b. Site 1053. In: Norris, R.D., Kroon, D., Klaus, A., et al.
862 (Eds.), *Proceedings of the Ocean Drilling Program, Initial Reports 171B*, 321-348. doi:
863 10.2973/odp.proc.ir.171B.107.1998

864 Shipboard Scientific Party, 2002. Site 1218. In: Lyle, M., Wilson, P.A., Janecek, T.R., et al.
865 (Eds.), Proceedings of the Ocean Drilling Program, Initial Reports 199, 1-126 (Online). doi:
866 10.2973/odp.proc.ir.199.111.2002

867 Sluijs, A., Zeebe, R.E., Bijl, P.K., Bohaty, S.M., 2013. A middle Eocene carbon cycle
868 conundrum. Nature Geoscience Advance Online Publication, 1-6. doi: 10.1038/NGEO1807

869 Sømme, T.O., Helland-Hansen, W., Granjeon, D., 2009. Impact of eustatic amplitude
870 variations on shelf morphology, sediment dispersal, and sequence stratigraphic interpretation:
871 Icehouse versus greenhouse systems. Geology 37, 587-590. doi: 10.1130/G25511A.1

872 Spofforth, D.J.A., Agnini, C., Pälike, H., Rio, D., Fornaciari, E., Giusberti, L., Luciani, V.,
873 Lanci, L., Muttoni, G., 2010. Organic carbon burial following the middle Eocene climatic
874 optimum in the central western Tethys. Paleoceanography 25, PA3210. doi:
875 10.1029/2009PA001738

876 Stickley, C.E., Koç, N., Brumsack, H.-J., Jordan, R.W., Suto, I., 2008. A siliceous microfossil
877 view of middle Eocene Arctic paleoenvironments: a window of biosilica production and
878 preservation. Paleoceanography 23, PA1S14. doi: 10.1029/2007PA001485

879 Stoll, H.M., Shimizu, N., Archer, D., Ziveri, P., 2007. Coccolithophore productivity response
880 to greenhouse event of the Paleocene-Eocene Thermal Maximum. Earth and Planetary
881 Science Letters 258, 192-206. doi: 10.1016/j.epsl.2007.03.037

882 Suto, I., 2004. Fossil marine diatom resting spore morpho-genus *Xanthiopyxis* Ehrenberg in
883 the North Pacific and Norwegian Sea. Paleontological Research 8, 283-310.

884 Suto, I., 2006. Taxonomy of the fossil marine diatom resting spore morpho-genera
885 *Xanthioisthmus* Suto gen. nov. and *Quadrocistella* Suto gen. nov. in the North Pacific and
886 Norwegian Sea. Journal of Micropalaeontology 25, 3-22.

887 Suto, I., Jordan, R.W., Watanabe, M., 2009. Taxonomy of middle Eocene diatom resting
888 spores and their allied taxa from the central Arctic Basin. Micropaleontology 55, 259-312.

889 Tappan, H., 1980. Paleobiology of plant protists. W.H. Freeman and Company, San
890 Francisco.

891 Toffanin, F., Agnini, C., Fornaciari, E., Rio, D., Giusberti, L., Luciani, V., Spofforth, D.J.A.,
892 Pälike, H., 2011. Changes in calcareous nannofossil assemblages during the Middle Eocene

893 Climatic Optimum: clues from the central-western Tethys (Alano section, NE Italy). *Marine*
894 *Micropaleontology* 81, 22-31. doi: 10.1016/j.marmicro.2011.07.002

895 Tréguer, P.J., De La Rocha, C.L., 2013. The World Ocean silica cycle. *Annual Review of*
896 *Marine Science* 5: 477-501. doi: 10.1146/annurev-marine-121211-172346

897 van Mourik, C.A., Brinkhuis, H., Williams, G.L., 2001. Mid- to late Eocene organic-walled
898 dinoflagellate cysts from ODP Leg 171B, offshore Florida. In: Kroon, D., Norris, R.D.,
899 Klaus, A. (Eds.), *Western North Atlantic Palaeogene and Cretaceous Palaeoceanography*.
900 *Geological Society of London Special Publications* 183, 225-251.

901 Wade, B.S., Kroon, D., 2002. Middle Eocene regional climate instability: evidence from the
902 western North Atlantic. *Geology* 30, 1011-1014.

903 Walker, J.C.G., Hays, P.B., Kasting, J.F., 1981. A negative feedback mechanism for the long-
904 term stabilization of Earth's surface temperature. *Journal of Geophysical Research* 86, 9776-
905 9782. doi:10.1029/JC086iC10p09776

906 Weber, M.E., 1998. Estimation of biogenic carbonate and opal by continuous non-destructive
907 measurements in deep-sea sediments: application to the eastern Equatorial Pacific. *Deep-Sea*
908 *Research I* 45, 1955-1975.

909 Witkowski, J., Harwood, D.M., Chin, K., 2011. Taxonomic composition, paleoecology and
910 biostratigraphy of Late Cretaceous diatoms from Devon Island, Nunavut, Canadian High
911 Arctic. *Cretaceous Research* 32, 277-300. doi: 10.1016/j.cretres.2010.12.009

912 Witkowski, J., Bohaty, S.M., McCartney, K., Harwood, D.M., 2012. Enhanced siliceous
913 plankton productivity in response to middle Eocene warming at Southern Ocean ODP Sites
914 748 and 749. *Palaeogeography, Palaeoclimatology, Palaeoecology* 326-328, 78-94. doi:
915 10.1016/j.palaeo.2012.02.006

916 Yool, A., Tyrrell, T., 2003. Role of diatoms in regulating the ocean's silicon cycle. *Global*
917 *Biogeochemical Cycles* 17, 1103. doi: 10.1029/2002GB002018

918 Zachos, J.C., Pagani, M., Sloan, L., Thomas, E., Billups, K., 2001. Trends, rhythms, and
919 aberrations in global climate 65 Ma to present. *Science* 292, 686-693.

920 Zachos, J.C., Dickens, G.R., Zeebe, R.E., 2008. An early Cenozoic perspective on greenhouse
921 warming and carbon-cycle dynamics. *Nature* 451, 279-283. doi: 10.1038/nature06588

Fig. 1. Paleogeographic map of the Atlantic Ocean at 40 Ma, showing the location of Site 1051 (closed circle) and other Atlantic ODP sites (open circles) referred to in this paper. Base map generated using Ocean Drilling Stratigraphic Network Plate Tectonic Reconstruction Service (www.odsn.de).

Fig. 2. Siliceous microfossil abundance records for ODP Site 1051: (a) relative abundance of major siliceous microfossil groups, (b) total siliceous microfossil (TSM) absolute abundance, (c) relative abundances of major diatom groups, and (d) diatom group absolute abundances, plotted with bulk and benthic $\delta^{13}\text{C}$ and $\delta^{18}\text{O}$ records (e-f). Correlation and/or stable isotope data are from Mita (2001), Bohaty et al. (2009) and Edgar et al. (2010). Abbreviations: mcd – meters composite depth; TSM Max – total siliceous microfossil abundance maximum; VPDB – Vienna Pee Dee Belemnite.

Fig. 3. ODP Site 1051 diatom assemblage records spanning the MECO event: (a) relative abundance of major neritic taxa, (b) relative abundance of major pelagic taxa, (c) relative abundance of major species of *Hemiaulus*, (d) relative abundance of major resting spore taxa. Correlation based on Edgar et al. (2010). Dashed vertical lines represent boundaries of assemblage intervals discussed in the text. Abbreviations: mcd – meters composite depth.

Fig. 4. Global paleobiogeographic distribution of key pelagic diatom taxa recorded at ODP Site 1051, including (a) *Distephanosira architecturalis* in middle Eocene through late Oligocene successions, and (b) *Triceratium inconspicuum* in middle Eocene successions. See Tables S6-S9 in the online Supplementary Materials for a list of references used in this compilation. Base maps: 40 Ma paleogeographic reconstruction generated using Ocean Drilling Stratigraphic Network Plate Tectonic Reconstruction service (www.odsn.de).

Fig. 5. Eocene through late Oligocene paleobiogeographic distribution of key pelagic diatom taxa recorded at ODP Site 1051: (a) *Hemiaulus polycystinorum* var. *mesolepta*, (b) *Coscinodiscus decrescens*, and (c) *Rocella praeinitida*. See Tables S10-S15 in the online Supplementary Materials for lists of references used in this compilation. Base maps: 40 Ma paleogeographic reconstruction generated using Ocean Drilling Stratigraphic Network Plate Tectonic Reconstruction service (www.odsn.de).

Fig. 6. Synthesis of siliceous microfossil records from ODP Site 1051 across the MECO event compared with key planktic foraminiferal assemblage data and isotope records: (a) Diatom accumulation rates, (b) radiolarian and silicoflagellate accumulation rates, (c-d) relative

abundance of major planktic foraminiferal groups, (e-f) bulk-carbonate and benthic $\delta^{18}\text{O}$ and $\delta^{13}\text{C}$ records, and (g) surface-to-deep $\delta^{13}\text{C}$ gradient ($\Delta\delta^{13}\text{C}_{\text{bulk carbonate-benthic}}$). Planktic foraminiferal assemblage and magnetostratigraphic data are from Edgar et al. (2010; 2013). Abbreviations: Max – TSM Maximum; VPDB – Vienna Pee Dee Belemnite; CK95 – Cande and Kent (1995); GTS2012 – Gradstein et al. (2012). Dashed vertical lines represent boundaries of assemblage intervals.

Fig. 7. Site 1051 reconstruction of sea surface temperature and nutrient availability changes across the MECO event (Stages I through IV) as interpreted from siliceous microfossil assemblage variations. Schematic drawings are not to scale.

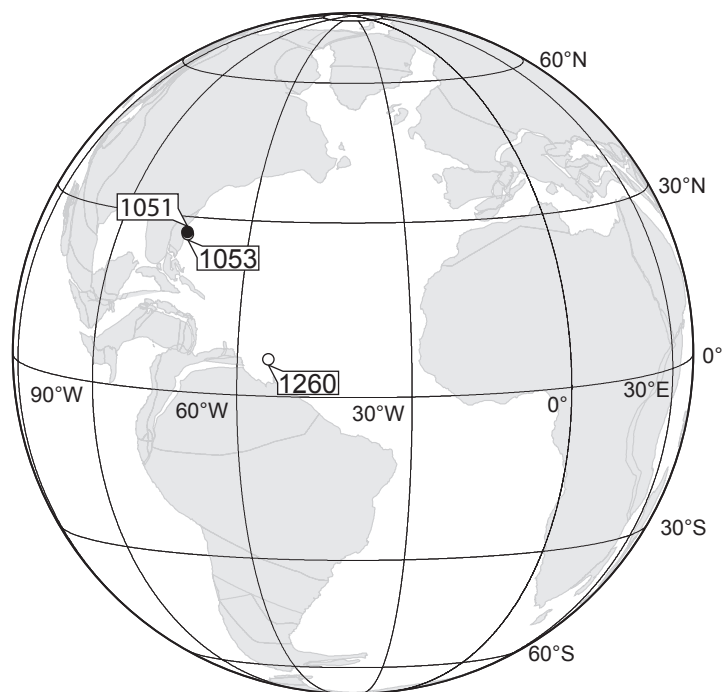
Fig. 8. ODP Site 1051 $\delta^{18}\text{O}$ record across Stage II through initial Stage IV (a), plotted against differences in timing between peak fluxes of diatoms (b) and radiolarians, and radiolarian: diatom abundance ratio (c). Abbreviations: CK95 – Cande and Kent (1995), VPDB – Vienna Pee Dee Belemnite; GTS2012 – Gradstein et al. (2012).

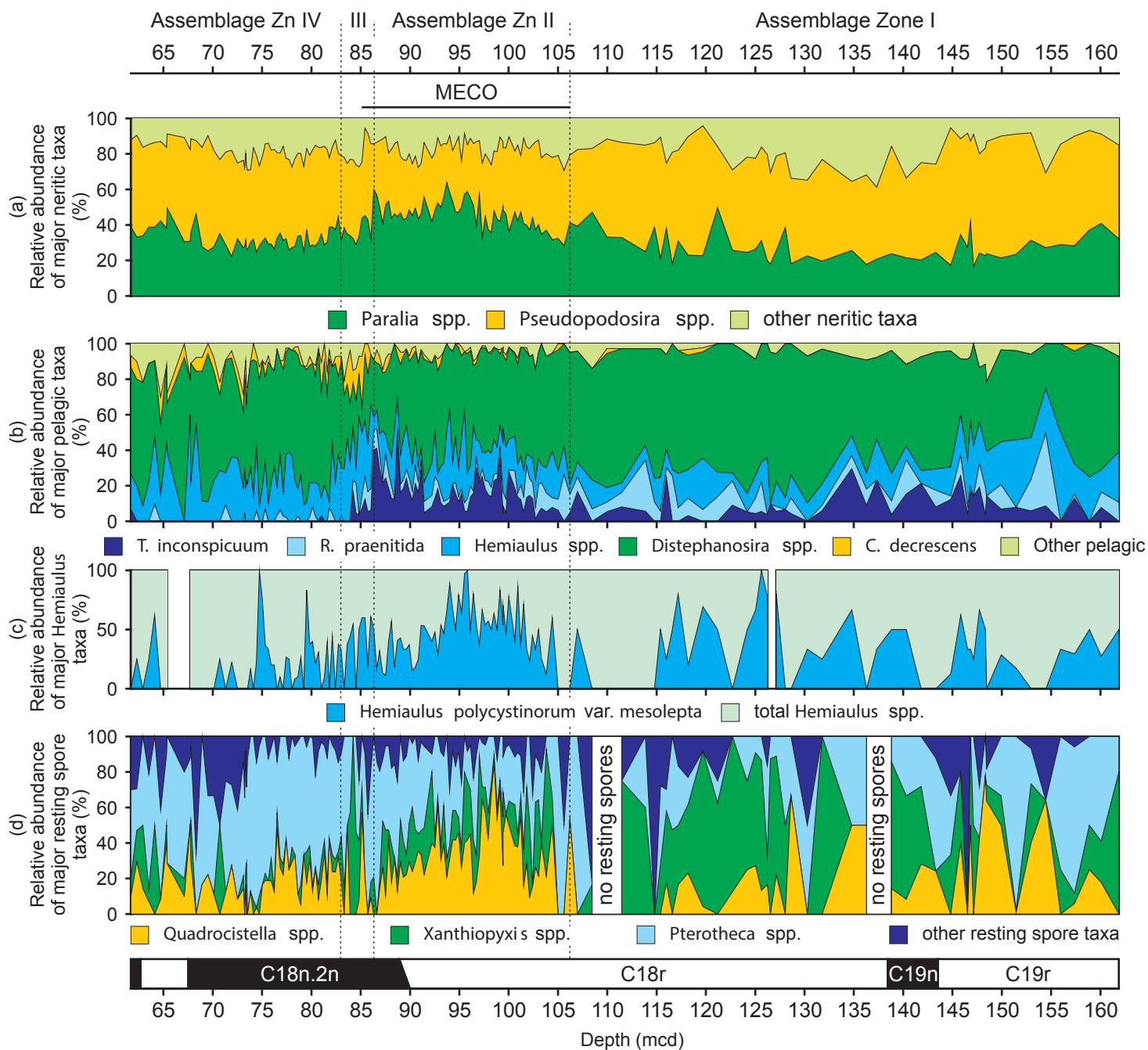
Fig. 9. (a) Multi-proxy compilation of interpreted changes in surface ocean productivity across the MECO in deep-sea and outcrop successions around the world, (b) comparison of biogenic opal mass accumulation rates at Site 1218 and pelagic diatom flux at Site 1051, (c) comparison of trends in total siliceous microfossil abundance at Sites 748 and 1051 (note difference in vertical scales), (d) fine-fraction and benthic $\delta^{18}\text{O}$ records from the Southern Ocean sites 738 and 748. Based on data from Lyle et al. (2005), Bijl et al. (2010), Luciani et al. (2010), Spofforth et al. (2010), and Witkowski et al. (2012). Stable isotope data are from Bohaty et al. (2009). Magnetostratigraphic data from Edgar et al. (2010). Abbreviations: MAR – mass accumulation rate; TSM – total siliceous microfossils; VPDB – Vienna Pee Dee Belemnite; CK95 – Cande and Kent (1995); GTS2012 – Gradstein et al. (2012). Base map in panel (a): 40 Ma paleogeographic reconstruction generated using Ocean Drilling Stratigraphic Network Plate Tectonic Reconstruction service (www.odsnet.de).

Plate I. Photomicrographs of key diatom taxa from the MECO interval of ODP Site 1051. All pairs represent high and low focus of the same specimen. Scale bar equals 20 μm , except for Figs. 8-10 and 17-18 (10 μm), and Fig. 4 (15 μm). **Fig. 1a-b.** *Rhaphoneis atlantica*, sample 171B-1050A-2H-5, 33-34 cm. **Fig. 2.** *Diplomenora cocconeiforma*?, sample 171B-1050A-2H-2, 33-34 cm. **Fig 3a-b.** *Mastogloia barbadensis*, sample 171B-1051A-10H-2, 36-37 cm. **Fig. 4.** *Mastogloia* sp. aff. *M. archaia*, sample 171B-1051A-8H-4, 96-97 cm. **Fig. 5.** *Lyrella* sp. aff. *L. praetexta*, sample 171B-1051A-9H-3, 36-37 cm. **Fig. 6.** *Strangulonema*

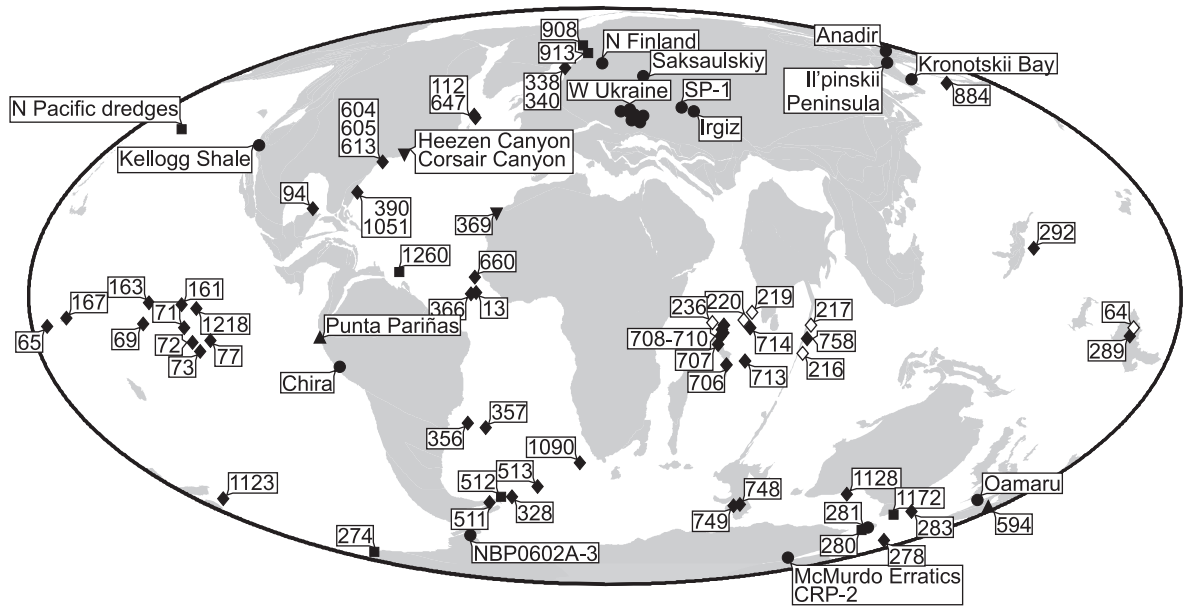
986 *barbadensis*, sample 171B-1050A-2H-2, 33-34 cm. **Fig. 7.** *Actinoptychus hillabyanus*, sample
987 171B-1051B-12H-4, 6-7 cm. **Fig. 8.** *Pseudopodosira bella*, sample 171B-1051A-10H5, 66-67
988 cm. **Fig. 9.** *Paralia* sp., oblong specimen, sample 171B-1051B-9H-1, 96-97 cm. **Fig. 10.**
989 *Paralia crenulata*, sample 171B-1051A-10H-5, 126-127 cm. **Fig. 11a-b.** *Abas wittii*, sample
990 171B-1051A-8H-4, 126-127 cm. **Fig. 12a-b.** *Hemiaulus immanis*, sample 171B-1051A-8H-2,
991 6-7 cm. **Fig. 13a-b.** *Hemiaulus polycystinorum* var. *mesolepta*, sample 171B-1050A-2H-2,
992 33-34 cm. **Fig. 14.** *Triceratium inconspicuum* var. *inconspicuum*, sample 171B-1051A-10H-
993 4, 36-37 cm. **Fig. 15.** *Triceratium inconspicuum* var. *trilobata*, sample 171B-1051B-15H-4, 4-
994 5 cm. **Fig. 16a-b.** *Coscinodiscus decrescens*, sample 171B-1051A-8H-2, 96-97 cm. **Figs. 17-**
995 **18.** *Distephanosira architecturalis*, samples 171B-1051B-12H-5, 6-7 cm (Fig. 17), 171B-
996 1051A-10H5, 66-67 cm (Fig. 18). **Fig. 19.** *Liostephanosira* sp., sample 171B-1050A-2H-2, 33-
997 34 cm. **Fig. 20a-b.** *Rocella praenitida*, sample 171B-1050A-3H-6, 33-34 cm. **Fig. 21a-b.**
998 *Xanthiopyxis oblonga*, sample 171B-1051A-10H-1, 6-7 cm. **Fig. 22a-b.** *Quadrocistella*
999 *montana*, sample 171B-1051A-13H-5, 6-7 cm. **Fig. 23a-b.** *Pterotheca aculeifera*, sample
1000 171B-1051A-19X-4, 126-127 cm.

1001 **Plate II.** Photomicrographs of other siliceous microfossils from the MECO interval of ODP
1002 Site 1051. All pairs represent high and low focus of the same specimen. Scale bar equals 20
1003 μm , except for Figs. 5a-b (10 μm). **Fig. 1a-b.** *Corbisema regina*, sample 171B-1051B-15H-1,
1004 4-5 cm. **Fig. 2a-b.** *Corbisema spinosa*, sample 171B-1051A-10H-1, 36-37 cm. **Fig. 3a-b.**
1005 *Ebriopsis cornuta*, sample 171B-1051A-8H-2, 96-97 cm. **Figs. 4-5.** Chrysophycean cysts,
1006 sample 171B-1051A-9H-6, 126-127 cm. **Fig. 6a-b.** *Ebriopsis crenulata*, sample 171B-
1007 1051A-15H-6, 66-67 cm. **Fig. 7a-b.** *Ebriopsis* sp., sample 171B-1051A-10H-1, 66-67 cm.
1008 **Figs. 8-9.** *Peridinites sphaericus*?, samples 171B-1051A-9H-6, 126-127 cm (Fig. 8), 171B-
1009 1050A-2H-2, 33-34 cm (Fig. 9). **Figs. 10-11.** *Macrora barbadensis*, samples 171B-1051A-
1010 10H-1, 6-7 cm (Fig. 10a-b), 171B-1051A-9H-2, 66-67 cm (Fig. 11a-b). **Fig. 12a-b.** *Macrora*
1011 *stella*, sample 171B-1051A-8H-2, 96-97 cm.

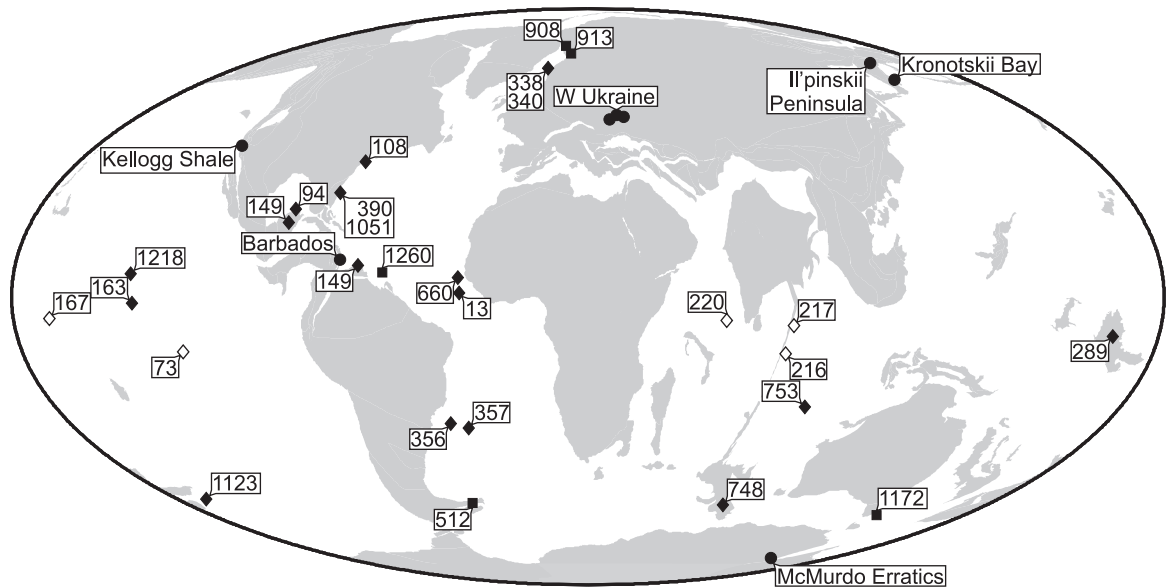




(a) *Distephanosira architecturalis*

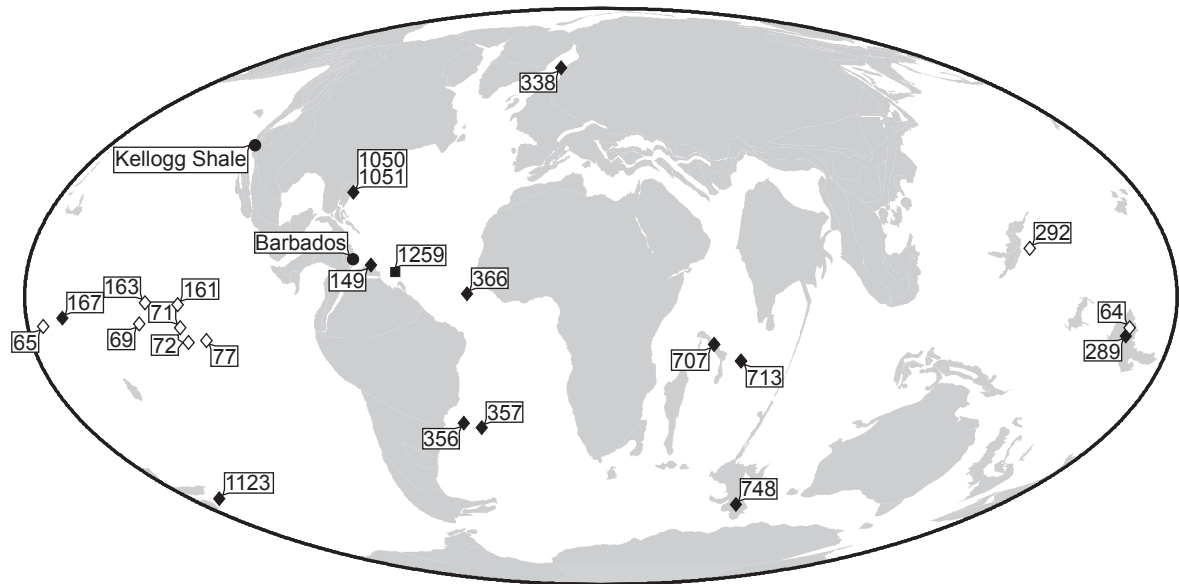


(b) *Triceratium inconspicuum*

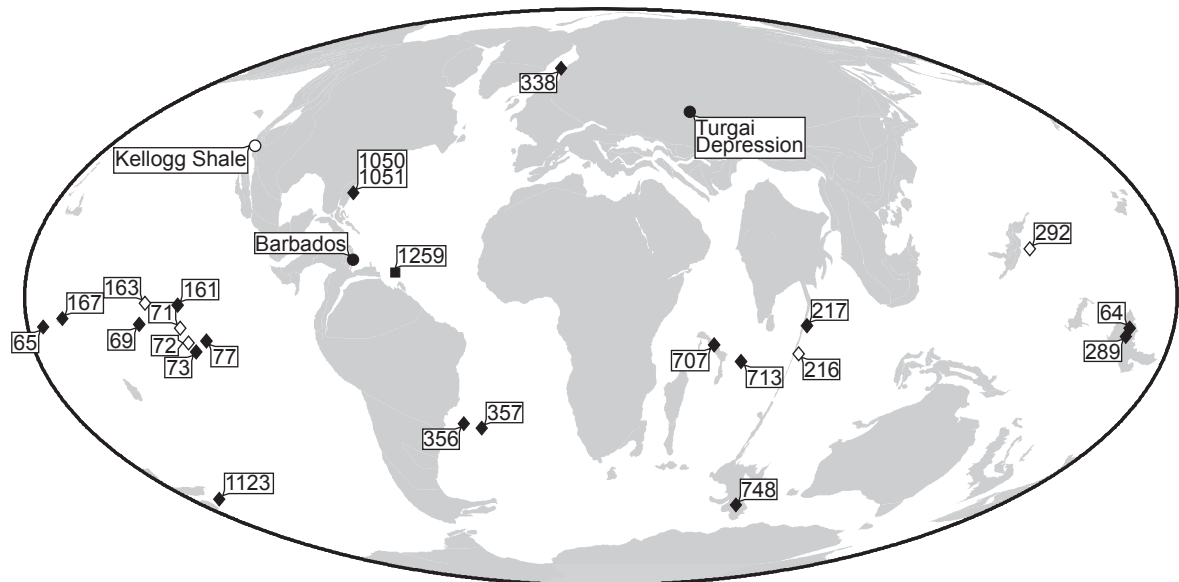


● coastal/neritic ▲ reworked ■ hemipelagic ▼ hemipelagic/pelagic ◆ pelagic
open symbols = absent

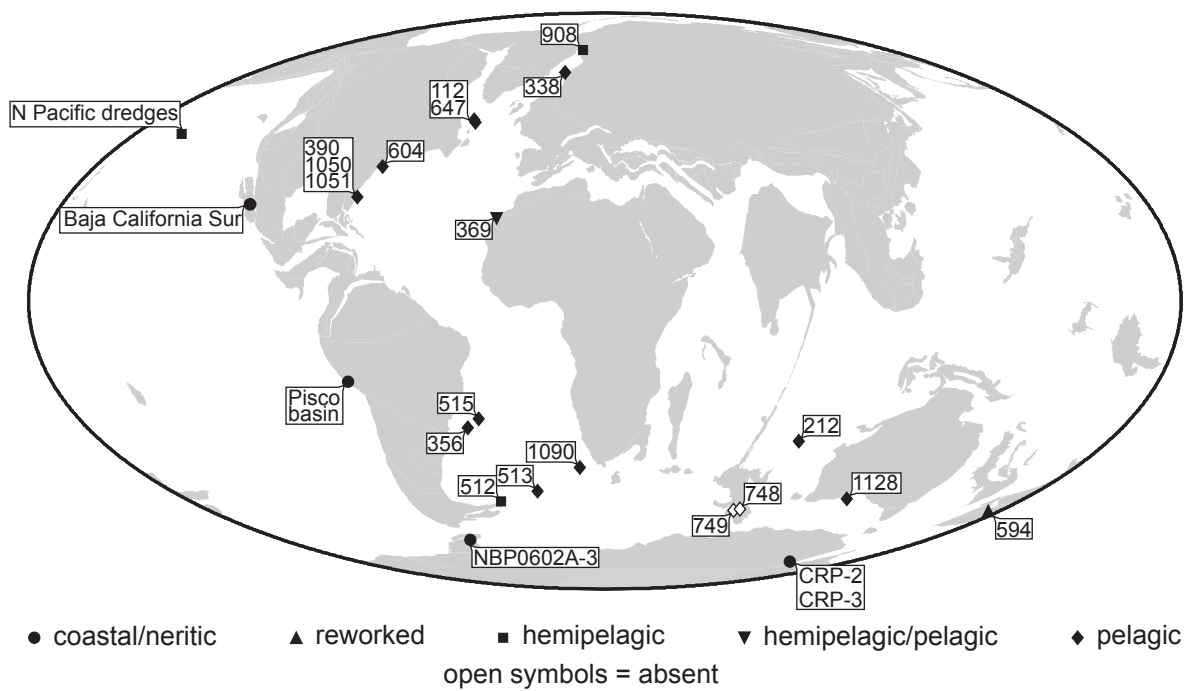
(a) *Hemiaulus polycystinorum* var. *mesolepta*

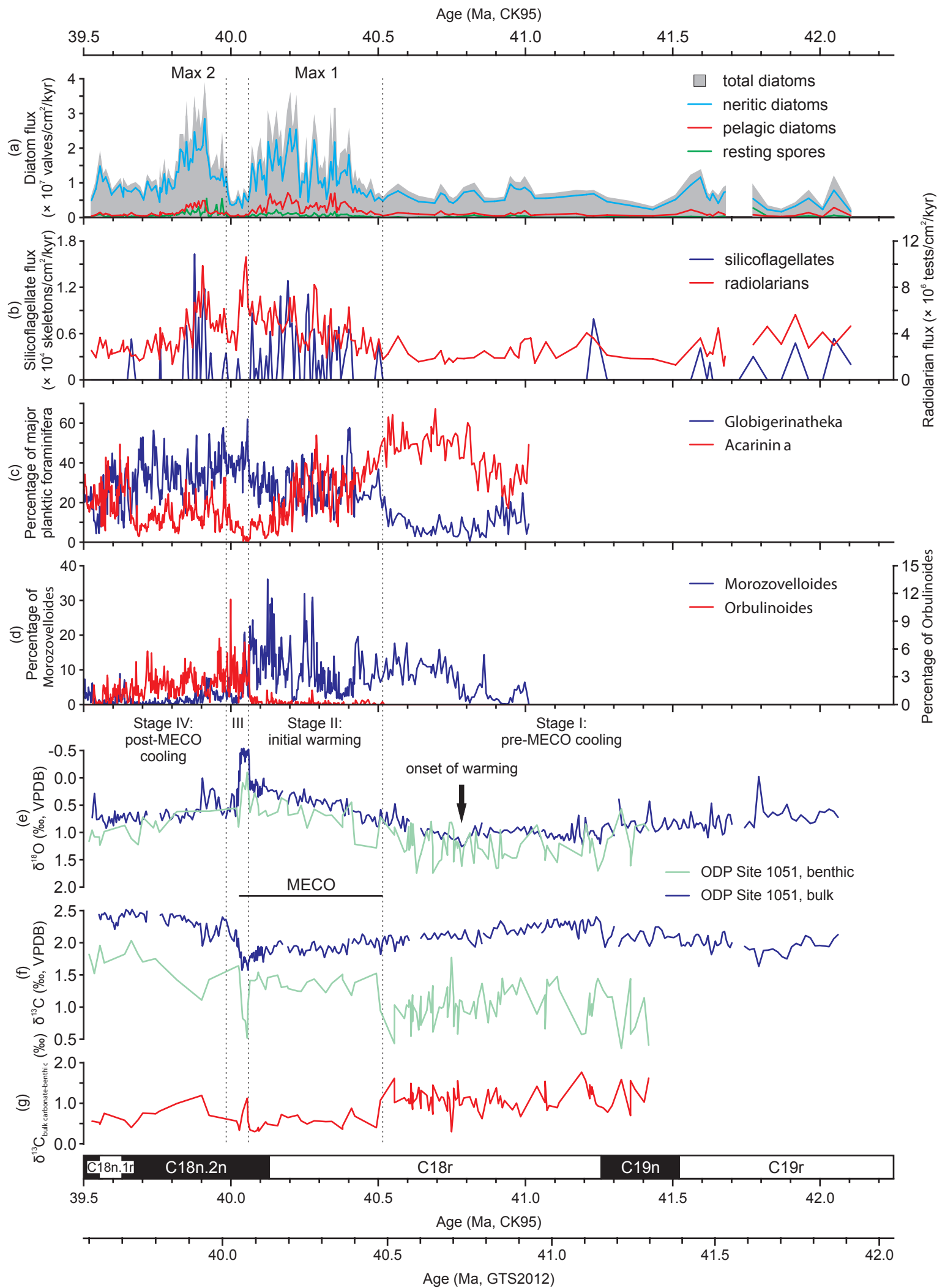


(b) *Coscinodiscus decrescens*

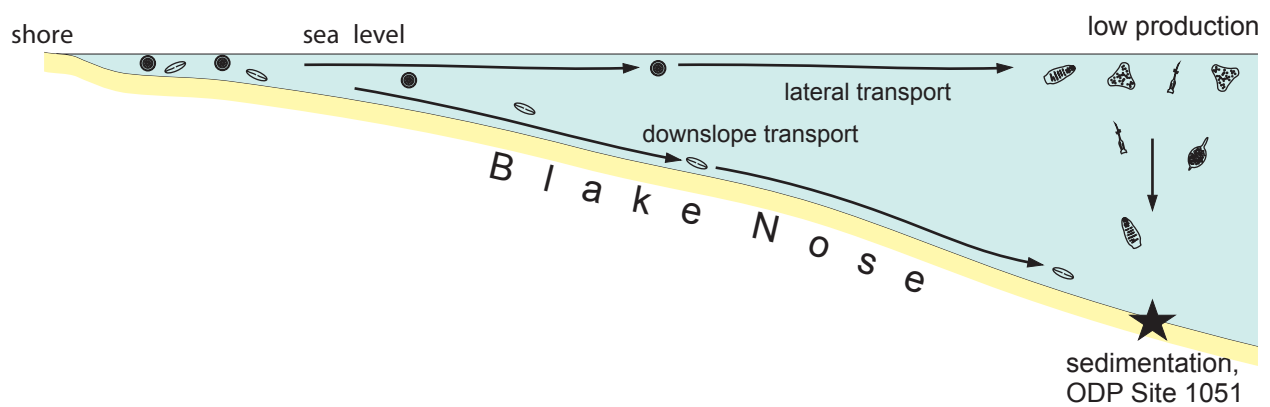


(c) *Rocella praenitida*



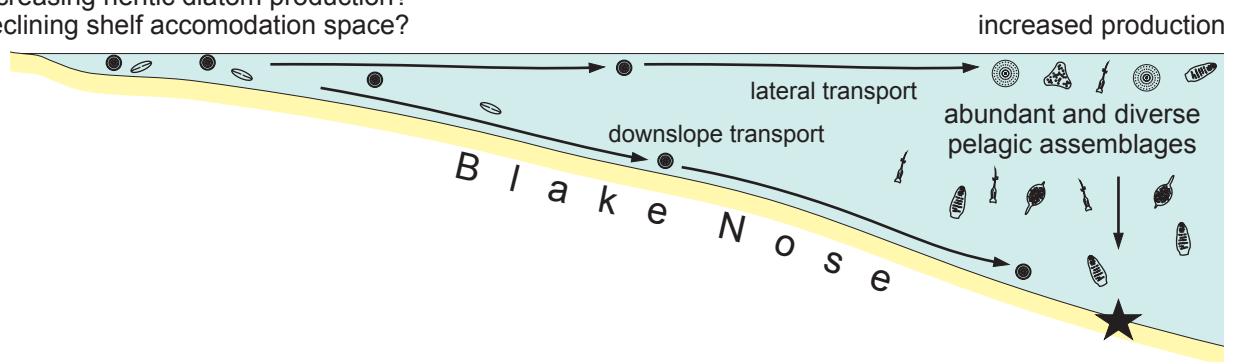


(a) Stage I: Prior to 40.52 Ma

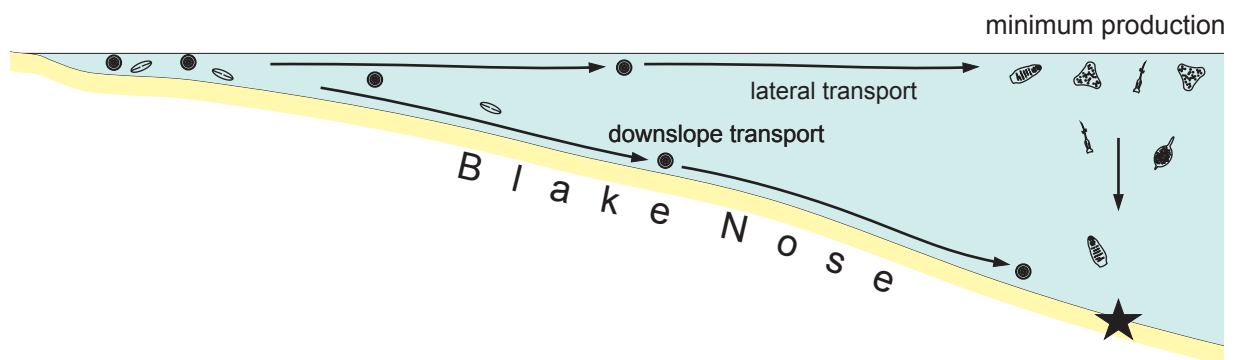


(b) Stage II: 40.52 —40.06 Ma

increasing neritic diatom production?
declining shelf accommodation space?

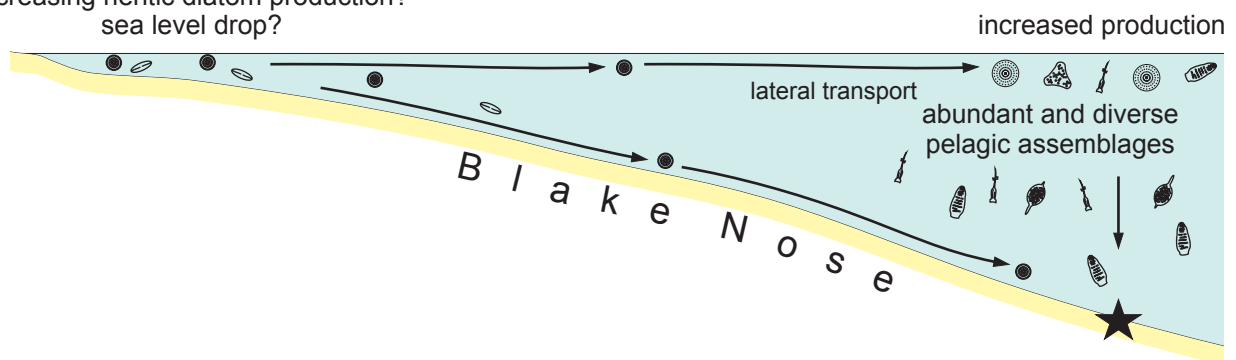


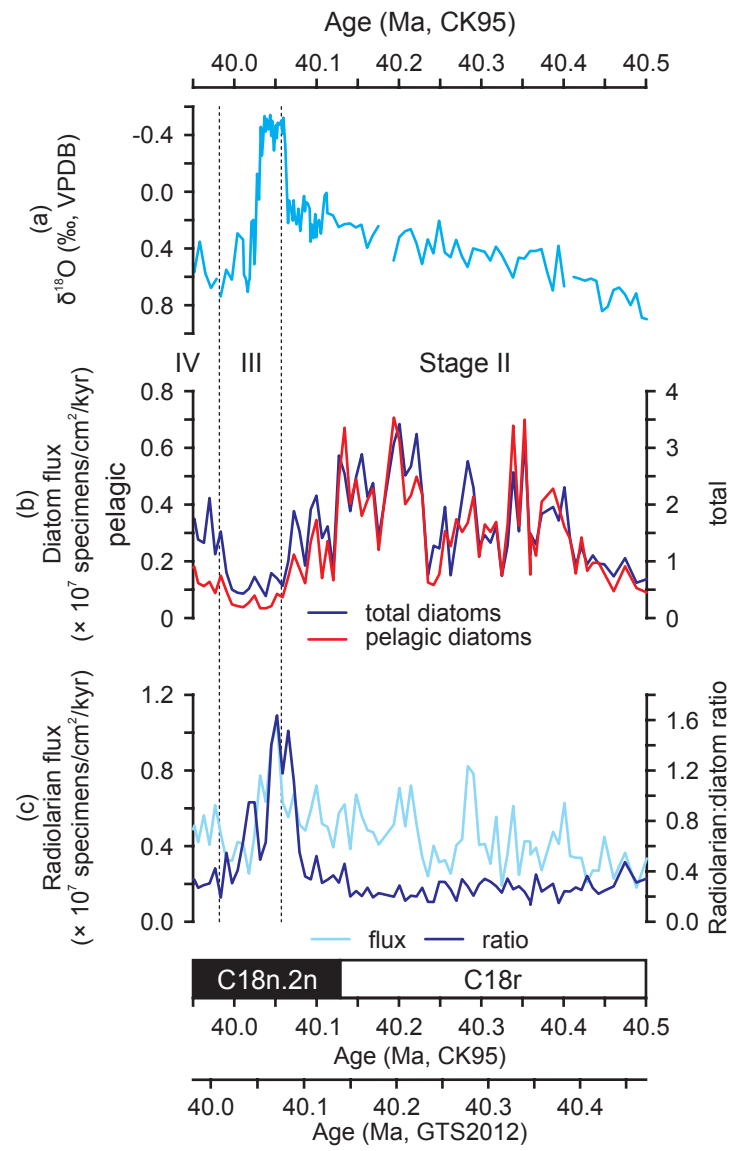
(c) Stage III: 40.06 —39.98 Ma



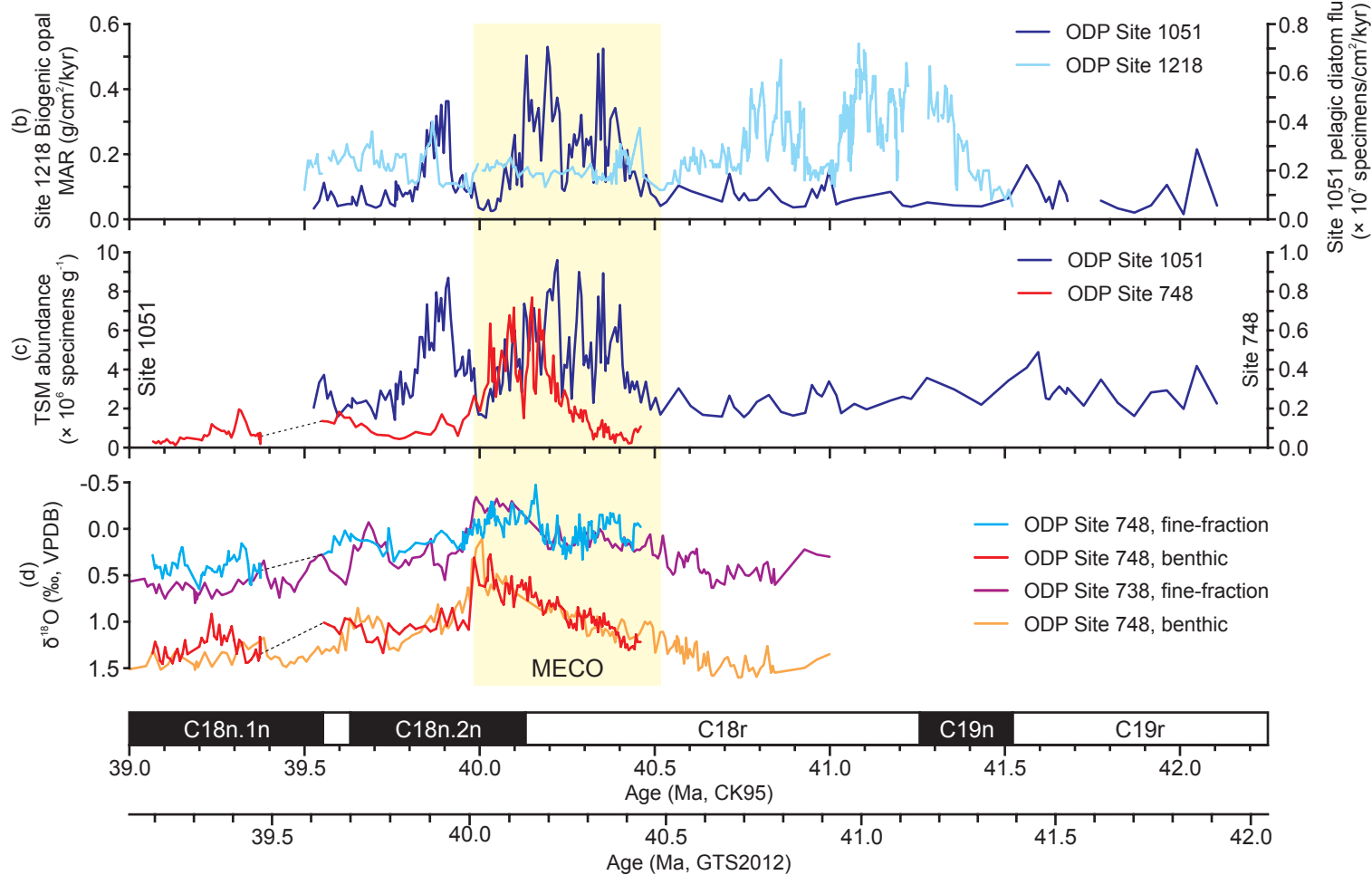
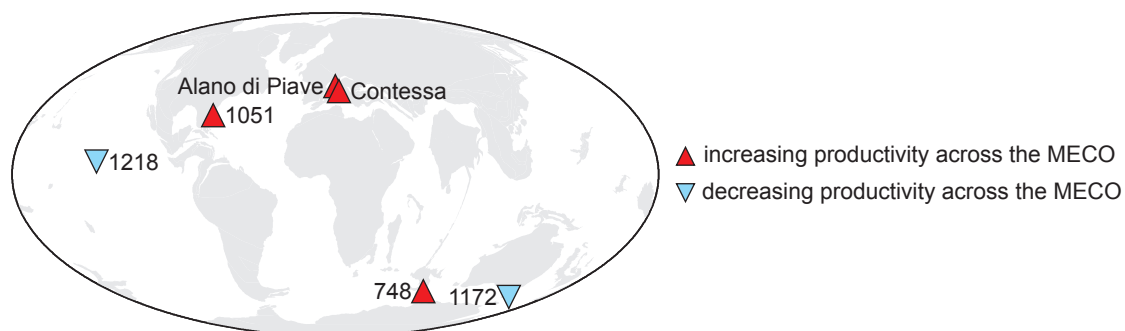
(d) Initial Stage IV: 39.98 —39.76 Ma

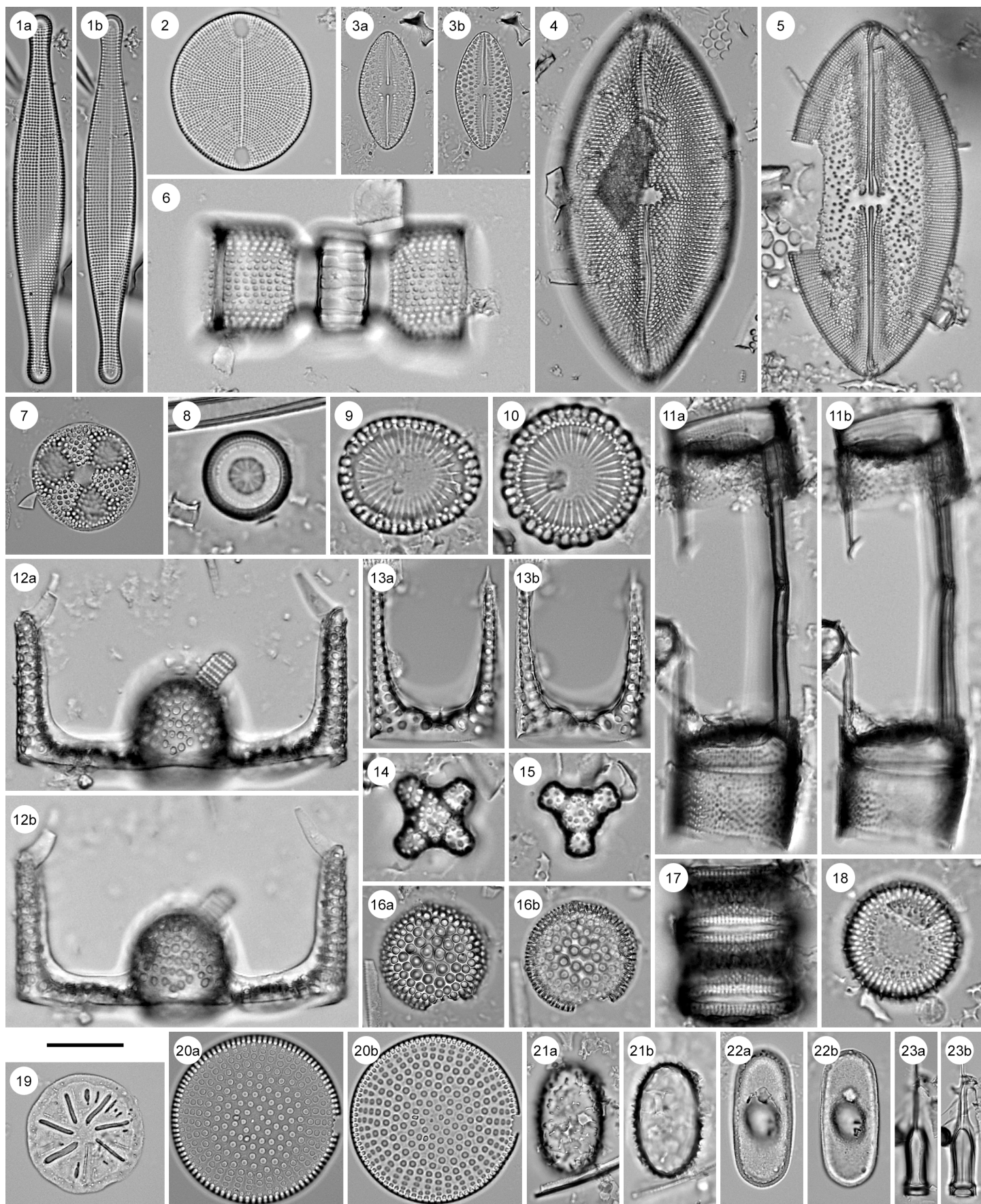
increasing neritic diatom production?
sea level drop?

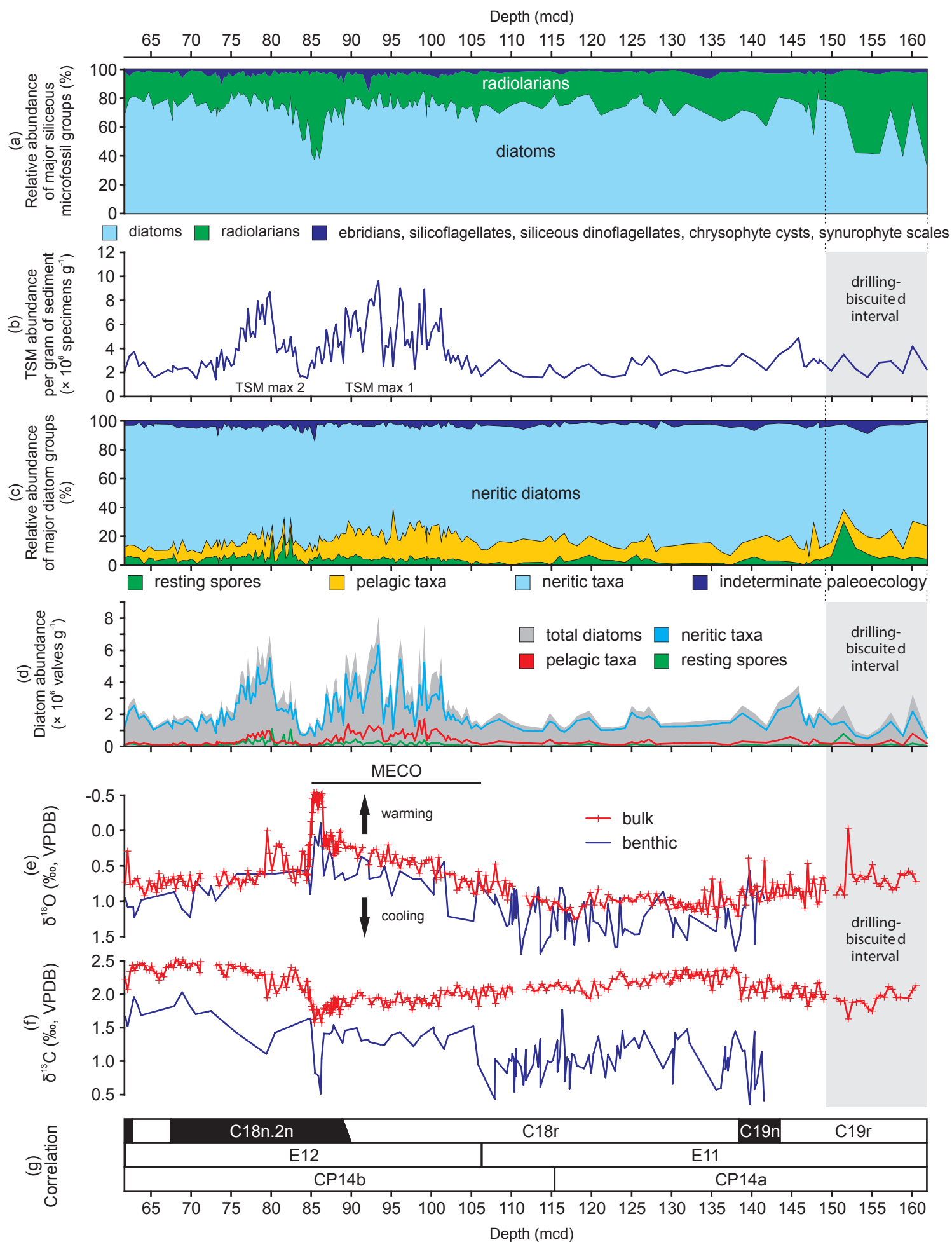


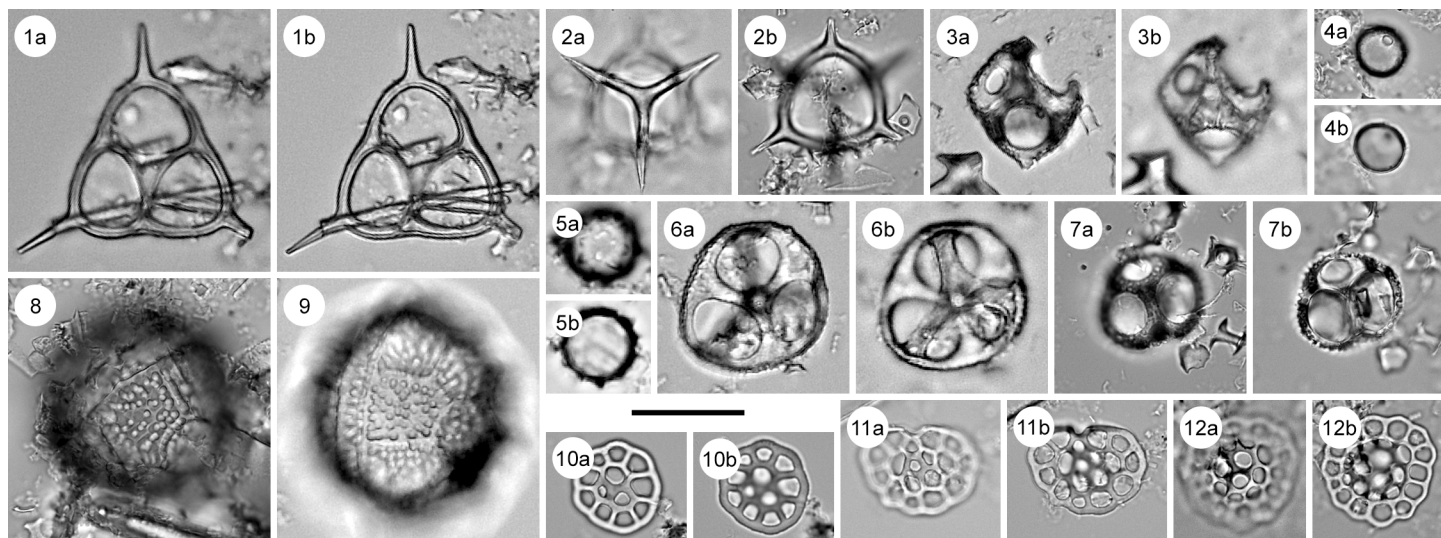


(a) Surface-water productivity changes across the MECO









Neritic diatoms		Pelagic diatoms	Resting spores
<i>Abas wittii</i>	<i>Paralia russica</i>	<i>Asterolampra insignis</i>	<i>Costopyxis trochlea</i>
<i>Actinoptychus hillabyanus</i>	<i>Paralia sulcata</i>	<i>Asterolampra marylandica</i>	<i>Pseudopyxilla</i> sp. 1
<i>Actinoptychus intermedius</i>	<i>Paralia</i> sp.	<i>Asterolampra</i> sp. cf. <i>A. affinis</i>	<i>Pterotheca aculeifera</i>
<i>Actinoptychus pericavatus</i>	<i>Peponia barbadensis</i>	<i>Asterolampra vulgaris</i>	<i>Pterotheca</i> sp. 1
<i>Actinoptychus senarius</i>	<i>Plagiogramma barbadense</i>	<i>Azpeitia tuberculata</i>	<i>Pterotheca</i> sp. 2
<i>Actinoptychus</i> sp. 1	<i>Porodiscus splendidus</i>	<i>Brightwellia hyperborea</i>	<i>Pterotheca</i> sp. 3
<i>Actinoptychus</i> sp. 2	<i>Pseudoauliscus radiatus</i>	<i>Coscinodiscus decrescens</i>	<i>Quadrocistella montana</i>
<i>Amphora</i> sp.	<i>Pseudopodosira bella</i>	<i>Coscinodiscus marginatus</i>	<i>Quadrocistella paliesa</i>
<i>Anuloplicata ornata</i>	<i>Pseudopodosira pileiformis</i>	<i>Distephanosira architecturalis</i>	<i>Quadrocistella rectagonuma</i>
<i>Arachnoidiscus clarus</i>	<i>Pseudopodosira westii</i>	<i>Distephanosira</i> sp. 1	<i>Quadrocistella</i> spp.
<i>Aulacodiscus</i> sp.	<i>Pseudopodosira</i> sp. cf. <i>P. hyalina</i>	<i>Distephanosira</i> sp. 2	<i>Syndendrium</i> sp.
<i>Auliscus johsonianus</i>	<i>Pseudopodosira</i> sp. cf. <i>P. pileiformis</i>	<i>Distephanosira</i> sp. 3	<i>Vallodiscus lanceolatus</i>
<i>Auliscus</i> sp.	<i>Pseudopodosira</i> sp. 1	<i>Hemiaulus immanis</i>	<i>Xanthiopyxis oblonga</i>
<i>Biddulphia punctata</i>	<i>Radialiplicata</i> sp.	<i>Hemiaulus polycystinorum</i> var. <i>mesolepta</i>	<i>Xanthiopyxis structuralis</i>
<i>Biddulphia tuomeyi</i>	<i>Rhaphoneis amphiceros</i>	<i>Hemiaulus reflexispinosus</i>	<i>Xanthiopyxis</i> sp. 1
<i>Biddulphia</i> sp. 1	<i>Rhaphoneis atlantica</i>	<i>Hemiaulus crenatus</i>	<i>Xanthioisthmus panduraeformis</i>
<i>Biddulphia</i> sp. 2	<i>Rhaphoneis</i> sp. 1	<i>Hemiaulus</i> sp. cf. <i>H. inaequilaterus</i>	Unknown resting spore #1
<i>Briggera</i> sp. 1	<i>Rhaphoneis</i> sp. 2	<i>Hemiaulus</i> sp.	Unknown resting spore #2
<i>Clavicula polymorpha</i>	<i>Rhaphoneis</i> sp. 3	<i>Liostephania</i> spp.	
<i>Clavularia barbadensis</i>	<i>Rhaphoneis</i> sp. 4	<i>Porpeia ornata</i>	
<i>Craspedodiscus barronii</i>	<i>Rhaphoneis</i> sp. 5	<i>Proboscia</i> sp.	
Cymatosiraceae	<i>Rutilaria areolata</i>	<i>Pyrgopyxis johnsoniana</i>	
<i>Dextradonator eximius</i>	<i>Rutilaria grevilleana</i>	<i>Pyrgopyxis prolongata</i>	
<i>Dextradonator jeremianus</i>	<i>Sheshukovia castellata</i>	<i>Riedelia claviger</i>	
<i>Diploneis</i> sp.	<i>Sheshukovia</i> sp. 1	<i>Riedelia longicornis</i>	
<i>Diplomenora cocconeiforma</i>	<i>Sheshukovia triorbica</i>	<i>Riedelia lyriformis</i>	
<i>Drepanotheca bivittata</i>	<i>Stictodiscus inflatus</i>	<i>Riedelia tenuicornis</i>	
<i>Endictya</i> sp.	<i>Stictodiscus parallelus</i>	<i>Rocella praenitida</i>	
<i>Euodia</i> sp.	<i>Strangulonema barbadense</i>	<i>Stephanopyxis superba</i>	
<i>Eunotogramma variabile</i>	<i>Thaumatonema barbadense</i>	<i>Stephanopyxis turris</i>	
<i>Eunotogramma productum</i>	<i>Thaumatonema costatum</i>	<i>Stephanopyxis</i> sp.	
<i>Eunotogramma</i> sp. cf. <i>E. laevis</i>	<i>Triceratium blanditum</i>	<i>Triceratium inconspicuum</i>	
<i>Grammatophora</i> sp.	<i>Triceratium capitatum</i>	<i>Triceratium inconspicuum</i> var. <i>trilobatum</i>	
<i>Hyalodiscus</i> sp.	<i>Triceratium denticulatum</i>	<i>Triceratium kanayae</i> var. <i>kanayae</i>	
<i>Lyrella</i> sp. aff. <i>L. praetexta</i>	<i>Triceratium irregulare</i>	<i>Triceratium kanayae</i> var. <i>quadriloba</i>	
<i>Mastogloia archaia</i>	<i>Triceratium mirificum</i>	<i>Triceratium</i> sp. aff. <i>T. favus</i>	
<i>Mastogloia barbadensis</i>	<i>Triceratium polycystinorum</i>	<i>Triceratium ventriculosum</i>	
<i>Medlinia abyssorum</i>	<i>Triceratium venosum</i>	<i>Trinacria cornuta</i>	
<i>Medlinia simbirskiana</i>	Unknown genus and species 1	<i>Trinacria subcapitata</i>	
Naviculoid diatoms		<i>Trinacria</i> sp. cf. <i>T. subcapitata</i>	
<i>Paralia crenulata</i>		<i>Trochosira</i> sp.	

Table 1. Taxonomic list of diatoms identified in this study.

Ebridians	Silicoflagellates
<i>Ammodochium rectangulare</i>	<i>Corbisema angularis</i>
<i>Ammodochium speciosum</i>	<i>Corbisema bimucronata</i>
<i>Ebriopsis cornuta</i>	<i>Corbisema hexacantha</i>
<i>Ebriopsis crenulata</i>	<i>Corbisema spinosa</i>
<i>Ebriopsis</i> sp.	<i>Corbisema triacantha</i>
' <i>Falsebria</i> ' sp.	<i>Dictyocha byronalis</i>
<i>Pseudoammodochium dictyoides</i>	<i>Naviculopsis</i> sp.

Table 2. Taxonomic list of ebridians and silicoflagellates identified in this study.

Dinoflagellates	Incertae sedis	Synurophyte scales
<i>Actiniscus pentasterias</i>	<i>‘Naviculopsis hyalina nordica’</i> sensu Ciesielski (1991)	<i>Macrora barbadensis</i>
<i>Carduifolia gracilis</i>		<i>Macrora stella</i>
<i>Peridinites sphaericus</i>		

Table 3. Taxonomic list of other siliceous microfossils indentified in this study.

	post-MECO cooling 83.0 – 61.7 mcd = ~39.98-39.53 Ma	Peak warming followed by abrupt cooling 86.3-83.0 mcd = ~40.06-39.98 Ma	Initial warming 106.2 – 86.3 mcd = ~40.52-40.06 Ma	Pre-MECO cooling ~148.5-106.2 mcd = ~41.68-40.52 Ma
	Assemblage Zone / Stage IV	Assemblage Zone / Stage III	Assemblage Zone / Stage II	Assemblage Zone / Stage I
Neritic diatoms	<i>Pseudopodosira</i> spp. <i>Paralia</i> spp. <i>Rhaphoneis</i> spp.	<i>Pseudopodosira</i> spp. <i>Paralia</i> spp. <i>Rhaphoneis</i> spp.	<i>Paralia</i> spp. <i>Pseudopodosira</i> spp. <i>Rhaphoneis</i> spp.	<i>Pseudopodosira</i> spp. (predominantly <i>P. bella</i>) <i>Paralia</i> spp. <i>Rutilaria</i> spp.
Pelagic diatoms	<i>Distephanosira</i> spp. <i>Hemiaulus</i> spp. (predominantly <i>H. immanis</i>) <i>Coscinodiscus decrescens</i> <i>Rocella praenitida</i>	<i>Hemiaulus</i> spp. <i>Distephanosira</i> spp. <i>Coscinodiscus decrescens</i> <i>Rocella praenitida</i> <i>Triceratium inconspicuum</i>	<i>Distephanosira</i> spp. <i>Hemiaulus</i> spp. (predominantly <i>H. polycystinorum</i> var. <i>mesolepta</i>) <i>Triceratium inconspicuum</i> <i>Rocella praenitida</i>	<i>Distephanosira</i> spp. <i>Hemiaulus</i> spp. <i>Rocella praenitida</i> <i>Triceratium inconspicuum</i>
Resting spores	<i>Pterotheca</i> spp. <i>Quadrocistella</i> spp. <i>Xanthiopyxis</i> spp.	Rapid variations	<i>Quadrocistella</i> spp. <i>Pterotheca</i> spp. <i>Xanthiopyxis</i> spp.	<i>Xanthiopyxis</i> spp. <i>Pterotheca</i> spp. <i>Quadrocistella</i> spp.

Table 4. Summary of taxonomic composition of diatom assemblages across the MECO event. In each cell, the most abundant taxon is listed as the first, and the least abundant as the last.

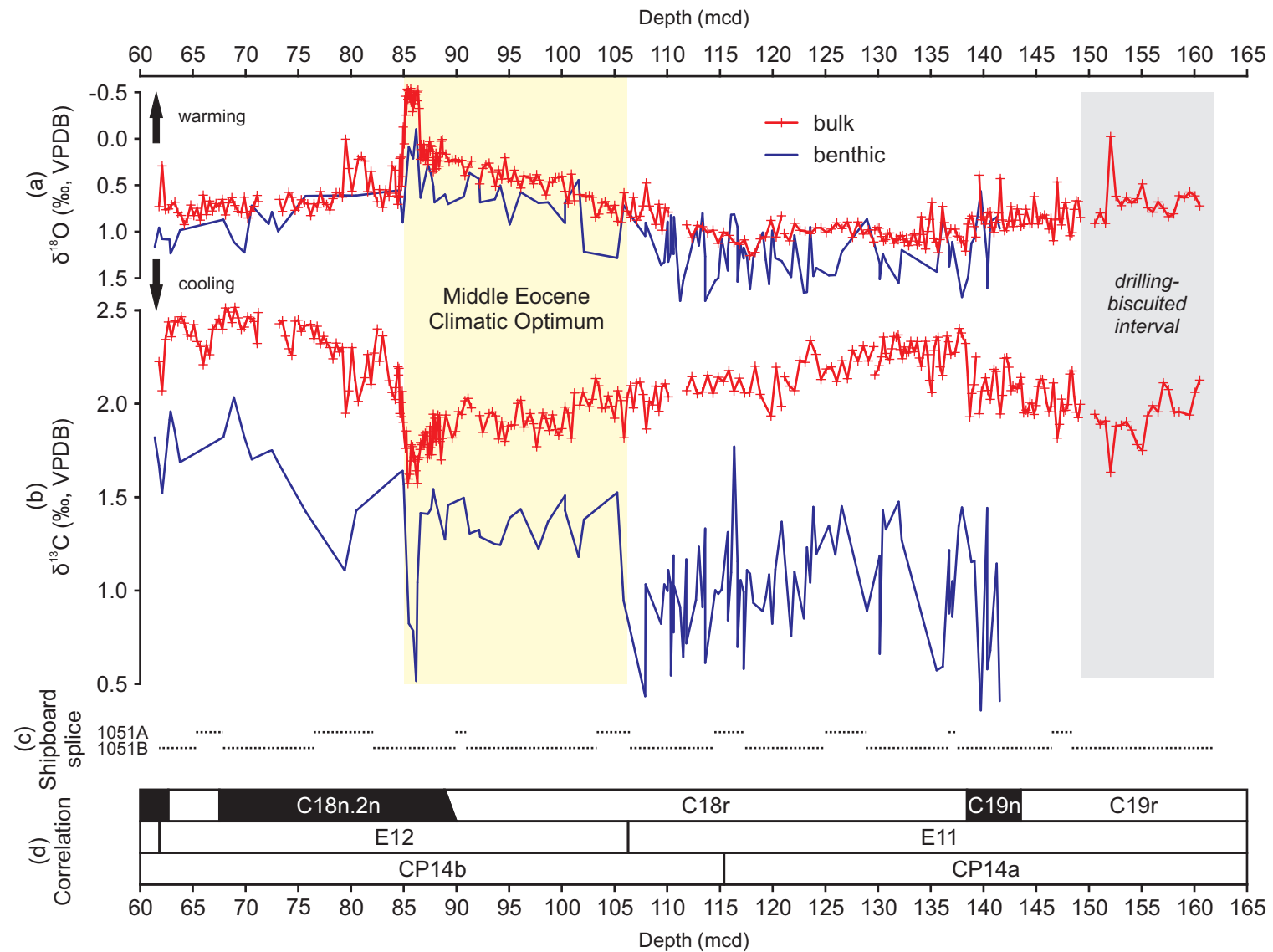


Fig. S1. ODP Site 1051 bulk-sediment and benthic $\delta^{18}\text{O}$ (a) and $\delta^{13}\text{C}$ (b) records, shipboard splice representation (Shipboard Scientific Party, 1998) (c), and magnetostratigraphic and biostratigraphic correlation of the study interval, including foraminiferal and calcareous nannofossil zones (d). Stable isotope data are from Bohaty et al. (2009) and Edgar et al. (2010). Correlation based on data from Edgar et al. (2010) and Mita (2001). Abbreviations: VPDB – Vienna Pee Dee Belemnite; mcd – meters composite depth.

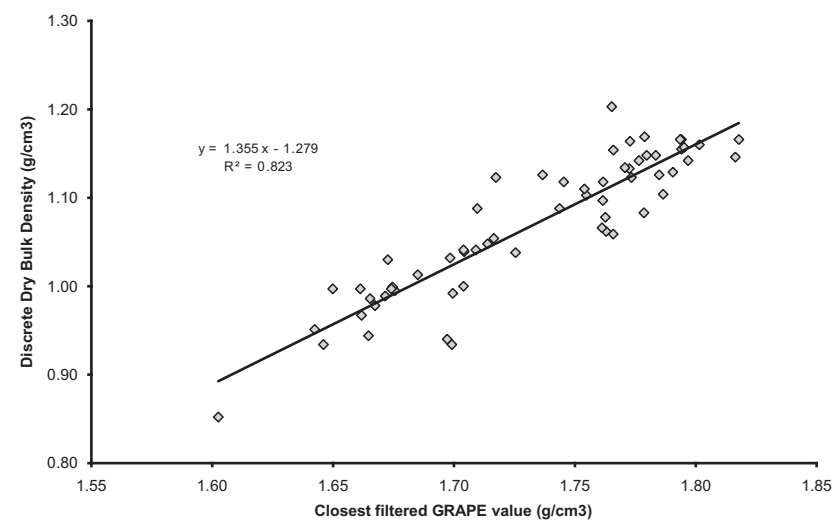


Fig. S2. Discrete dry bulk sediment density measurements (DBD) calibrated to gamma ray attenuation method (GRAPE) wet bulk sediment density estimates. Data source: Shipboard Scientific Party (1998).

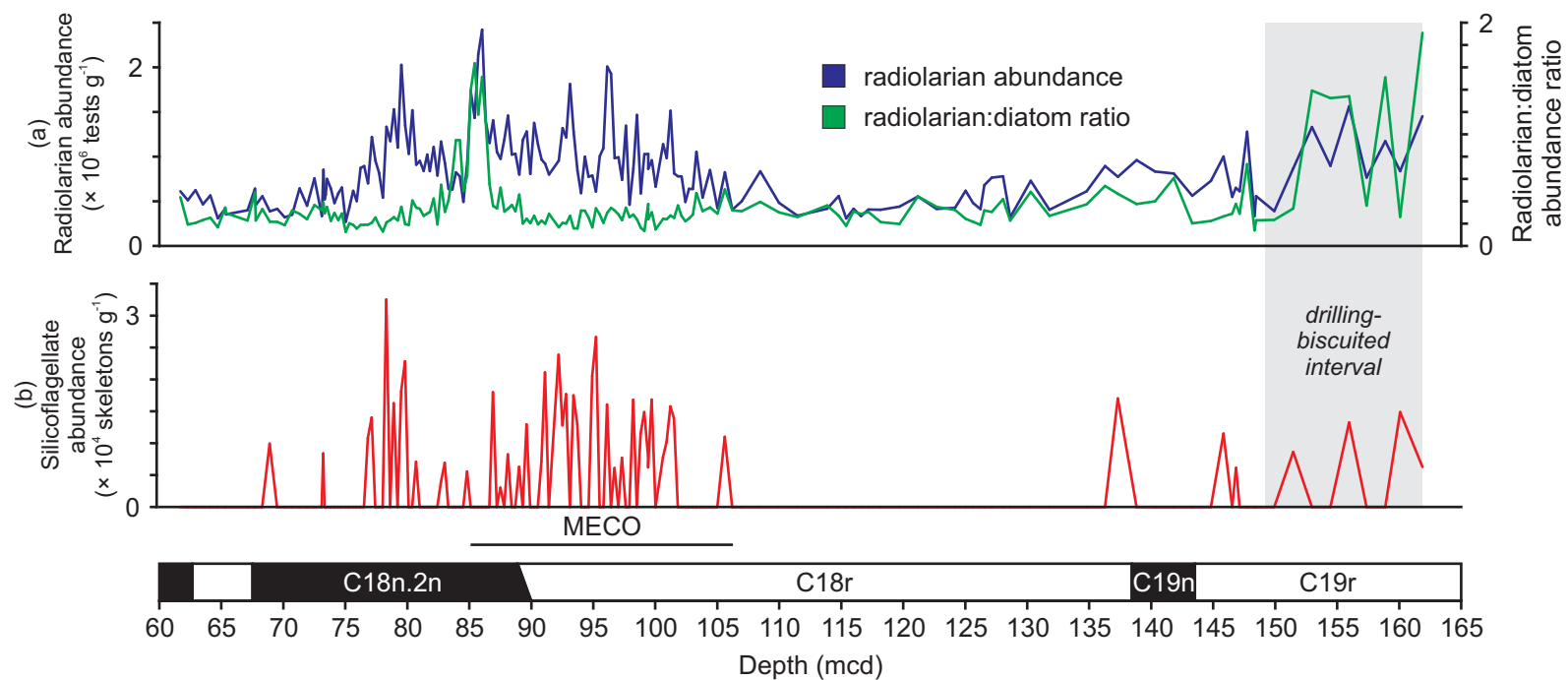


Fig. S3. ODP Site 1051 absolute abundance of radiolarians, plotted against radiolarian:diatom abundance ratio (a), and absolute abundance of silicoflagellates (b). Magnetostratigraphic correlation based on Edgar et al. (2010). Abbreviations: mcd – meters composite depth.

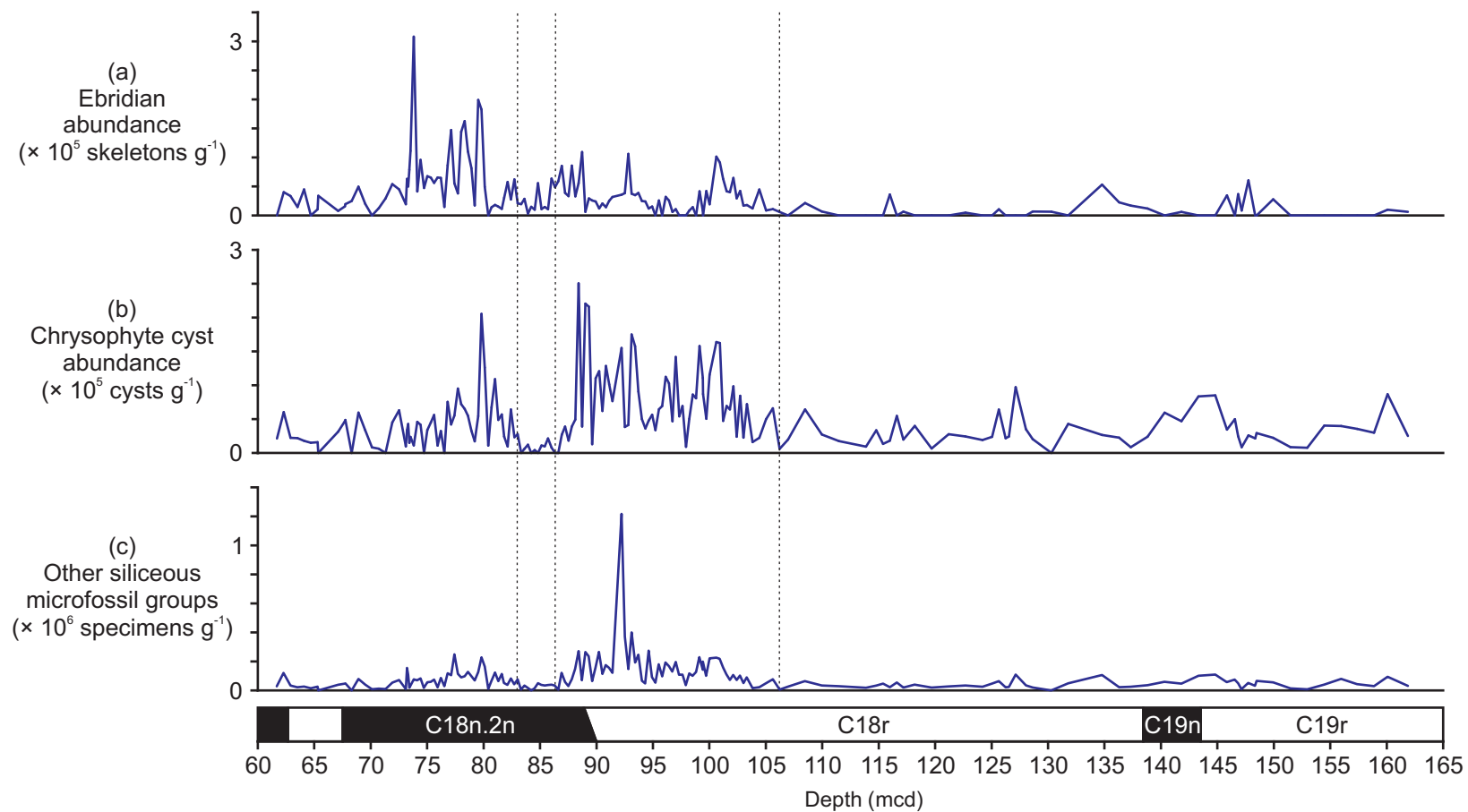


Fig. S4. Site 1051 absolute abundances of ebridians (a), chrysophyte cysts (b) and other siliceous microfossils (synurophyte scales and siliceous dinoflagellates) (c) plotted on depth axis. Magnetostratigraphic correlation based on Edgar et al. (2010).

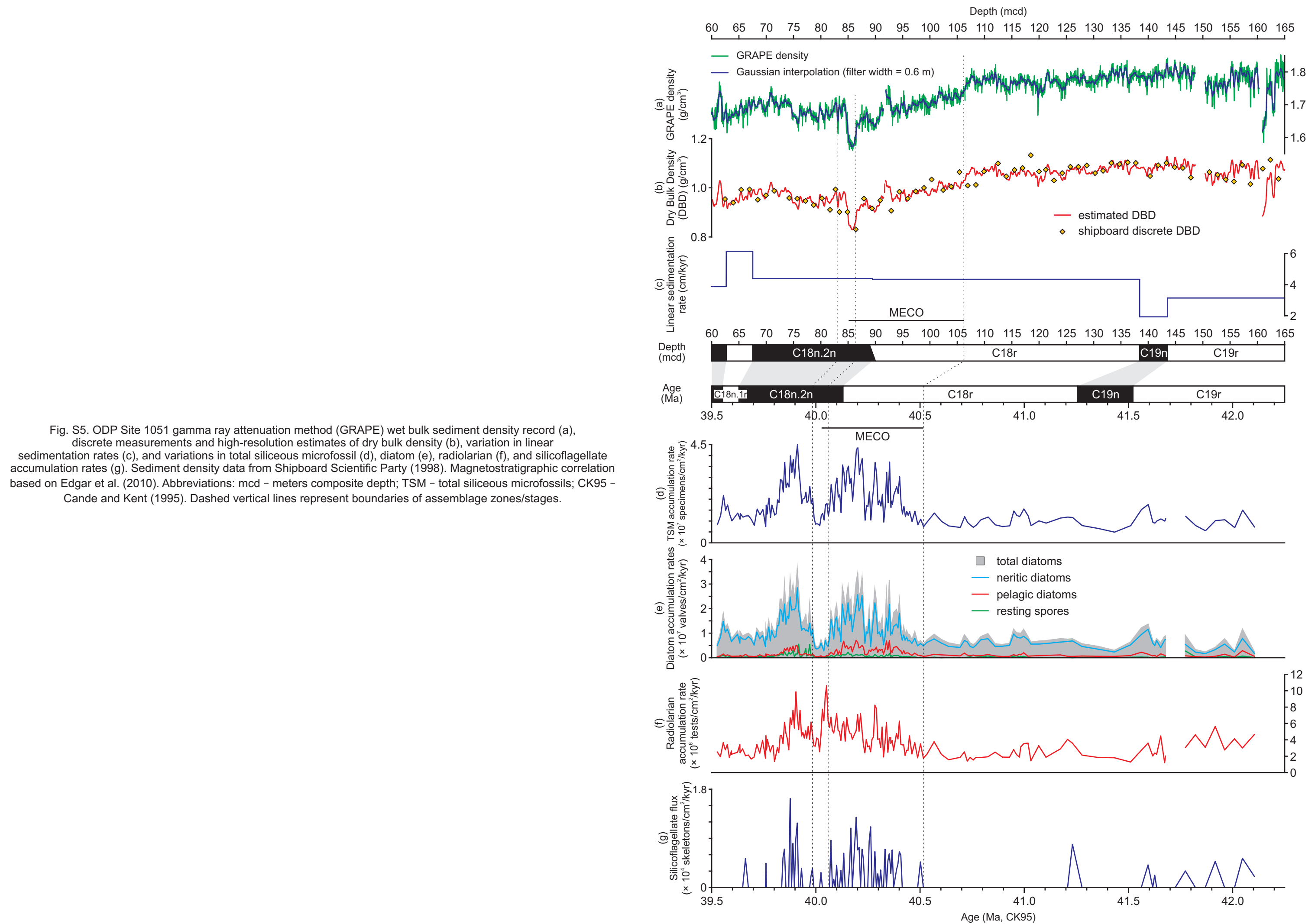


Fig. S5. ODP Site 1051 gamma ray attenuation method (GRAPE) wet bulk sediment density record (a), discrete measurements and high-resolution estimates of dry bulk density (b), variation in linear sedimentation rates (c), and variations in total siliceous microfossil (d), diatom (e), radiolarian (f), and silicoflagellate accumulation rates (g). Sediment density data from Shipboard Scientific Party (1998). Magnetostratigraphic correlation based on Edgar et al. (2010). Abbreviations: mcd – meters composite depth; TSM – total siliceous microfossils; CK95 – Cande and Kent (1995). Dashed vertical lines represent boundaries of assemblage zones/stages.

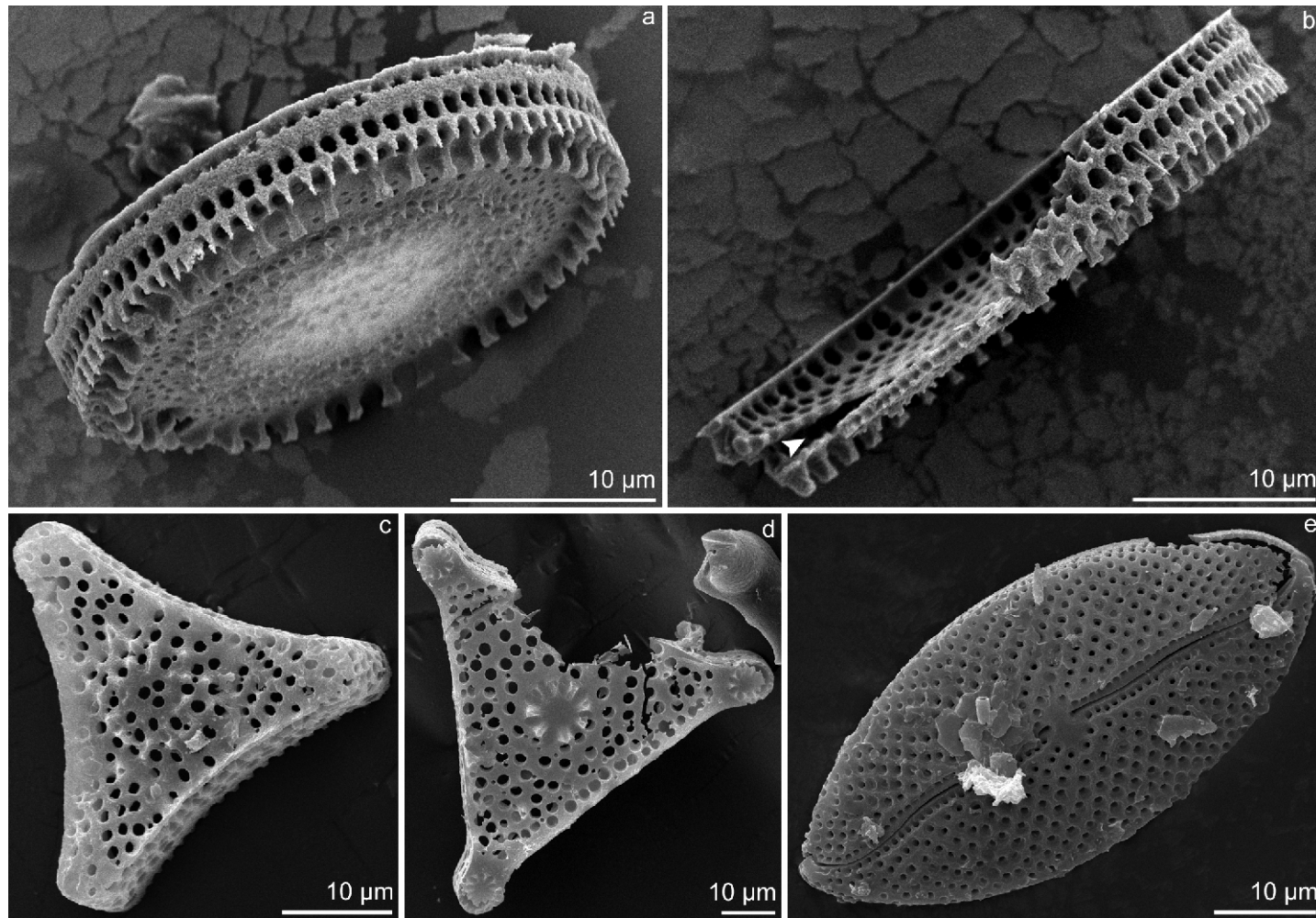


Fig. S6. Scanning electron micrographs of *Distephanosira architecturalis* from Russia, and diatoms from the MECO interval of Site 1051. (a) oblique external view of *D. architecturalis*. (b) a fractured valve of *D. architecturalis* reveals an empty chamber underneath the valve face (arrowhead). (c) *Triceratium inconspicuum*, showing minor breakage and minor dissolution (lack of fragile occlusions to the areolae). (d) *Medlinia abyssorum*, showing moderate breakage and moderate dissolution (occlusions and polar pore fields are absent). (e) *Mastogloia* sp., showing moderate breakage and dissolution.

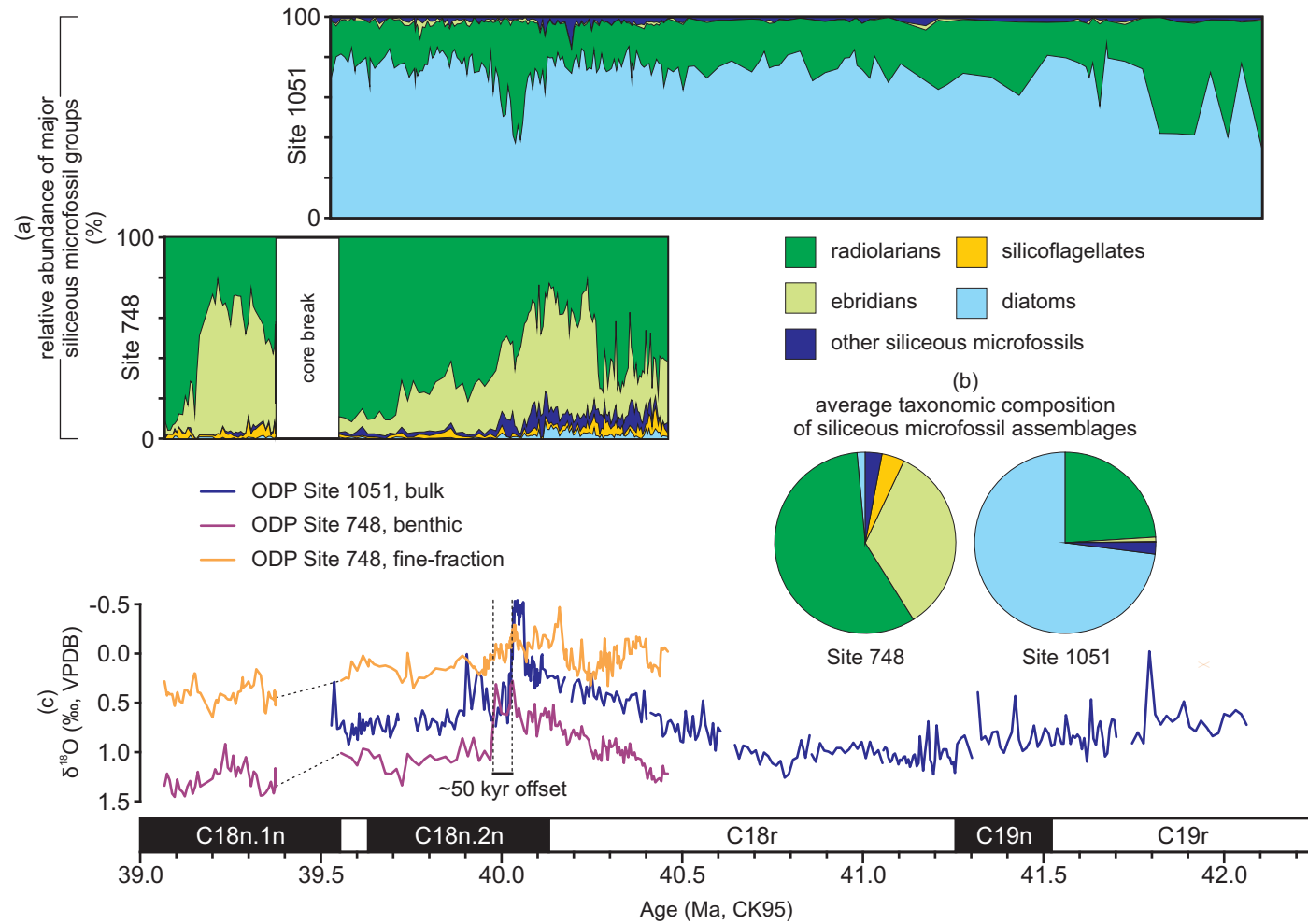


Fig. S7. Comparison of relative abundances of major siliceous microfossil groups at sites 748 and 1051 (a), comparison of average taxonomic composition of the siliceous microfossil assemblages from the MECO intervals of sites 748 and 1051 (b), and $\delta^{18}\text{O}$ records from sites 748 and 1051 showing the ~50 kyr misalignment of the peak of the MECO based on the currently available age models for each site (c). Stable isotope data are from Bohaty et al. (2009). Abbreviations: CK95 - Cande and Kent (1995).

Table S1. Site 1051 diatom abundance, recorded as total number of specimens found in the examined slide area.

[illegible]

[illegible]

[illegible]

[illegible]

Table S1 (continued).

[illegible]

[illegible]

[illegible]

[illegible]

[illegible]

								1	2	3	4	5	6	7	8	9	10	11	12	13	14	15	16	17	18	19	20	21	22	23	24	25
99.43	1051	A	10H	5	126	127	B	18	0.75							7				10												59
99.43	1051	A	10H	5	126	127	C	18	0.75			1				7				8												80
99.72	1051	B	11H	3	67	68	D	18	0.75				1			4				1				1		2						64
99.72	1051	B	11H	3	67	68	C	18	0.75			1				2				5						2						50
100.02	1051	A	10H	6	36	37	B	18	0.75							5				4						1						34
100.02	1051	A	10H	6	36	37	A	18	0.75							7				7									1			35
100.62	1051	B	11H	4	7	8	B	18	0.75				1			14				1						1	1					82
100.62	1051	B	11H	4	7	8	C	18	0.75							7		1		6				1		10						64
100.92	1051	A	10H	6	126	127	B	18	0.75				1			4		1	3							2		1				43
100.92	1051	A	10H	6	126	127	C	18	0.5							8			1					2		2						36
101.22	1051	A	10H	7	6	7	D	18	0.75							2				3					1	3						55
101.22	1051	A	10H	7	6	7	B	18	0.75				1			1		1		3												41
101.52	1051	B	11H	4	97	98	A	18	0.75							3				4							1		2			54
101.52	1051	B	11H	4	97	98	C	18	0.75			1	1			7				2						3						63
101.82	1051	B	11H	4	127	128	A	18	0.75							3				1							3					65
101.82	1051	B	11H	4	127	128	B	18	0.75							5											2					32
102.12	1051	B	11H	5	7	8	A	18	0.75							5											2					31
102.12	1051	B	11H	5	7	8	B	18	1							5				1					1		4					51
102.42	1051	B	11H	5	37	38	A	18	1.25							2				4					1		2		1			33
102.42	1051	B	11H	5	37	38	B	18	1							1				2												27
102.72	1051	B	11H	5	67	68	A	18	0.75							4				1							6					56
102.72	1051	B	11H	5	67	68	B	18	0.75							10				2							1					50
103.02	1051	B	11H	5	97	98	A	18	0.75							2				3							3					44
103.02	1051	B	11H	5	97	98	B	18	0.75							2				2												69
103.32	1051	B	11H	5	127	128	A	18	0.75							4				2							2					54
103.32	1051	B	11H	5	127	128	D	18	0.75							4																63
103.82	1051	A	11H	2	66	67	B	18	0.75							1												1				33
103.82	1051	A	11H	2	66	67	A	18	2.25							1																36
104.42	1051	A	11H	2	126	127	B	18	0.75							1									2					1		39
104.42	1051	A	11H	2	126	127	D	18	0.75							1														1		37
105.02	1051	A	11H	3	36	37	C	18	1							5													1			22
105.02	1051	A	11H	3	36	37	A	18	1.25							1																34
105.62	1051	A	11H	3	96	97	A	18	0.75				1			4													1			40
105.62	1051	A	11H	3	96	97	B	18	0.75							2		1														35
106.22	1051	A	11H	4	6	7	B	18	2							1									1							36
106.22	1051	A	11H	4	6	7	C	18	1.75																							27
106.97	1051	B	12H	2	6	7	A	18	0.75							2				1												28
106.97	1051	B	12H	2	6	7	B	18	0.75							1																48
108.47	1051	B	12H	3	6	7	C	18	1							3									1		1					61
108.47	1051	B	12H	3	6	7	D	18	1							6											1					56
109.97	1051	B	12H	4	6	7	A	18	1.5							1				1												34
109.97	1051	B	12H	4	6	7	D	18	1.5							3											1					37
111.47	1051	B	12H	5	6	7	B	18	1.5																							29
111.47	1051	B	12H	5	6	7	D	18	1.5							3				1	1											29
113.87	1051	B	12H	6	96	97	B	18	1							2				2												49
113.87	1051	B	12H	6	96	97	C	18	1																							40
114.79	1051	A	12H	3	6	7	D	18	0.75							3																18
114.79	1051	A	12H	3	6	7	B	18	0.75																							32
115.39	1051	A	12H	3	66	67	A	18	0.75										1		2											15
115.39	1051	A	12H	3	66	67	B	18	1.25							2																21
115.99	1051	A	12H	3	126	127	D	18	0.75															1		1			1			27
115.99	1051	A	12H	3	126	127	B	18	1.75							4				1					1							29
116.6	1051	A	12H	4	37	38	B	18	0.75							5																23
116.6	1051	A	12H	4	37	38	D	18	1.75							2																30
117.19	1051	A	12H	4	96	97	B	18	1.75							2											1					24
117.19	1051	A	12H	4	96	97	D	18	1.75							1																38
118.19	1051	B	13H	2	6	7	A	18	1							4																40
118.19	1051	B	13H	2	6	7	B	18	1							3																31
119.69	1051	B	13H	3	6	7	A	18	1							1				1												32
119.69	1051	B	13H	3	6	7	B	18	1											1												35
121.19	1051	B	13H	4	6	7	A	18	1							3																51
121.19	1051	B	13H	4	6	7	B	18	1							2																49
122.69	1051	B	13H	5	6	7	C	18	1							2				1								1				41
122.69	1051	B	13H	5	6	7	D	18	1							3				1												44
124.19	1051	B	13H	6	6	7	B	18	1.5							2																35
124.19	1051	B	13H	6	6	7	C	18	1.5							1				1												32
125.04	1051	A	13H	4	6	7	B	18	0.75										1													22
125.04	1051	A	13H	4	6	7	D	18	0.75							2				1												30
125.64	1051	A	13H	4	66	67	C</																									

										1	2	3	4	5	6	7	8	9	10	11	12	13	14	15	16	17	18	19	20	21	22	23	24	25
149.94	1051	B	16X	3	3	4	B	18	1.5									3				2					1		1					34
149.94	1051	B	16X	3	3	4	D	18	1.5									1		1	3						2				1			36
151.47	1051	B	16X	4	6	7	B	18	1.5																									76
151.47	1051	B	16X	4	6	7	D	18	1							1		1					1											50
152.97	1051	B	16X	5	6	7	A	18	1.5																									73
152.97	1051	B	16X	5	6	7	B	18	1.5									1																101
154.47	1051	B	16X	6	6	7	A	18	2.5									2																73
154.47	1051	B	16X	6	6	7	C	18	2.25									4																63
155.97	1051	B	16X	CC	6	7	A	18	0.75												3													59
155.97	1051	B	16X	CC	6	7	D	18	0.75				1					3																59
157.38	1051	B	17X	2	6	7	B	18	1.5									3				1												43
157.38	1051	B	17X	2	6	7	D	18	1									1																36
158.88	1051	B	17X	3	6	7	D	18	1									3																57
158.88	1051	B	17X	3	6	7	C	18	1									1																100
160.08	1051	B	17X	3	6	7	A	18	1			1						1				1												46
160.08	1051	B	17X	3	6	7	C	18	0.75									8							1									50
161.88	1051	B	17X	4	36	37	C	18	1									3																124
161.88	1051	B	17X	4	36	37	?	18	1				1					1					1						1					107

Table S3. Paleoecology of neritic diatoms recorded in the study interval of Site 1051.

Taxon	Life form	Inference based on	References
<i>Abas wittii</i>	Neritic plankton?	Reported primarily from neritic localities; Morphological adaptations	–
<i>Actinoptychus hillabyanus</i>	Benthic	Analogy to living species	Round et al. (1990)
<i>Actinoptychus intermedius</i>			
<i>Actinoptychus pericavatus</i>			
<i>Actinoptychus senarius</i>			
<i>Actinoptychus</i> sp. 1			
<i>Actinoptychus</i> sp. 2			
<i>Amphora</i> sp.	Benthic	Analogy to living species	Round et al. (1990)
<i>Anuloplicata ornata</i>	Tychoplanktic	Morphological adaptations	–
<i>Arachnoidiscus clarus</i>	Benthic	Analogy to living species	Round et al. (1990)
<i>Aulacodiscus</i> sp.	Benthic	Analogy to living species	Tiffany (2008)
<i>Auliscus johnsonianus</i>	Benthic	Analogy to living species	Round et al. (1990)
<i>Auliscus</i> sp.			
<i>Biddulphia punctata</i>	Benthic	Analogy to living species	Round et al. (1990)
<i>Biddulphia tuomeyi</i>			
<i>Biddulphia</i> sp. 1			
<i>Biddulphia</i> sp. 2			
<i>Briggera</i> sp. 1	Benthic	Reported primarily from neritic localities; Morphological adaptations	–
<i>Clavicula polymorpha</i>	Benthic	Morphological adaptations	–
<i>Clavularia barbadensis</i>	Benthic	Reported primarily from neritic localities	–
<i>Craspedodiscus barronii</i>	Neritic plankton?	Reported primarily from neritic localities	Round et al. (1990)
Cymatosiraceae	Benthic / tychoplanktic	Analogy to living species	Hasle et al. (1983)
<i>Dextradonator eximius</i>	Neritic plankton?	Reported primarily from neritic localities; Morphological adaptations	–
<i>Dextradonator jeremianus</i>			
<i>Diplomenora cocconeiforma</i>	Benthic	Analogy to living species	Blazé (1984)
<i>Diploneis</i> sp.	Benthic	Analogy to living species	Round et al. (1990)
<i>Drepanotheca bivittata</i>	Tychoplanktic?	Reported primarily from neritic localities	–
<i>Endictya</i> sp.	Benthic	Analogy to living species	Round et al. (1990)
<i>Eunotogramma variabile</i>	Benthic	Analogy to living species	Round et al. (1990)
<i>Eunotogramma productum</i>			
<i>Eunotogramma</i> sp. cf. <i>E. laevis</i>			
<i>Euodia</i> sp.	Benthic / tychoplanktic?	Morphological adaptations	–
<i>Grammatophora</i> sp.	Benthic	Analogy to living species	Round et al. (1990)
<i>Hyalodiscus</i> sp.	Benthic	Analogy to living species	Round et al. (1990)
<i>Lyrella</i> sp. aff. <i>L. praetexta</i>	Benthic	Analogy to living species	Round et al. (1990)
<i>Mastogloia archaia</i>	Benthic	Analogy to living species	Round et al. (1990)
<i>Mastogloia barbadensis</i>			
<i>Medlinia abyssorum</i>	Tychoplanktic	Reported primarily from neritic localities; Morphological adaptations	Witkowski et al. (2011a)
<i>Medlinia simbirskiana</i>			

Naviculoid diatoms	Benthic	Analogy to living genera	Round et al. (1990)
<i>Paralia crenulata</i>	Tychoplanktic	Analogy to living species	Mcquoid and Nordberg (2003)
<i>Paralia russica</i>			
<i>Paralia sulcata</i>			
<i>Paralia</i> sp.			
<i>Peponia barbadensis</i>	Benthic	Reported primarily from neritic localities	–
<i>Plagiogramma barbadense</i>	Benthic	Analogy to living species	Round et al. (1990)
<i>Porodiscus splendidus</i>	Benthic	Reported primarily from neritic localities; Morphological adaptations	–
<i>Pseudauliscus radiatus</i>	Benthic	Morphological adaptations	–
<i>Pseudopodosira bella</i>	Tychoplanktic	Analogy to living species	Tanimura and Sato (1997); Witkowski et al., (2000)
<i>Pseudopodosira pileiformis</i>			
<i>Pseudopodosira westii</i>			
<i>Pseudopodosira</i> sp. cf. <i>P. hyalina</i>			
<i>Pseudopodosira</i> sp. cf. <i>P. pileiformis</i>			
<i>Pseudopodosira</i> sp. 1			
<i>Radialiplicata</i> sp.	Tychoplanktic	Morphological adaptations	–
<i>Rhaphoneis amphiceros</i>	Benthic (reported also as tycho planktic)	Analogy to living species	Hasle and Syvertsen (1997); Sato et al. (2011)
<i>Rhaphoneis atlantica</i>			
<i>Rhaphoneis</i> sp. 1			
<i>Rhaphoneis</i> sp. 2			
<i>Rhaphoneis</i> sp. 3			
<i>Rhaphoneis</i> sp. 4			
<i>Rhaphoneis</i> sp. 5			
<i>Rutilaria areolata</i>	Neritic plankton	Analogy to living species	Ross (1995)
<i>Rutilaria grevilleana</i>			
<i>Sheshukovia castellata</i>	Benthic / tycho planktic?	Reported primarily from neritic localities; Morphological adaptations	–
<i>Sheshukovia</i> sp. 1			
<i>Sheshukovia triorbica</i>			
<i>Stictodiscus inflatus</i>	Neritic plankton?	Reported primarily from neritic localities	–
<i>Stictodiscus parallelus</i>			
<i>Strangulonema barbadense</i>	Benthic / tycho planktic?	Reported primarily from neritic localities	–
<i>Thaumatonema barbadense</i>	Benthic / tycho planktic?	Reported primarily from neritic localities	–
<i>Thaumatonema costatum</i>			
<i>Triceratium</i> sp. aff. <i>T. favus</i>	Neritic plankton	Analogy to living species	Round et al. (1990)
<i>Triceratium blanditum</i>	Most probably a group of non-congeneric taxa	Reported primarily from neritic localities; Morphological adaptations	–
<i>Triceratium capitatum</i>			
<i>Triceratium denticulatum</i>			
<i>Triceratium irregulare</i>			
<i>Triceratium mirificum</i>			
<i>Triceratium polycistinum</i>			
<i>Triceratium venosum</i>	Benthic / Tycho planktic?		
<i>Triceratium ventriculosum</i>			
Unknown genus and species 1	Benthic / tycho planktic?	Morphological adaptations	–

Table S4. Paleoecology of pelagic diatoms recorded in the study interval of Site 1051.

Taxon	Inference based on	References
<i>Asterolampra insignis</i>	Analogy to living species	Round et al. (1990); Tiffany and Hernández-Becerril (2005)
<i>Asterolampra marylandica</i>		
<i>Asterolampra</i> sp. cf. <i>A. affinis</i>		
<i>Asterolampra vulgaris</i>		
<i>Azpeitia tuberculata</i>	Analogy to living species	Round et al. (1990)
<i>Brightwellia hyperborea</i>	Global geographic distribution	–
<i>Coscinodiscus decrescens</i>	Analogy to living species	Round et al. (1990)
<i>Coscinodiscus marginatus</i>		
<i>Distephanosira architecturalis</i>	Morphological adaptations, Global geographic distribution	–
<i>Distephanosira</i> sp. 1		
<i>Distephanosira</i> sp. 2		
<i>Distephanosira</i> sp. 3		
<i>Hemiaulus crenatus</i>	Analogy to living species	Round et al. (1990)
<i>Hemiaulus immanis</i>		
<i>Hemiaulus polycystinorum</i> var. <i>mesolepta</i>		
<i>Hemiaulus reflexispinosus</i>		
<i>Hemiaulus</i> sp. cf. <i>H. inaequilaterus</i>		
<i>Hemiaulus</i> sp.		
<i>Liostephania</i> spp.	<i>Internal casts formed within valves of Asterolampra</i> spp.	Hanna and Brigger (1970)
<i>Porpeia ornata</i>	Analogy to living species	
<i>Proboscia</i> sp.	Analogy to living species	Round et al. (1990)
<i>Pyrgopyxis johnsoniana</i>	Morphological adaptations; Global geographic distribution	–
<i>Pyrgopyxis prolongata</i>		
<i>Riedelia claviger</i>	Morphological adaptations; Global geographic distribution	–
<i>Riedelia longicornis</i>		
<i>Riedelia lyriformis</i>		
<i>Riedelia tenuicornis</i>		
<i>Rocella praenitida</i>	Morphological adaptations; Global geographic distribution	–
<i>Stephanopyxis superba</i>	Analogy to living species	Round et al. (1990)
<i>Stephanopyxis turris</i>		
<i>Stephanopyxis</i> sp.		
<i>Triceratium inconspicuum</i>	Global geographic distribution	–
<i>Triceratium inconspicuum</i> var. <i>trilobatum</i>		
<i>Triceratium kanayae</i> var. <i>kanayae</i>		
<i>Triceratium kanayae</i> var. <i>quadriloba</i>		
<i>Trinacria cornuta</i>	Morphological adaptations; Global geographic distribution	–
<i>Trinacria subcapitata</i>	Morphological adaptations; Global geographic distribution	–
<i>Trochosira</i> sp.	Morphological adaptations	–

Table S5. Paleoeecology of resting spore taxa recorded in the study interval of Site 1051.

Taxon	Inference based on	References
<i>Costopyxis trochlea</i>	Morphological adaptations	Suto et al. (2009), Witkowski et al. (2011a)
<i>Pseudopyxilla</i> sp. 1		–
<i>Pterotheca aculeifera</i>		Suto et al. (2009)
<i>Pterotheca</i> sp. 1		
<i>Pterotheca</i> sp. 2		
<i>Pterotheca</i> sp. 3		
<i>Quadrocistella montana</i>		Suto (2004)
<i>Quadrocistella paliesae</i>		
<i>Quadrocistella rectagonuma</i>		
<i>Syndendrium</i> sp.		–
<i>Vallodiscus lanceolatus</i>		Suto (2005)
<i>Xanthiopyxis oblonga</i>		Fenner (1978); Suto (2006)
<i>Xanthiopyxis structuralis</i>		
<i>Xanthiopyxis</i> sp. 1		Suto (2006)
<i>Xanthioisthmus panduraeformis</i>		Suto (2004)
Unknown resting spore sp. 1		–
Unknown resting spore sp. 2		–

Table S6. Paleobiogeographic distribution of *Distephanosira architecturalis*.

Date	Reported as	Authorship	Reference		Locality	Age	Setting	Water depth
1892	<i>Melosira architecturalis</i>	Brun in Schmidt et al.	Schmidt et al.	taf. 177, figs. 45-50	Oamaru, New Zealand	late Eocene-earliest Oligocene	coastal/neritic	—
1957	<i>Cyclotella hanna</i> e	Kanaya	Kanaya	p. 82, pl. 3, figs. 19-14	Mt. Diablo Area, California	middle Eocene	coastal/neritic	—
1968	<i>Melosira architecturalis</i>	Brun in Schmidt et al.	Gleser and Sheshukova-Poretzkaya	p. 120, pl. I, fig. 3	Dniepropetrovsk district, Sumy district, Ukraine	late Eocene	coastal/neritic	—
1969	<i>Melosira architecturalis</i>	Brun in Schmidt et al.	Gleser	p. 68, p. 73, pl. IV, fig. 3	Irgiz region, Kazakhstan	late Eocene	coastal/neritic	—
1969	<i>Melosira architecturalis</i>	Brun in Schmidt et al.	Gleser and Sheshukova-Poretzkaya	pl. II, fig. 1	Ukraine	late Eocene	coastal/neritic	—
1974	<i>Melosira architecturalis</i>	Brun in Schmidt et al.	Gleser and Jouse	p. 53, pl. 1, figs. 1-3	DSDP Site 13	middle Eocene	pelagic	4588 m
1974	<i>Melosira architecturalis</i>	Brun in Schmidt et al.	Gleser et al.	pl. XXX, fig. 1; pl. XXXI, fig. 1, pl. XXXVII, fig. 2	Western Kazakhstan; NE USSR	late Eocene-early Oligocene	coastal/neritic	—
1976	<i>Melosira architecturalis</i>	Brun in Schmidt et al.	Hajós	p. 824, pl. 1, figs. 5-6	DSDP Site 280	early Oligocene	?hemipelagic	4191 m
					DSDP Site 281	late Eocene	neritic	1601 m
					DSDP Site 283	late Eocene	pelagic	4766 m
1976	<i>Melosira architecturalis</i>	Brun in Schmidt et al.	Schrader and Fenner	p. 989, pl. 14, fig. 13; pl. 29, figs. 7-8; pl. 35, fig. 14	DSDP Site 338	late Eocene-late Oligocene	pelagic	1297 m
					DSDP Site 340	late Eocene	pelagic	1217 m
1977	<i>Melosira architecturalis</i>	Brun in Schmidt et al.	Gombos	p. 595, pl. 26, figs. 5-7	DSDP Site 328B	late Eocene through late Oligocene	abyssal	5013 m
1978	<i>Melosira architecturalis</i>	Brun in Schmidt et al.	Ryan et al.	pp. 242, 244, 248	Heezen and Corsair Canyons	early middle Eocene through late Eocene	hemipelagic and pelagic	1168-1503 m
1978	Diatom sp. A	—	Bukry	pl. 16, fig. 12	DSDP Site 390A	middle Eocene	pelagic	2670 m
1978	<i>Melosira architecturalis</i>	Brun in Schmidt et al.	Schrader	tables 1-2	DSDP Site 366	late Eocene-Oligocene	pelagic	2853 m
					DSDP Site 369/369A	Oligocene	pelagic	1752 m
1978	<i>Melosira architecturalis</i>	Brun in Schmidt et al.	Dzinoridze et al.	p. 300, pl. 1, figs. 10-11	DSDP Sites 338, 340	late Eocene	as in Schrader and Fenner (1976)	
1978	<i>Melosira architecturalis</i>	Brun in Schmidt et al.	Fenner	p. 524, pl. 16, figs. 7-12	DSDP Site 356	middle Eocene	pelagic	3203 m
1979	<i>Melosira architecturalis</i>	Brun in Schmidt et al.	Dzinoridze et al.	p. 18, fig. 77 (misabeled as <i>Actinocyclus</i> sp.)	DSDP Sites 338, 340	late Eocene	as in Schrader and Fenner (1976)	
1982	<i>Stictodiscus</i> sp.	—	Tynni	p. 23, pl. 2, figs. 2, 4	Northern Finland	?Eocene	coastal/neritic	—
1983	<i>Melosira architecturalis</i>	Brun in Schmidt et al.	Gombos	p. 570	DSDP Site 512	middle Eocene	?hemipelagic	1844 m
1983	<i>Melosira architecturalis</i>	Brun in Schmidt et al.	Gombos and Ciesielski	p. 602	DSDP Site 511	late Eocene-early Oligocene	pelagic	2589 m
					DSDP Site 513	early Oligocene	pelagic	4373 m
1984	<i>Melosira architecturalis</i>	Brun in Schmidt et al.	Barron et al.	p. 156, pl. 7, figs. 1-3	Kellogg Shale	middle Eocene	coastal/neritic	—
1984a	<i>Melosira architecturalis</i>	Brun in Schmidt et al.	Fenner	p. 1264	DSDP Site 65	Oligocene/late Oligocene	pelagic	6130 m
					DSDP Site 69/69A	middle Eocene-early Oligocene	pelagic	4978 m
					DSDP Site 71A	early Oligocene	pelagic	4419 m
					DSDP Site 72	early Oligocene	pelagic	4326 m
					DSDP Site 73	early Oligocene	pelagic	4387 m
					DSDP Site 77B	early Oligocene	pelagic	4291 m
					DSDP Site 161A	early Oligocene	pelagic	4939 m
					DSDP Site 163	middle Eocene	pelagic	5230 m
DSDP Site 167	middle Eocene-early Oligocene	pelagic	3176 m					

					DSDP Site 289	late Eocene-Oligocene	pelagic	2206 m
					DSDP Site 292	early Oligocene	pelagic	2943 m
					DSDP Site 357	middle Eocene	pelagic	2086 m
1984b	<i>Melosira architecturalis</i>	Brun in Schmidt et al.	Fenner	p. 335	DSDP Site 94	early-middle Eocene	pelagic	1793 m
1984b	<i>Melosira architecturalis</i>	Brun in Schmidt et al.	Fenner	text-fig. 5	DSDP Site 274	late Oligocene	hemipelagic	3326 m
1984b	<i>Melosira architecturalis</i>	Brun in Schmidt et al.	Fenner	text-fig. 5	DSDP Site 278	middle-late Oligocene	?pelagic	3708 m
1985	<i>Melosira architecturalis</i>	Brun in Schmidt et al.	Fenner	p. 734, figs. 12.4-12.5	Global distribution	early Eocene-late Oligocene	—	—
1986	<i>Melosira architecturalis</i>	Brun in Schmidt et al.	Gleser et al.	p. 853, pl. 1, fig. 1	Ol'ga and Kronotskii Canyons	middle Eocene	?coastal/neritic	—
1986	<i>Melosira architecturalis</i>	Brun in Schmidt et al.	Ciesielski	p. 876	DSDP Site 594	middle Miocene	reworked	1204 m
1987a	<i>Melosira architecturalis</i>	Brun in Schmidt et al.	Abbott	p. 789	DSDP Site 604	middle Eocene	reworked	2361 m
1987b	<i>Melosira architecturalis</i>	Brun in Schmidt et al.	Abbott	p. 418	DSDP Site 613	middle Eocene-late Eocene	pelagic	2309 m
1987	<i>Melosira architecturalis</i>	Brun in Schmidt et al.	Gombos	p. 795	DSDP Site 605	early-middle Eocene	pelagic	2361 m
1989	<i>Melosira architecturalis</i>	Brun in Schmidt et al.	Desikachary and Sreelatha	p. 177, pl. 78, fig. 3	Oamaru, New Zealand	late Eocene-earliest Oligocene	coastal/neritic	—
1989	<i>Melosira architecturalis</i>	Brun in Schmidt et al.	Baldauf and Monjanel	p. 342	DSDP Site 112	early Oligocene	hemipelagic	3657 m
1989	<i>Melosira architecturalis</i>	Brun in Schmidt et al.	Baldauf and Pokras	p. 29	ODP Site 647	early Oligocene	hemipelagic	3869 m
					ODP Site 660	middle Eocene	pelagic	4012 m
1990	<i>Melosira architecturalis</i>	Brun in Schmidt et al.	Fenner and Mikkelsen	p. 446, pl. 1, fig. 8	ODP Site 706	early Oligocene	pelagic	2515 m
					ODP Site 707	late Eocene-early Oligocene	pelagic	1152 m
					ODP Site 708	early Oligocene	pelagic	4121 m
					ODP Site 709	late Eocene-early Oligocene	pelagic	3051 m
					ODP Site 710	early Oligocene	pelagic	3834 m
					ODP Site 711	late Eocene-early Oligocene	pelagic	4428 m
					ODP Site 713	middle Eocene	pelagic	2909 m
					ODP Site 714	late Oligocene	pelagic	2031.5 m
1991	<i>Melosira architecturalis</i>	Brun in Schmidt et al.	Fourtanier	p. 201, pl. 26, fig. 8	ODP Site 758	late Oligocene	pelagic	2923 m
1992	<i>Melosira architecturalis</i>	Brun in Schmidt et al.	Strelnikova	pl. IV, figs. 2-5	Oamaru; DSDP Site 340	middle Eocene	as in Schmidt et al. (1892), and Schrader and Fenner (1976)	
1992	<i>Melosira architecturalis</i>	Brun in Schmidt et al.	Koizumi	p. 240, pl. 1, fig. 1	Chira, Peru	late Eocene	coastal/neritic	—
1992	<i>Distephanosira architecturalis</i>	(Brun) Gleser	Gleser et al.	p. 68, pl. 56, figs. 1-9	Global distribution	early Eocene-late Oligocene	—	—
1995	<i>Melosira architecturalis</i>	Brun in Schmidt et al.	Gladenkov and Barron	p. 31, pl. 2, fig. 2	ODP Site 884	late Oligocene	pelagic	3827 m
1996	<i>Distephanosira architecturalis</i>	(Brun) Gleser	Scherer and Koç	p. 86, pl. 4, figs. 14-17	ODP Site 908	early Oligocene-late Oligocene	hemipelagic	1273 m
					ODP Site 913	late Eocene-early Oligocene	hemipelagic	3318 m
1996	<i>Distephanosira architecturalis</i>	(Brun) Gleser	Gleser	p. 395	SP-1 Borehole	middle Eocene	?coastal/neritic	—
1999	<i>Melosira architecturalis</i>	(Brun) Gleser	Shipboard Scientific Party	Table 8	ODP Site 1123	middle-late Eocene	pelagic	3290 m
2000	<i>Distephanosira architecturalis</i>	(Brun) Gleser	Harwood and Bohaty	p. 92, pl. 8, figs. b-c	McMurdo Erratics	middle Eocene-Oligocene	coastal/neritic	—
2003	<i>Distephanosira architecturalis</i>	(Brun) Gleser	Tsoy	p. 381, pl. 1, fig. 8	Ol'ga and Kronotskii Canyons	middle Eocene	?coastal/neritic	—
2003	<i>Distephanosira architecturalis</i>	(Brun) Gleser	Sanfilippo and Fourtanier	p. 13, pl. 3, fig. 5	ODP Site 1128	Oligocene	pelagic	3874 m
2004	<i>Distephanosira architecturalis</i>	(Brun) Gleser	Sluijs et al.	fig. 3	ODP Site 1170	late Eocene-early Oligocene	hemipelagic	2704 m
					ODP Site 1171	late Eocene-early Oligocene	hemipelagic	2148 m
					ODP Site 1172	late Eocene-early Oligocene	hemipelagic	2620 m
2010	<i>Melosira architecturalis</i>	Brun in Schmidt et al.	Renaudie et al.	pp. 123-126	ODP Site 1260	middle Eocene	hemipelagic	2549 m
2011	<i>Distephanosira architecturalis</i>	Brun in Schmidt et al.	Bohaty et al.	p. 103, fig. 14-9	SHALDRIL II Site NBP0602A-3	late Eocene	coastal/neritic	340 m
2012	<i>Distephanosira architecturalis</i>	(Brun) Gleser	Witkowski et al.	pl. IV, figs. 5a-b	ODP Site 748B	middle Eocene	pelagic	1290 m
2012	<i>Distephanosira architecturalis</i>	(Brun) Gleser	Manchester et al.	p. 470, pl. 1, fig. 10	Punta Parinas vicinity	early Oligocene	reworked	—
2013	<i>Distephanosira architecturalis</i>	(Brun) Gleser	Gladenkov	p. 102	Il'Pinskii Peninsula, Kamchatka	middle Eocene	coastal/neritic	—
in press	<i>Distephanosira architecturalis</i>	(Brun) Gleser	Barron et al.	p. 26, pl. 4, fig. 20	ODP Site 1090	late Eocene	pelagic	3700 m
unpubl.	<i>Distephanosira architecturalis</i>	(Brun) Gleser	Bohaty, Barron, Fourtanier	—	ODP Site 1218	middle Eocene	pelagic	4828 m
unpubl.	<i>Distephanosira architecturalis</i>	(Brun) Gleser	Witkowski	—	Boromlya, Kursk district	late Eocene	coastal/neritic	—

Table S7. List of deep-sea sites, where *Distephanosira architecturalis* is reported as absent.

Date	Reference		Locality	Age	Setting	Water depth
1984a	Fenner	p. 1264	DSDP Site 216	middle Eocene-Oligocene	pelagic	2237 m
			DSDP Site 217	middle Eocene-Oligocene	pelagic	3010 m
			DSDP Site 220	middle Eocene	pelagic	4034 m
1990	Fenner and Mikkelsen	p. 446	DSDP Site 219	middle Eocene-late Eocene	pelagic	1764 m
			DSDP Site 236	late Eocene	pelagic	4504 m

Table S8. Paleobiogeographic distribution of *Triceratium inconspicuum* .

Date	Taxon	Authorship	Reference		Locality	Age	Setting	Water depth
1861	<i>Triceratium inconspicuum</i>	Greville	Greville	p. 70, pl. VIII, fig. 10	Barbadoes deposit	?middle Eocene (maximum age from Saunders et al., 1984)	?pelagic	—
1887	<i>Triceratium inconspicuum?</i>	Greville	Schmidt et al.	taf. 77, figs 25-28	Springfield, Barbadoes	?middle Eocene (maximum age from Saunders et al., 1984)	?pelagic	—
1949	<i>Triceratium inconspicuum</i>	Greville	Proschkina-Lavrenko et al.	p. 166, tab. 62, fig. 6	Kharkovskiy Yarus, Starobel'sk, Voroshilovgrad district	lower Oligocene (probably misdated)	coastal	—
1957	<i>Triceratium (Amphitetras) inconspicuum</i>	Greville	Kanaya	p. 103, pl. 7, fig. 8	Mt. Diablo area, California	middle Eocene	coastal	—
1976	<i>Triceratium inconspicuum</i>	Greville	Schrader and Fenner	p. 1003	DSDP Site 338	late Eocene	pelagic	1297 m
1978	<i>Triceratium inconspicuum</i> var. <i>trilobata</i>	Fenner	Fenner	p. 534, pl. 30, figs 23-26	DSDP Site 356	middle Eocene	pelagic	3203 m
1983	<i>Triceratium inconspicuum</i> var. <i>trilobata</i>	Fenner	Gombos	p. 571	DSDP Site 512	middle Eocene	hemipelagic	1844 m
1984b	<i>Triceratium inconspicuum</i> var. <i>trilobata</i>	Fenner	Fenner	text-figs. 2-3	DSDP Site 94	middle Eocene	pelagic	1793 m
					DSDP Site 149	middle Eocene	pelagic	3972 m
					DSDP Site 390A	middle Eocene	pelagic	2670 m
1984	<i>Triceratium inconspicuum</i> var. <i>trilobata</i>	Fenner	Barron et al.	p. 158, pl. 6, figs 6-7	Kellogg Shale, California	middle Eocene	coastal	—
1984a	<i>Triceratium inconspicuum</i>	Greville	Fenner	p. 1265	DSDP Site 357	middle Eocene	pelagic	2086 m
					DSDP Site 163	middle Eocene	pelagic	5230 m
					DSDP Site 289	late Eocene	pelagic	2206 m
					DSDP Site 220	middle Eocene	pelagic	4034 m
1985	<i>Triceratium inconspicuum</i> var. <i>trilobata</i>	Fenner	Fenner	p. 740, fig. 8.12-8.16	DSDP Site 13	middle Eocene	pelagic	4588 m
					DSDP Site 94	middle Eocene	pelagic	1793 m
					DSDP Site 108	middle Eocene	pelagic	1855 m
					DSDP Site 390A	middle Eocene	pelagic	2670 m
1992	<i>Triceratium inconspicuum</i> var. <i>trilobata</i>	Fenner	Harwood and Maruyama	p. 708	ODP Site 748	middle Eocene	pelagic	1290 m
1986	<i>Lisitzinia inconspicua</i> var. <i>trilobata</i>	(Fenner) Gleser	Gleser et al.	p. 858, pl. I, figs 4a-b	Ol'ga and Kronotskii Canyons, eastern Kamchatka	middle Eocene	coastal	—
1989	<i>Triceratium inconspicuum</i>	Greville	Baldauf and Pokras	p. 29	ODP Site 660	middle Eocene	pelagic	4327 m
1989	<i>Lisitzinia inconspicua</i> var. <i>trilobata</i>	Fenner	Shipboard Scientific Party	p. 179	ODP Site 753	middle Eocene	pelagic	1176 m
1996	<i>Triceratium inconspicuum</i>	Greville	Scherer and Koç	p. 89, pl. 8, fig. 4	ODP Site 908	early/late Oligocene	reworked	1273 m
					ODP Site 913	middle Eocene	hemipelagic	3318 m
2000	<i>Triceratium inconspicuum</i> var. <i>trilobata</i>	Fenner	Harwood and Bohaty	p. 94, pl. 4, fig. L	MTD-95 erratic, McMurdo Sound, Antarctica	middle Eocene	?coastal	—
2002	<i>Lisitzinia inconspicua</i>	(Greville) Gleser	Olshynskaya	p. 122, pl. II, figs 7-8; pl. III, figs 1-2	Nikol'skoe, Ukraine	Eocene	coastal	—
2003	<i>Lisitzinia inconspicua</i> var. <i>trilobata</i>	Gleser	Tsoy	p. 381, figs 2a,b	Ol'ga and Kronotskii Canyons, eastern Kamchatka	middle Eocene	coastal	—
2009	<i>Triceratium inconspicuum</i> var. <i>trilobata</i>	Fenner	Stickley et al.	p. 12	ODP Site 1172	middle-late Eocene	hemipelagic	2620 m
2010	<i>Triceratium inconspicuum</i>	Greville	Renaudie et al.	pp. 123-126	ODP Site 1260A	middle Eocene	hemipelagic	2549 m
2012	<i>Triceratium inconspicuum</i> var. <i>trilobata</i>	Fenner	Witkowski et al.	pl. IV, figs 4a-b	ODP Site 748	middle Eocene	pelagic	1290 m
2013	<i>Triceratium inconspicuum</i> var. <i>trilobata</i>	Fenner	Gladnikov	p. 102, pl. I, figs. 1a-b	Il'pinskiy Peninsula, Kamchatka	early Eocene	coastal	—
unpubl.	<i>Triceratium inconspicuum</i> var. <i>trilobata</i>	Fenner	Bohaty et al.	—	ODP Site 1218	middle Eocene	pelagic	4828 m
unpubl.	<i>Triceratium inconspicuum</i>	Greville	Witkowski	—	ODP Site 1050	middle Eocene	pelagic	2300 m

Table S9. List of deep-sea sites, where *Triceratium inconspicuum* is reported as absent.

Date	Reference		Locality	Age	Setting	Water depth
1984a	Fenner	p. 1265	DSDP Site 73	middle Eocene	pelagic	4387 m
			DSDP Site 167	middle Eocene	pelagic	3176 m
			DSDP Site 216	Eocene	pelagic	2237 m
			DSDP Site 217	middle Eocene	pelagic	3010 m

Table S10. Paleobiogeographic distribution of *Hemiaulus polycystinorum* var. *mesolepta* .

Date	Taxon	Authorship	Reference		Locality	Age	Setting	Water depth
1884	<i>Hemiaulus polycystinorum</i> var. <i>mesolepta</i>	Grunow	Grunow	p. 65, pl. II(B), fig. 43	Barbadoes deposit	?middle Eocene (maximum age from Saunders et al., 1984)	?pelagic	—
1957	<i>Hemiaulus polycystinorum</i> var. <i>mesolepta</i>	Grunow	Kanaya	pp. 104-105, pl. VII, figs. 12-15	Mt. Diablo Area	middle Eocene	coastal	—
1978	<i>Hemiaulus polycystinorum</i> var. <i>mesolepta</i>	Grunow	Fenner	p. 521, pl. 23, fig. 5, pl. 24, fig. 7	DSDP Site 356	middle Eocene	pelagic	3203 m
1984a	<i>Hemiaulus polycystinorum</i> var. <i>mesolepta</i>	Grunow	Fenner	p. 1264	DSDP Site 167	middle-late Eocene	pelagic	3176 m
					DSDP Site 289	late Eocene	pelagic	2206 m
					DSDP Site 357	middle Eocene	pelagic	2086 m
1984	<i>Hemiaulus polycystinorum</i> var. <i>mesolepta</i>	Grunow	Barron et al.	p. 156, pl. 8, fig. 5	Kellogg Shale	middle Eocene	coastal	—
1985	<i>Hemiaulus polycystinorum</i> var. <i>mesolepta</i>	Grunow	Fenner	p. 733, fig. 8.10	DSDP Site 149	middle Eocene	pelagic	3972 m
					DSDP Site 338	middle Eocene	pelagic	1297 m
					DSDP Site 356	middle Eocene	pelagic	3203 m
					DSDP Site 366	middle Eocene-early Oligocene	pelagic	2853 m
					DSDP Site 366A	late Oligocene	pelagic	2853 m
					DSDP Site 369	Oligocene	pelagic	1752 m
1990	<i>Hemiaulus polycystinorum</i> var. <i>mesolepta</i>	Grunow	Fenner and Mikkelsen	p. 444	ODP Site 707	late Eocene/early Oligocene	pelagic	1152 m
					ODP Site 713A	middle Eocene	pelagic	2909 m
1999	<i>Hemiaulus polycystinorum</i> var. <i>mesolepta</i>	Grunow	Shipboard Scientific Party	p. 21	ODP Site 1123	middle-late Eocene	pelagic	3290 m

Table S11. List of deep-sea sites, where *Hemiaulus polycystinorum* var. *mesolepta* is reported as absent.

Date	Reference		Locality	Age	Setting	Water depth
1984a	Fenner	p. 1264	DSDP Site 64A	Eocene-early Oligocene	pelagic	2052 m
			DSDP Site 65	Eocene-Oligocene	pelagic	6130 m
			DSDP Site 69	Eocene-early Oligocene	pelagic	4978 m
			DSDP Site 71	Early Oligocene	pelagic	4419 m
			DSDP Site 72	Early Oligocene	pelagic	4326 m
			DSDP Site 77B	Early Oligocene	pelagic	4291 m
			DSDP Site 161A	late Eocene-early Oligocene	pelagic	4939 m
			DSDP Site 163	middle Eocene-early Oligocene	pelagic	5230 m
			DSDP Site 292	early Oligocene	pelagic	2943 m

Table S12. Paleobiogeographic distribution of *Coscinodiscus decrescens*.

Date	Taxon	Authorship	Reference		Locality	Age	Setting	Water depth
1878	<i>Coscinodiscus decrescens</i>	Grunow	Schmidt et al.	taf. 61, figs. 8-9	Springfield, Barbadoes	?middle Eocene	?pelagic	—
1969	<i>Coscinodiscus decrescens</i> var. <i>decrescens</i>	?Gleser	Gleser	pl. II, fig. 2	Turgai Depression	late Eocene	coastal	—
1974	<i>Coscinodiscus decrescens</i>	Grunow	Gleser et al.	pl. XXV, fig. 1	Western Siberia	late Eocene	—	—
1978	<i>Coscinodiscus decrescens</i>	Grunow	Fenner	p. 514, pl. 7, fig. 4	DSDP Site 356	middle Eocene	pelagic	3203 m
1984a	<i>Coscinodiscus decrescens</i>	Grunow	Fenner	p. 1261	DSDP Site 357	middle Eocene	pelagic	2086 m
					DSDP Site 64A	Eocene-early Oligocene	pelagic	2052 m
					DSDP Site 65	late Eocene	pelagic	6130 m
					DSDP Site 69	early Oligocene	pelagic	4978 m
					DSDP Site 73	early Oligocene	pelagic	4387 m
					DSDP Site 77B	early Oligocene	pelagic	4291 m
					DSDP Site 161A	Eocene	pelagic	4939 m
					DSDP Site 167	middle-late Eocene	pelagic	3176 m
					DSDP Site 289	late Eocene	pelagic	2206 m
					DSDP Site 217	late Eocene	pelagic	3010 m
2003	<i>Coscinodiscus decrescens</i>	Grunow	Tsoy	p. 380	Kronotskii Bay	middle Eocene	coastal	—
2007	<i>Coscinodiscus decrescens</i>	Grunow	Danelian et al.	fig. 7c	ODP Site 1259	middle Eocene	pelagic	2354 m

Table S13. List of deep-sea sites, where *Coscinodiscus decrescens* is reported as absent.

Date	Reference		Locality	Age	Setting	Water depth
1984a	Fenner	p. 1261	DSDP Site 71A	early Oligocene	pelagic	4419 m
			DSDP Site 72	ealry Oligocene	pelagic	4326 m
			DSDP Site 163	middle Eocene	pelagic	5230 m
			DSDP Site 292	early Oligocene	pelagic	2943 m
			DSDP Site 216	Eocene-Oligocene	pelagic	2237 m

Table S14. Paleobiogeographic distribution of *Rocella praenitida*.

Date	Taxon	Authorship	Reference		Locality	Age	Setting	Water depth
1976	<i>Coscinodiscus praenitidus</i>	Fenner	Schrader and Fenner	p. 972, pl. 14, figs 7-9, 12; pl. 35, fig. 24; pl. 36, fig. 5	DSDP Site 338	late Oligocene	pelagic	1297 m
1978	<i>Coscinodiscus praenitidus</i>	Fenner	Fenner	p. 516, pl. 1, figs 6, 9, 15; pl. 3, fig. 3	DSDP Site 356	middle Eocene	pelagic	3203 m
1978	<i>Coscinodiscus praenitidus</i>	Fenner	Schrader	table 2	DSDP Site 369A	Oligocene	pelagic	1752 m
1978	<i>Stictodiscus?</i> sp.	—	Bukry	pl. 16, fig. 5	DSDP Site 390A	middle Eocene	pelagic	2670 m
1983a	<i>Coscinodiscus praenitidus</i>	Fenner	Gombos	p. 569	DSDP Site 512	middle Eocene	hemipelagic	1844 m
1983	<i>Coscinodiscus praenitidus</i>	Fenner	Gombos and Ciesielski	p. 601, pl. 22, figs 4-5	DSDP Site 513	late Oligocene	pelagic	4373 m
1983b	<i>Coscinodiscus praenitidus</i>	Fenner	Gombos	p. 799	DSDP Site 515	late Oligocene	hemipelagic	4252 m
1986	<i>Rocella praenitida</i>	(Fenner) Fenner	Kim and Barron	p. 177	San Hilario, Baja California Sur, Mexico	late Oligocene	?neritic	—
1986	<i>Coscinodiscus praenitidus</i>	Fenner	Ciesielski	p. 876, pl. 6, fig. 11	DSDP Site 594	middle Miocene	reworked	1204 m
1987	<i>Coscinodiscus praenitidus</i>	Fenner	Abbott	p. 789	DSDP Site 604	?middle Eocene	?reworked	2361 m
1988	<i>Coscinodiscus praenitidus</i>	Fenner	Machare et al.	p. 35	Cerro Callejon de Piedra	early Miocene	neritic	—
1989	<i>Rocella praenitida</i>	(Fenner) Fenner	Baldauf and Monjanel	p. 342	DSDP Site 112 ODP Site 647	early Oligocene	hemipelagic hemipelagic	3657 m 3869 m
1996	<i>Rocella praenitida</i>	(Fenner) Fenner	Scherer and Koç	p. 88, pl. 7, figs 9-11	ODP Site 908	early-late Oligocene	hemipelagic	1273 m
2000	<i>Rocella praenitida</i>	(Fenner) Fenner	Scherer et al.	p. 436, pl. 5, fig. 2	CRP-2/2A	late Oligocene-early Miocene	hemipelagic	178 m
2001	<i>Rocella praenitida</i>	(Fenner) Fenner	Harwood and Bohaty	p. 329, pl. 5, figs 4-5	CRP-3	early Oligocene	neritic	295 m
2003	<i>Rocella praenitida</i>	(Fenner) Fenner	Sanfilippo and Fourtanier	p. 13	ODP Site 1128	early Oligocene	pelagic	3874 m
2011	<i>Rocella praenitida</i>	(Fenner) Fenner	Bohaty et al.	p. 106, fig. 14.5-14.7	SHALDRIL II Site NBP0602A-3	late Eocene	coastal/neritic	340 m
2012	<i>Rocella praenitida</i>	(Fenner) Fenner	Prema and Desikachary	p. 67, figs 6, 9	DSDP Site 212	middle Eocene	pelagic	6243 m
in press	<i>Rocella praenitida</i>	(Fenner) Fenner	Barron et al.	pl. 4, fig. 11	ODP Site 1090	Oligocene	pelagic	3700 m

Table S15. List of deep-sea sites, where *Rocella praenitida* is reported as absent.

Date	Reference		Locality	Age	Setting	Water depth
unpubl.	Witkowski	—	ODP Site 748	middle Eocene	pelagic	1290 m
			ODP Site 749	middle Eocene	pelagic	1203 m

Supplementary references

- Abbott, W.H., 1987a. Diatom occurrences, Deep Sea Drilling Project Site 604. In: van Hinte, J.E., Wise, S.W., Jr., et al. (Eds.), Initial Reports of the Deep Sea Drilling Project 93, 789-792. doi: 10.2973/dsdp.proc.93.125.1987
- Abbott, W.H., 1987b. Diatom occurrences, Deep Sea Drilling Project Sites 612 and 613. In: Poag, C.W., Watts, A.B., et al. (Eds.), Initial Reports of the Deep Sea Drilling Project 95, 417-418. doi: 10.2973/dsdp.proc.95.113.1987
- Baldauf, J.G., Monjanel, A.-L., 1989. An Oligocene diatom biostratigraphy for the Labrador Sea: DSDP Site 112 and ODP Hole 647A. In: Srivastava, S.P., Arthur, M., Clement, B., et al. (Eds.), Proceedings of the Ocean Drilling Program, Scientific Results 105, 323-347. doi: 10.2973/odp.proc.sr.105.129.1989
- Baldauf, J.G., Pokras, E.M., 1989. Diatom biostratigraphy of Leg 108 sediments: Eastern Tropical Atlantic Ocean. In: Ruddiman, W., Sarntheim, M., et al. (Eds.), Proceedings of the Ocean Drilling Program, Scientific Results 108, 23-34. doi: 10.2973/odp.proc.sr.108.123.1989
- Baldauf, J.G., Clement, B., Aksu, A.E., de Vernal, A., Firth, J., Hall, F., Head, M.J., Jarrard, R., Kaminski, M.A., Lazarus, D., Monjanel, A.-L., Berggren, W.A., Gradstein, F., Knuttel, S., Mudie, P., Russell, M.D., Jr., 1989. Magnetostratigraphic and biostratigraphic synthesis of Ocean Drilling Program Leg 105: Labrador Sea and Baffin Bay. In: Srivastava, S.P., Arthur, M., Clement, B., et al. (Eds.), Proceedings of the Ocean Drilling Program, Scientific Results 105, 935-956. doi: 10.2973/odp.proc.sr.105.165.1989
- Barron, J.A., Bukry, D., Gersonde, R., in press. Diatom and silicoflagellate biostratigraphy for the late Eocene: ODP 1090 (sub-Antarctic Atlantic). Nova Hedwigia Beiheft.
- Barron, J.A., Bukry, D., Poore, R.Z., 1984. Correlation of the middle Eocene Kellogg Shale of northern California. Micropaleontology 30, 138-170.
- Blazé, K.L., 1984. Morphology and taxonomy of *Diplomenora* gen. nov. (Bacillariophyta). British Phycological Journal 19, 217-225.
- Bohaty, S.M., Zachos, J.C., Florindo, F., Delaney, M.L., 2009. Coupled greenhouse warming and deep-sea acidification in the middle Eocene. Paleoclimatology 24, PA2207. doi: 10.1029/2008PA001676
- Bohaty, S.M., Kulhanek, D.W., Wise, S.W., Jr., Jemison, K., Warny, S., Sjunneskog, C., 2011. Age assessment of Eocene-Pliocene drill cores recovered during SHALDRILL II Expedition, Antarctic Peninsula. In: Anderson, J.B., Wellner, J.S. (Eds.), Tectonic, Climatic and Cryospheric Evolution of the Antarctic Peninsula, Special Publication 063, American Geophysical Union. doi: 10.1029/2010SP001049.
- Bukry, D., 1978. Cenozoic coccolith, silicoflagellate, and diatom biostratigraphy, Deep Sea Drilling Project, Leg 44. In: Benson, W.E., Sheridan, R.E., et al. (Eds.), Initial Reports of the Deep Sea Drilling Project 44, 807-863. doi:10.2973/dsdp.proc.44.137.1978
- Cande, S.C., Kent, D.V., 1995. Revised calibration of the geomagnetic polarity timescale for the Late Cretaceous and Cenozoic. Journal of Geophysical Research 100, 6093-6095.
- Ciesielski, P.F., 1986. Middle Miocene to Quaternary diatom biostratigraphy of Deep Sea Drilling Project Site 594, Chatham Rise, Southwest Pacific. In: Kennett, J.P., von der Borch, C.C., et al. (Eds.), Initial Reports of the Deep Sea Drilling Project 90, 863-885. doi: 10.2973/dsdp.proc.90.115.1986
- Danelian, T., Saint Martin, S., Blanc-Valleron, M.-M., 2007. Middle Eocene radiolarian and diatom accumulation in the equatorial Atlantic (Demerara Rise, ODP Leg 207). Possible links with climatic

and palaeoceanographic changes. *Comptes Rendus Palevol* 6, 103-114. doi: 10.1016/j.crpv.2006.08.002

Desikachary, T.V., Sreelatha, P., 1989. Oamaru Diatoms. *Bibliotheca Diatomologica* Band 19. J. Cramer, Berlin – Stuttgart, 330 pp, 145 pls.

Dzinoridze, R.N., Jousé, A.P., Koroleva-Golikova, G.S., Kozlova, G.E., Nagaeva, G.S., Petrushevskaya, M.G., Strelnikova, N.I., 1978. In: Talwani, M., Udintsev, G., et al. (Eds.), Initial Reports of the Deep Sea Drilling Project 38 Supplement, 289-427. doi:10.2973/dsdp.proc.38394041s.119.1978

Dzinoridze, R.N., Jousé, A.P., Strelnikova, N.I., 1979. Description of the diatoms. In: Ushakov, P.V. (Ed.), The history of the microplankton of the Norwegian Sea, Nauka, Moskva, 32-70 (in Russian).

Edgar, K.M., Wilson, P.A., Sexton, P.F., Gibbs, S.J., Roberts, A.P., Norris, R.D., 2010. New biostratigraphic, magnetostratigraphic and isotopic insights into the Middle Eocene Climatic Optimum in low latitudes. *Palaeogeography, Palaeoclimatology, Palaeoecology* 297, 670-682. doi: 10.1016/j.palaeo.2010.09.016

Fenner, J., 1978. Cenozoic diatom biostratigraphy of the equatorial Southern Atlantic Ocean. In: Perch-Nielsen, K., Supko, P.R., et al. (Eds.), Initial Reports of the Deep Sea Drilling Project 39 Supplement, 491-624. doi: 10.2973/dsdp.proc.38394041s.201.1978

Fenner, J., 1984a. Middle Eocene to Oligocene planktonic diatom stratigraphy from deep sea drilling sites in the South Atlantic, Equatorial Pacific, and Indian Oceans. In: Hay, W.W., Sibuet, J.-C., et al., Initial Reports of the Deep Sea Drilling Project 75, 1245-1271. doi: 10.2973/dsdp.proc.75.149.1984

Fenner, J., 1984b. Eocene-Oligocene planktic diatom stratigraphy in the low latitudes and the high southern latitudes. *Micropaleontology* 30, 319-342.

Fenner, J., 1985. Late Cretaceous to Oligocene planktic diatoms. In: Bolli, H.M., Saunders, J.B., Perch-Nielsen, K. (Eds.), *Plankton stratigraphy*, Cambridge University Press, Cambridge, 713-762.

Fenner, J., Mikkelsen, N., 1990. Eocene-Oligocene diatoms in the Western Indian Ocean: taxonomy, biostratigraphy, and paleoecology. In: Duncan, R.A., Backman, J., et al. (Eds.), *Proceedings of the Ocean Drilling Program, Scientific Results* 115, 433-463. doi:10.2973/odp.proc.sr.115.207.1990.

Fourtanier, E., 1991b. Diatom biostratigraphy of equatorial Indian Ocean Site 758. In: Weissel, J., Peirce, J., et al. (Eds.), *Proceedings of the Ocean Drilling Program, Scientific Results* 121, 189-208. doi:10.2973/odp.proc.sr.121.137.1991

Gladenkov, A.Y., 2013. First finds of Eocene diatoms in the marine Paleogene reference section in the Il'pinskii Peninsula, Northeastern Kamchatka. *Stratigraphy and Geological Correlation* 21, 96-106.

Gladenkov, A.Y., Barron, J.A., 1995. Oligocene and early middle Miocene diatom biostratigraphy of Hole 884B. In: Rea, D.K., Basov, I.A., Scholl, D.W., Allan, J.F. (Eds.), *Proceedings of the Ocean Drilling Program, Scientific Results* 145, 21-41. doi: 10.2973/odp.proc.sr.145.105.1995

Gleser, S.I., 1969. Комплексы диатомовых, кремневых жгутиковых водорослей и эбрии из верхнеэоценовых отложений юго-западной части Тургайского прогиба. Биостратиграфический сборник 4, 67-86 (in Russian).

Gleser, S.I., 1996. Problems of Eocene siliceous phytoplankton zonation (exemplified by the Caspian Eocene deposits). *Stratigraphy and Geological Correlation* 4, 392-402.

- Gleser, S.I., Jousé, A.P., 1974. Diatoms and silicoflagellates in the Eocene of the equatorial Atlantic. In: Jousé, A.P., Gleser, S.I. (Eds.), *Micropaleontology of Oceans and Seas*, Nauka, Moscow, pp. 49-62 (in Russian).
- Gleser, S.I., Sheshukova-Poretzkaya, V.N., 1968. Late Eocene Bacillariophyta, Chrysophyta, Pyrrophyta and Ebrideae of the north-eastern margin of the Ukrainian crystalline massif. *Paleontologicheskii Sbornik* 5, 117-124.
- Gleser, S.I., Sheshukova-Poretzkaya, V.N., 1969. К истории формирования позднеэоценовой морской диатомовой флоры Украины. *Вестник Ленградского Университета* 9, 60-73.
- Gleser, S.I., Dolmatova, L.M., Lupikina, E.G., 1986. Marine Palaeogenic diatoms algae from eastern Kamchatka. *Botanicheskii Zhurnal* 71, 851-859 (in Russian).
- Gleser, S.I., Jousé, A.P., Makarova, I.B., Proshkina-Lavrenko, A.I., Sheshukova-Poretzkaya, V.S., 1974. Diatoms of the USSR: Fossil and Recent, vol. 1. Nauka, Moskva (in Russian).
- Gleser, S.I., Makarova, I.V. (ed.), Moiseeva, A.I., Nikolaev, V.A., 1992. The diatoms of the USSR: Fossil and Recent, vol. 2, fasc. II. Nauka, St. Petersburg (in Russian).
- Gombos, A.M., Jr., 1977. Paleogene and Neogene diatoms from the Falkland Plateau and Malvinas Outer Basin: Leg 36, Deep Sea Drilling Project. In: Barker, P., Dalziel, I.W.D., et al. (Eds.), *Initial Reports of the Deep Sea Drilling Project 36*, 575-687. doi:10.2973/dsdp.proc.36.111.1977.
- Gombos, Jr., A.M., 1983. Middle Eocene diatoms from the South Atlantic. In: Ludwig, W.J., Krashennnikov, V.A., et al. (Eds.), *Initial Reports of the Deep Sea Drilling Project 71*, 565-581. doi: 10.2973/dsdp.proc.71.123.1983
- Gombos, Jr., A.M., 1987. Middle Eocene diatoms from the North Atlantic, Deep Sea Drilling Project Site 605. In: van Hinte, J.E., Wise, S.W., Jr., et al. (Eds.), *Initial Reports of the Deep Sea Drilling Project 93*, 793-799. doi: 10.2973/dsdp.proc.93.126.1987
- Gombos, A.M., Jr., Ciesielski, P.F., 1983. Late Eocene to early Miocene diatoms from the Southwest Atlantic. In: Ludwig, W.J., Krashennnikov, V.A., et al. (Eds.), *Initial Reports of the Deep Sea Drilling Project 71*, 583-634. doi: 10.2973/dsdp.proc.71.124.1983
- Greville, R.K., 1861. Descriptions of new and rare diatoms. Series II. *Transactions of the Microscopical Society*, New Series 9, 67-73.
- Grunow, A., 1884. Die Diatomeen von Franz-Josefs-Land. *Denkschriften der Kaiserlichen Akademie der Wissenschaften. Mathematisch-Naturwissenschaftliche Classe* 48, 53-112 (in German).
- Hajós, M., 1976. Upper Eocene and lower Oligocene Diatomaceae, Archaeomonadaceae, and Silicoflagellatae in Southwestern Pacific sediments, DSDP Leg 29. In: Hollister, C.D., Craddock, C., et al. (Eds.), *Initial Reports of the Deep Sea Drilling Project 35*, 817-883. doi:10.2973/dsdp.proc.35.29chap1.1976
- Hanna, G D., Brigger, A.L., 1970. Observations on *Liostephanina*. In: Gerloff, J., Cholnoky, B.J. (Ed.), *Diatomaceae II. Friedrich Hustedt Gedenkband. Nova Hedwigia, Beiheft* 31, 89-100.
- Harwood, D.M., Bohaty, S.M., 2000. Marine diatom assemblages from Eocene and younger erratics, McMurdo Sound, Antarctica. In: Stillwell, J.D., Feldmann, R.M. (Eds.), *Paleobiology and paleoenvironments of Eocene rocks, McMurdo Sound, East Antarctica. Antarctic Research Series* 76, 73-98.

- Harwood, D.M., Bohaty, S.M., 2001. Early Oligocene siliceous microfossil biostratigraphy of Cape Roberts Project Core CRP-3, Victoria Land Basin, Antarctica. *Terra Antarctica* 8, 315-338.
- Harwood, D.M., Maruyama, T., 1992. Middle Eocene to Pleistocene diatom biostratigraphy of Southern Ocean sediments from the Kerguelen Plateau, Leg 120. In: Wise, S.W., Jr., Schlich, R., et al. (Eds.), *Proceedings of the Ocean Drilling Program 120*, 683-733. doi: 10.2973/odp.proc.sr.120.160.1992.
- Hasle, G.R., Syvertsen, E.E., 1997. Marine diatoms. In: Tomas, C.R. (Ed.), *Identifying Marine Phytoplankton*. Academic Press, San Diego, 5-386.
- Hasle, G.R., von Stosch, H.A., Syvertsen, E.E., 1983. Cymatosiraceae, a new diatom family. *Bacillaria* 6, 9-156.
- Jones, D.M., Kingston, M.J., Marlow, M.S., Cooper, A.K., Barron, J.A., Wingate, F.H., Arnal, R.E., 1981. Age, mineralogy, physical properties, and geochemistry of dredge samples from the Bering Sea continental margin. *United States Geological Survey Open File Report 81-1297*, 1-69.
- Kanaya, T., 1957. Eocene diatom assemblages from the Kellogg and "Sidney" Shales, Mt. Diablo area, California. *Scientific Reports of Tohoku University, Sendai, Japan, 2nd series* 28, 27-124.
- Kim, W.H., Barron, J.A., 1986. Diatom biostratigraphy of the Upper Oligocene to Lowermost Miocene San Gregorio Formation, Baja California Sur, Mexico. *Diatom Research* 1, 169-187.
- Koizumi, I., 1992. Diatomaceous sediments along the Pacific coastal areas of South America and their evolution. *Journal of the Faculty of Science, Hokkaido University. Series 4, Geology and Mineralogy* 23, 227-245.
- Machare, J., Devries, T., Barron, J., Fourtanier, E., 1988. Oligo-Miocene transgression along the Pacific margin of South America: new paleontological and geological evidence from the Pisco basin (Peru). *Géodynamique* 3, 25-37.
- Manchester S.R., Herrera, F., Fourtanier, E., Barron, J., Martinez, J.-N., 2012. Oligocene age of the classic Belén fruit and seed assemblage of north coastal Peru based on diatom biostratigraphy. *Journal of Geology* 120, 467-476.
- Mita, I., 2001. Data report: Early to Late Eocene calcareous nannofossil assemblages of Sites 1051 and 1052, Blake Nose, Northwestern Atlantic Ocean. In: Kroon, D., Norris, R.D., Klaus, A. (Eds.), *Proceedings of the Ocean Drilling Program, Scientific Results 171B*, 1-28 (Online). doi:10.2973/odp.proc.sr.171B.122.2001
- Olshynskaya, A., 2002. Morphological and taxonomic characteristics of some Paleogene diatoms of Ukraine. *International Journal on Algae* 4, 118-126.
- Prema, P., Desikachary, T.V., 2012. Eocene diatoms from the Indian Ocean region. *Phykos* 42, 65-73.
- Proshkina-Lavrenko, A.N. (Ed.), 1949. *Diatomovyi analiz. Kniga 2. Opredelitel iskopaemykh i sovremennykh diatomovykh vodorosley. Poryadki Centrales i Mediales*. Gosgeoltekhizdat, Leningrad, 240 pp., 101 pls (in Russian).
- Renaudie, J., Danelian, T., Saint Martin, S., Le Callonec, L., Tribovillard, N., 2010. Siliceous phytoplankton response to a Middle Eocene warming event recorded in the tropical Atlantic (Demerara Rise, ODP Site 1260A). *Palaeogeography, Palaeoclimatology, Palaeoecology* 286, 121-134. doi: 10.1016/j.palaeo.2009.12.004.

Ryan, W.B.F., Cita, M.B., Miller, E.L., Hanselman, D., 1978. Bedrock geology in New England submarine canyons. *Oceanologica Acta* 1, 233-254.

Sanfilippo, A., Fourtanier, E., 2003. Oligocene radiolarians, diatoms and ebridians from the Great Australian Bight (ODP Leg 182, Site 1128). In: Hine, A.C., Feary, D.A., Malone, M.J. (Eds.), *Proceedings of the Ocean Drilling Program, Scientific Results 182*, 1-24 (Online). doi: 10.2973/odp.proc.sr.182.004.2003

Saunders, J.B., Bernoulli, D., Müller-Merz, E., Oberhänsli, H., Perch-Nielsen, K., Riedel, W.R., Sanfilippo, A., Torrini, R., Jr., 1984. Stratigraphy of the late Middle Eocene to Early Oligocene in the Bath Cliff section, Barbados, West Indies. *Micropaleontology* 30, 390-425.

Sato, S., Watanabe, T., Nagumo, T., Tanaka, J., 2011. Valve morphogenesis in an araphid diatom *Rhaphoneis amphiceros* (Rhaphoneidaceae, Bacillariophyta). *Phycological Research* 59, 236-243. doi: 10.1111/j.1440-1835.2011.00621.x

Scherer, R.P., Koç, N., 1996. Late Paleogene diatom biostratigraphy and paleoenvironments of the northern Norwegian-Greenland Sea. In: Thiede, J., Myhre, A.M., et al. (Eds.), *Proceedings of the Ocean Drilling Program, Scientific Results 151*, 75-99. doi: 10.2973/odp.proc.sr.151.155.1996

Scherer, R.P., Bohaty, S.M., Harwood, D.M., 2000. Oligocene and lower Miocene siliceous microfossil biostratigraphy of Cape Roberts Project Core CRP-2/2A, Victoria Land Basin, Antarctica. *Terra Antarctica* 7, 417-442.

Schmidt, A., Schmidt, M., Fricke, F., Heiden, H., Müller, O., Hustedt, F., 1874-1959. *Atlas der Diatomaceen-kunde*. Leipzig-Berling. Reprint 1984, Koeltz Scientific Books, Koenigstein (in German).

Schrader, H.-J., 1978. Diatoms in DSDP Leg 41 Sites. In: Lancelot, Y., Seibold, E., et al. (Eds.), *Initial Reports of the Deep Sea Drilling Project 41*, 791-812. doi: 10.2973/dsdp.proc.41.119.1978.

Schrader, H.-J., Fenner, J., 1976. Norwegian Sea Cenozoic diatom biostratigraphy and taxonomy. In: Talwani, M., Udintsev, G., et al. (Eds.), *Initial Reports of the Deep Sea Drilling Project 38*, 921-1099. doi: 10.2973/dsdp.proc.38.130.1976.

Shipboard Scientific Party, 1989. Site 753. In: Peirce, J., Weissel, J., et al. (Eds.), *Proceedings of the Ocean Drilling Program, Initial Reports 121*, 171-189. doi: 10.2973/odp.proc.ir.121.107.1989

Shipboard Scientific Party, 1998. Site 1051. In: Norris, R.D., Kroon, D., Klaus, A., et al. (Eds.), *Proceedings of the Ocean Drilling Program, Initial Reports 171B*, 171-239. doi: 10.2973/odp.proc.ir.171B.105.1998

Shipboard Scientific Party, 1999. Site 1123: North Chatham drift – a 20-Ma record of the Pacific deep western boundary current. In: Carter, R.M., McCave, I.N., Richter, C., Carter, L., et al. (Eds.), *Proceedings of the Ocean Drilling Program, Initial Reports 181*, 1-184 (Online). doi: 10.2973/odp.proc.ir.181.107.2000

Sluijs, A., Brinkhuis, H., Stickley, C.E., Warnaar, J., Williams, G.L., Fuller, M., 2004. Dinoflagellate cysts from the Eocene-Oligocene transition in the Southern Ocean: results from ODP Leg 189. In: Exon, N.F., Kennett, J.P., Malone, M.J. (Eds.), *Proceedings of the Ocean Drilling Program, Scientific Results 189*, 1-42 (Online). doi: 10.2973/odp.proc.sr.189.104.2003.

Stickley, C.E., Brinkhuis, H., Schellenberg, S.A., Sluijs, A., Röhl, U., Fuller, M., Grauert, M., Huber, M., Warnaar, J., Williams, G.L., 2004. Timing and nature of the deepening of the Tasmanian Gateway. *Paleoceanography* 19, PA4027. doi: 10.1029/2004PA001022.

Stickley, C.E., Brinkhuis, H., McGonigal, K.L., Chaproniere, G.C.H., Fuller, M., Kelly, D.C., Nürnberg, D., Pfuhl, H.A., Schellenberg, S.S., Schoenfeld, J., Suzuki, N., Touchard, Y., Wei, W., Williams, G.L., Lara, J., Stant, S.A., 2004. Late Cretaceous-Quaternary biomagnetostratigraphy of ODP Sites 1168, 1170, 1171, and 1172, Tasmanian Gateway. In: Exon, N.F., Kennett, J.P., Malone, M.J. (Eds.), Proceedings of the Ocean Drilling Program, Scientific Results 189, 1-57 (Online). doi: 10.2973/odp.proc.sr.189.111.2004

Strelnikova, N.I., 1992. Paleogenov'e diatomov'e vodorosli. St. Petersburg University Press, St. Petersburg (in Russian).

Suto, I., 2004. Fossil marine diatom resting spore morpho-genus *Xanthiopyxis* Ehrenberg in the North Pacific and Norwegian Sea. Paleontological Research 8, 283-310.

Suto, I., 2005. *Vallodiscus* gen. nov., a new fossil resting spore morpho-genus related to the marine diatom genus *Chaetoceros* (Bacillariophyceae). Phycological Research 53, 11-29.

Suto, I., 2006. Taxonomy of the fossil marine diatom resting spore morpho-genera *Xanthioisthmus* Suto gen. nov. and *Quadrocistella* Suto gen. nov. in the North Pacific and Norwegian Sea. Journal of Micropalaeontology 23, 3-22.

Suto, I., Jordan, R.W., Watanabe, M., 2009. Taxonomy of middle Eocene diatom resting spores and their allied taxa from the central Arctic Basin. Micropaleontology 55, 259-312.

Tanimura, Y., Sato, H., 1997. *Pseudopodosira kosugii*: a new Holocene diatom found to be a useful indicator to identify former sea-levels. Diatom Research 12, 357-368.

Tiffany, M.A., 2008. Valve development in *Aulacodiscus*. Diatom Research 23, 185-212.

Tiffany, M.A., Hernández-Becerril, D.U., 2005. Valve development in the diatom family Asterolampraceae H.L. Smith 1872. Micropaleontology 51, 217-258.

Tsoy, I., 2003. Eocene diatoms and silicoflagellates from the Kronotskii Bay deposits (East Kamchatka). Stratigraphy and Geological Correlation 11, 376-390.

Tynni, R., 1982. The reflection of geological evolution in Tertiary and interglacial diatoms and silicoflagellates in Finnish Lapland. Geological survey of Finland Bulletin 320, 1-40.

Witkowski, A., Lange-Bertalot, H., Metzeltin, D., 2000. Diatom flora of marine coasts I. In: Lange-Bertalot, H. (Ed.), Iconographia Diatomologica 7. Gantner Verlag, Ruggell.

Witkowski, J., Harwood, D.M., Chin, K., 2011. Taxonomic composition, paleoecology and biostratigraphy of Late Cretaceous diatoms from Devon Island, Nunavut, Canadian High Arctic. Cretaceous Research 32, 277-300. doi: 10.1016/j.cretres.2010.12.009

Witkowski, J., Bohaty, S.M., McCartney, K., Harwood, D.M. (2012). *Enhanced siliceous plankton productivity in response to middle Eocene warming at Southern Ocean ODP Sites 748 and 749*. Palaeogeography, Palaeoclimatology, Palaeoecology 326-328, 78-94. doi: 10.1016/j.palaeo.2012.02.006